AD-A142 427 PERFORMANCE OF DIGITAL COMMUNICATIONS OVER SELECTIVE FADING CHANNELS(U) ILLINOIS UNIV AT URBANA COORDINATED SCIENCE LAB F D GARBER SEP 83 R-998 N00014-79-C-0424 1/2

UNCLASSIFIED F/G 17/2.1 NL

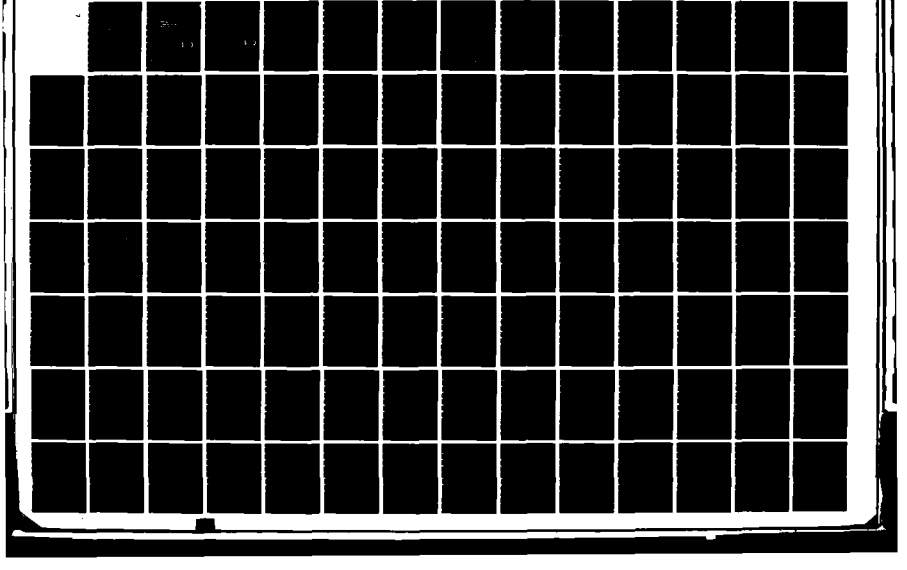

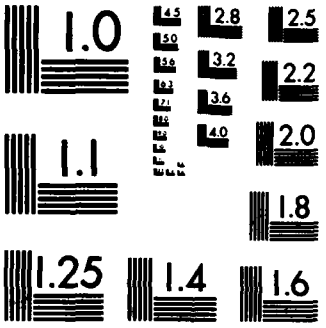


MICROCOPY RESOLUTION TEST CHART
NATIONAL BUREAU OF STANDARDS-1963-A

REPORT R-998 SEPTEMBER 1983 UILU-ENG 83-2219



# PERFORMANCE OF DIGITAL COMMUNICATIONS OVER SELECTIVE FADING CHANNELS

FREDERICK DWIGHT GARBER







UNIVERSITY OF ILLINOIS AT URBANA-CHAMPAIGN

UNCLASSIFIED

SECURITY CLASSIFICATION OF THIS PAGE (When Data Entered)

| REPORT DOCUMENTATION PAGE | READ INSTRUCTIONS BEFORE COMPLETING FORM |
|---|---|
| 1. REPORT NUMBER | 2. GOVT ACCESSION NO. AD-A142 427 / 3. RECIPIENT'S CATALOG NUMBER |
| 4. TITLE (and Subtitle) PERFORMANCE OF DIGITAL COMMUNICATIONS OVER SELECTIVE FADING CHANNELS | 5. TYPE OF REPORT & PERIOD COVERED Technical Report |
| | 6. PERFORMING ORG. REPORT NUMBER R-998; UILU-ENG 83-2219 |
| 7. AUTHOR(s) Frederick Dwight Garber | 8. CONTRACT OR GRANT NUMBER(s) N00014-79-C-0424 |
| 9. PERFORMING ORGANIZATION NAME AND ADDRESS Coordinated Science Laboratory University of Illinois at Urbana-Champaign Urbana, IL 61801 | 10. PROGRAM ELEMENT, PROJECT, TASK AREA & WORK UNIT NUMBERS |
| 11. CONTROLLING OFFICE NAME AND ADDRESS Joint Services Electronics Program | 12. REPORT DATE September 1983 |
| | 13. NUMBER OF PAGES 149 |
| 14. MONITORING AGENCY NAME & ADDRESS(if different from Controlling Office) | 15. SECURITY CLASS. (of this report) UNCLASSIFIED |
| | 15a. DECLASSIFICATION/ DOWNGRADING SCHEDULE |

16. DISTRIBUTION STATEMENT (of this Report)

Approved for public release; distribution unlimited

17. DISTRIBUTION STATEMENT (of the abstract entered in Block 20, if different from Report)



18. SUPPLEMENTARY NOTES

19. KEY WORDS (Continue on reverse side if necessary and identify by block number)

fading channels, intersymbol interference, differential phase-shift keying, frequency-shift keying, equalization

20. ABSTRACT (Continue on reverse side if necessary and identify by block number)

The performance of digital communications over selective wide-sense-stationary uncorrelated-scattering (WSSUS) fading channels is investigated. The emphasis is on the evaluation of the performance of binary differential phase-shift keyed (DPSK) and binary frequency-shift (FSK) communications with primary emphasis on the effects of intersymbol interference produced by the frequency-selective character of WSSUS fading channels.

The error probability of DPSK and FSK are evaluated for several models of WSSUS frequency-selective fading channels. The analysis is focused on the

DD FORM 1 JAN 73 1473

UNCLASSIFIED

SECURITY CLASSIFICATION OF THIS PAGE (When Data Entered)

performance evaluation for Rayleigh fading channels. The expressions for the probability of error for these systems are formulated in a way that allows the identification of the key parameters of the communication system.

The performance of DPSK and FSK are evaluated for several signaling formats. The design parameters considered are the shapes of the basic data-pulse waveforms for both DPSK and FSK, the modulation index, and the relative phase between successive transmitted signals for FSK. It is shown that the system error probability is highly dependent on these system parameters.

The interaction between the various elements of the communication system is examined. We show that the average error probability can be approximated in terms of one or two rms type channel measurements. A technique for obtaining bounds on system performance in terms of the key system and channel parameters is described and applied to the evaluation of both DPSK and FSK systems for several channel models and signaling formats. A method of approximating the performance of systems employing complicated pulse shapes and channels which are difficult to fully characterize is discussed. It is shown that the techniques for obtaining bounds and approximations for Rayleigh channels are easily applied to the more general frequency-selective Rician fading channels.

The applicability of adaptive equalization techniques to digital communications over WSSUS frequency-selective fading channels is discussed. We describe the characteristics of adaptive equalizers that are commonly employed for fading-channel communications. It is found that adaptive equalizers can be used to establish a coherent communications environment as well as to reduce the effects of ISI. The results of cited simulation and experimental studies are compared to the analytical results for the error probabilities of the DPSK and FSK systems. We develop a method of obtaining estimates of adaptive equalizer performance for practical systems.

# PERFORMANCE OF DIGITAL COMMUNICATIONS OVER SELECTIVE FADING CHANNELS

BY

FREDERICK DWIGHT GARBER

B.S., Tri-State College, 1975
M.S., University of Illinois, 1978

THESIS

Submitted in partial fulfillment of the requirements
for the degree of Doctor of Philosophy in Electrical Engineering
in the Graduate College of the
University of Illinois at Urbana-Champaign, 1983

Thesis Adviser: Professor M. B. Pursley

Urbana, Illinois

# PERFORMANCE OF DIGITAL COMMUNICATIONS OVER SELECTIVE FADING CHANNELS

Frederick Dwight Garber, Ph.D.
Department of Electrical Engineering
University of Illinois at Urbana-Champaign, 1983

## ABSTRACT

The performance of digital communications over selective wide-sense-stationary uncorrelated-scattering (WSSUS) fading channels is investigated. The emphasis is on the evaluation of the performance of binary differential phase-shift keyed (DPSK) and binary frequency-shift keyed (FSK) communications with primary emphasis on the effects of intersymbol interference produced by the frequency-selective character of WSSUS fading channels.

The error probabilities of DPSK and FSK are evaluated for several models of WSSUS frequency-selective fading channels. The analysis is focused on the performance evaluation for Rayleigh fading channels. The expressions for the probability of error for these systems are formulated in a way that allows the identification of the key parameters of the communication system.

The performances of DPSK and FSK are evaluated for several signaling formats. The design parameters considered are the shapes of the basic data-pulse waveforms for both DPSK and FSK, the modulation index, and the relative phase between successive transmitted signals for FSK. It is shown that the system error probability is highly dependent on these system parameters.

The interaction between the various elements of the communication system is examined. We show that the average error probability can be approximated in terms of one or two rms type channel measurements. A technique for

obtaining bounds on system performance in terms of the key system and channel parameters is described and applied to the evaluation of both DPSK and FSK systems for several channel models and signaling formats. A method of approximating the performance of systems employing complicated pulse shapes and channels which are difficult to fully characterize is discussed. It is shown that the techniques for obtaining bounds and approximations for Rayleigh channels are easily applied to the more general frequency-selective Rician fading channels.

The applicability of adaptive equalization techniques to digital communications over WSSUS frequency-selective fading channels is discussed. We describe the characteristics of adaptive equalizers that are commonly employed for fading-channel communications. It is found that adaptive equalizers can be used to establish a coherent communications environment as well as to reduce the effects of ISI. The results of cited simulation and experimental studies are compared to the analytical results for the error probabilities of the DPSK and FSK systems. We develop a method of obtaining estimates of adaptive equalizer performance for practical systems.

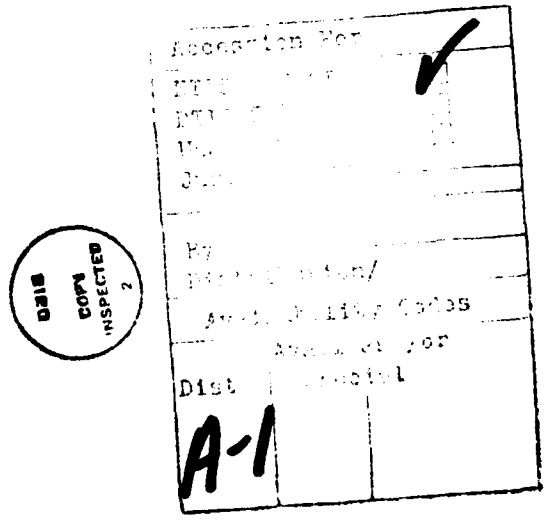

## ACKNOWLEDGEMENT

I would like to thank my thesis advisor, Professor Michael B. Pursley, for his guidance, support, and encouragement throughout the course of this work. I am also grateful to Professors B. E. Hajek, R. J. McEliece, H. V. Poor, and D. V. Sarwate for serving on the doctoral committee.

TABLE OF CONTENTS

# CHAPTER 1

## INTRODUCTION

Several problems arise in the consideration of slow-frequency-hopped (SFH) spread-spectrum communications which motivate the study of the performance of digital communications over selective fading channels [1-4]. In many applications of SFH systems, the channel (or transmission medium) cannot be adequately modeled as a non-dispersive additive white Gaussian noise channel. In cases where the characteristics of the channel are significantly different from this ideal, the channel is commonly referred to as a fading channel. Fading channels may exhibit such undesirable properties as a time-varying amplitude response, the spreading of transmitted signals in the frequency domain (time-selectivity), and dispersion in time (frequency-selectivity) which may produce significant intersymbol interference (ISI). In cases where it is impractical to obtain accurate channel estimates and incorporate these estimates in the detection process, the random character of the fading channel precludes the use of coherent demodulation. Binary differential phase-shift keying (DPSK) and frequency-shift keying (FSK) are of particular interest for applications of SFH systems in selective fading channels, since these forms of digital communications do not require the receiver to establish phase coherence at the beginning of each hop [2,3,5]. The primary focus of this thesis is the evaluation of the average probability of error for DPSK and FSK communications in selective fading channels. The analyses of these systems are of considerable importance independent of applications to spread-spectrum communications. Furthermore, the results on the average error probabilities for DPSK and FSK can also be used in the performance evaluation of SFH systems [2-4].

Previous analyses of various forms of digital communications over fading channels which are selective only in time show that system performance parameters such as signal-to-noise ratio and average error probability are not significantly degraded unless the degree of time selectivity is quite large [2,3,6-12]. When coupled with the measurements of the time-selectivity of practical channels [7,13], these results indicate that the time-selective nature of the channel is not a limiting factor for the performance of these systems. In this thesis, we are primarily concerned with the effects of intersymbol interference produced by the frequency-selective character of fading channels. Thus, models of strictly frequency-selective channels are used in the evaluation of the average probability of error.

Two common examples where fading phenomena are encountered in practice are ionospheric high-frequency "skywave" and tropospheric scatter channels [6-8]. A channel model which accurately describes the characteristics of these and other examples of fading environments is the wide-sense-stationary uncorrelated-scattering (WSSUS) fading channel, which is discussed at length in [9] and [10]. This model is quite general and includes, for example, the doubly-selective Rician channel as a special case.

Experimental investigations [8,14,15] of the multipath characteristics of fading channels show that no one multipath model adequately describes the properties of various frequency-selective channels encountered in practice. These investigations also indicate that there are many situations where the multipath parameters of the channel do not remain constant during the time required for transmission of a long data sequence. In Chapter 2, four examples of multipath propagation models for WSSUS frequency-selective channels are described.

In Chapters 3 and 4, we evaluate the average probabilites of error for binary DPSK and FSK over WSSUS frequency-selective fading channels. The analysis is focused on Rayleigh fading channels, since the adverse effects of frequency-selective fading are most evident for such channels. The primary goal of the analysis in Chapters 3 and 4 is to formulate expressions for the system error probability that provide insight to the nature of the fading mechanism. The expressions for the probability of error for these systems ar developed in a way that allows the identification of the key parameters of th communication system.

One of the fundamental design parameters for DPSK systems is the shape of the data-pulse waveform. Since the spectral characteristics of the transmitted signal are largely determined by the properties of this waveform, it is reasonable to expect that the performance of DPSK in a frequency-selective fading environment is highly dependent on the choice of the pulse waveform. For FSK communications, the character of the transmitted signal depends on the frequency separation between the two FSK tones and the relative phases between successive transmitted signals as well as the shape of the data-pulse waveform. Previous investigations of DPSK and FSK over frequency-selective fading channels [2,5,16-18] indicate that the error probabilities are strongly dependent on these parameters.

We examine the interaction between the characteristics of the fading channel, the transmitted signal, and the nonlinear detection that arises in both DPSK and FSK demodulation. We show that in many cases of practical interest, the performance of these systems can be approximated in terms of one or two parameters which can be obtained from rms type channel measurements (e.g., see [13]). It is found that the error probabilities for DPSK and FSK

depend on a number of common factors and that, in certain cases, the effects of frequency selectivity on both DPSK and FSK systems can be characterized by the same channel measurement. A technique for obtaining bounds on system performance is described and applied to the evaluation of both DPSK and FSK systems for several examples of channel models and signaling formats. We then present a method for approximating the performance of systems employing complicated pulse shapes and channels that are difficult to fully characterize. By using the results of [19], it is shown that the techniques for obtaining bounds and approximations for Rayleigh channels can easily be applied to the more general frequency-selective Rician fading channels.

In many practical systems, the effects of intersymbol interference (ISI) in a frequency-selective fading channel can severely limit the performance of conventional digital communications. For a number of years, considerable attention has been given to adaptive signal processing or "equalization" techniques for digital communications over certain non-fading channels [20-21]. For channels of this type, such as telephone lines and line-of-sight (LOS) microwave links, both linear and nonlinear equalizers (typically in the configuration of tapped-delay-line (TDL) filters) have been used effectively to reduce the effects of ISI [22]. More recently, there has been considerable interest in applications of similar equalization techniques to improve the performance of digital communications over WSSUS frequency-selective fading channels [23]. While the random character of fading channels presents a number of additional difficulties which must be overcome, both simulation studies [24] and experimental evidence [14] indicate that reliable communications can be achieved even in fading environments that produce unacceptably high error probabilities for unequalized systems.

In Chapter 5, we describe adaptive equalizers that are commonly employed for fading-channel communications. It is found that the main attributes of adaptive equalizers are the reduction of the effects of ISI and the ability to establish coherent communications. We briefly discuss the results of several simulation studies and experimental investigations. These results are compared to the results presented in Chapters 3 and 4. By examining the basic properties of TDL equalizers, we develop a method of obtaining estimates of adaptive equalizer performance for practical systems.

# CHAPTER 2

## CHANNEL MODELS

In this chapter, we discuss the key characteristics of the wide-sense-stationary uncorrelated-scattering (WSSUS) fading channel model used in the performance evaluation of the communication systems discussed in subsequent chapters. This channel model is described in detail in [9] and is employed in the analysis of a variety of digital communication systems in [2,5,9,11,16,17,24,25].

We employ narrowband signal models (see [6]) so that if the input to the channel is

$$\tilde{s}(t) = \mathrm{Re}\{s(t)\exp(j2\pi f_c t)\} , \tag{2.1}$$

then the output is given by

$$\tilde{r}(t) = \mathrm{Re}\{r(t)\exp(j2\pi f_c t)\} , \tag{2.2}$$

where

$$r(t) = \alpha s(t) + \int_{-\infty}^{\infty} h(t,\xi)s(t-\xi)\, d\xi + n(t) , \tag{2.3}$$

and n(t) is the equivalent (see [11]) low-pass Gaussian noise with (one-sided) spectral intensity $N_0$. For the general case of Rician fading, the received signal r(t) consists of three components: a single specular component, a diffuse or Rayleigh-faded component, and the channel noise. The fading process is characterized by the ensemble autocovariance of the response function h(t,ξ),

$$E\{h(t,\tau)h^*(x,\xi)\} = 2\sigma^2\rho(t-x,\xi)\delta(\tau-\xi) , \tag{2.4}$$

where $\delta(\cdot)$ is the Dirac delta function and $2\sigma^2$ is the total power in the

fading process, so that $\int_{-\infty}^{\infty} \rho(0,\xi)\, d\xi = 1$. Alternatively, the quantity $\sigma^2$ can be interpreted as the average power received when a (real) sinusoid of unity peak value is transmitted over the channel.

If $\alpha > 0$ in (2.1), there is a specular (non-faded) component present in the channel output. In this case the channel is termed a Rician fading channel (as in [12,19]). If $\alpha = 0$, there is no specular component in the received signal and the channel is a Rayleigh fading channel as is considered in [2,5,11,16,17]. The autocovariance function in (2.4) represents the second-order statistics of a channel that is selective in both time and frequency (i.e., doubly selective). Doubly selective channels are the most general examples in the class of WSSUS fading channels [9].

The effects of time-selective fading on DPSK communications are considered in [3] for several data pulse shapes and a variety of fading channel models. In [11], the performance of binary FSK communication via time-selective fading channels is calculated for one example of a fading channel. In each case the performance is evaluated as a function of parameters related to the bandwidth of the Doppler power density spectrum [11]. While it is probably true that most fading channels are time-selective to some degree, it is also true that, for a given fading channel, the normalized Doppler spread (see [3]) decreases with increasing channel data rate. Moreover, the results in [11] and [3], when coupled with measured Doppler spreads for typical channels [7],[13], indicate that the time-selective nature of the channel is not a limiting factor in determining the performance of practical systems. In the analyses that follow, we consider channels that are selective only in frequency, i.e., that are strictly frequency-selective.

For strictly frequency-selective fading channels, the autocovariance function (2.4) of the fading process becomes [9]

$$2\sigma^2 \rho(t-x,\xi)\delta(\tau-\xi) = 2\sigma^2 g(\xi)\delta(\tau-\xi) \ , \tag{2.5}$$

where $g(\xi)$ is the delay power-density spectrum of the fading process. The inverse Fourier transform of $g(\xi)$ is called the frequency correlation function [9] and is given by

$$G(\Omega) = \int_{-\infty}^{\infty} g(\xi) e^{j2\pi\Omega\xi} \, d\xi \ . \tag{2.6}$$

There are several ways in which the degree of frequency-selectivity can be specified. One is to define the selectivity as the "bandwidth" of the frequency correlation function $G(\Omega)$. For example, in [16] and [17], the distance between the "1/e" points of $G(\Omega)$ is used as a measure of frequency-selectivity. Alternatively, the degree of selectivity can be defined in terms of the delay power-density spectrum $g(\xi)$.

In any physical channel the transmitted signal undergoes a propagation delay $\tau_d$ (say) which, for the analyses of non-selective or non-fading channels, is usually assumed to be a known deterministic quantity that is compensated for at the receiver. In the case of frequency-selective channels, the transmitted signal may experience a continuum of random propagation delays, with mean value $\xi_d$ given by

$$\xi_d = \int_{-\infty}^{\infty} \xi g(\xi) \, d\xi \ , \tag{2.7}$$

which is referred to as the mean path delay. A parameter that is commonly used to specify the selectivity of the channel in terms of relative delay is the "multipath spread" [5] which is defined by

$$\text{m.s.} = 2\{\int_{-\infty}^{\infty} (\xi - \xi_d)^2 g(\xi)\, d\xi\}^{1/2} \tag{2.8}$$

(see [13], where techniques for measuring this channel parameter are discussed).

We are concerned with relative delays only and we assume that the receiver has compensated for the mean path delay $\xi_d$. Equivalently, we let $\xi_d = 0$ in order to establish a time reference. Parameters that are used in the sequel to specify the degree of frequency-selectivity are the rms delay,

$$M = \{\int_{-\infty}^{\infty} \xi^2 \cdot g(\xi)\, d\xi\}^{1/2} \tag{2.9}$$

which is equal to half the spread parameter defined in [5] and the rms multipath spread, defined by $\mu = M/T$, where T is the data symbol duration. This latter parameter is related to the normalized data rate [16,17], since it is a function of the ratio of the transmitted data rate and the channel correlation bandwidth.

Since the delay power-density spectrum, $g(\xi)$ in (2.5) (and hence the function $\rho(0,\xi)$ in (2.4)) can be viewed as the Fourier transform of the correlation function $G(\Omega)$ in (2.6), it is necessarily a nonnegative, real-valued function. We also assume that $g(\xi)$ is symmetric, i.e., $g(\xi) = g(-\xi)$. This assumption can be made without loss of generality since we consider only symmetric binary signaling, and the average probability of error depends on the fading channel model only through an ensemble average (2.4) of the channel statistics.

In the analysis that follows, the evaluation of the average probability of error for DPSK and FSK is considered for four examples of delay power-density spectra: the Gaussian, exponential, triangular and rectangular delay

densities. The Gaussian delay power-density spectrum is given by

$$g(\xi) = \frac{1}{\sqrt{2\pi}\, M} e^{-\xi^2/2M^2} , \tag{2.10}$$

with corresponding frequency correlation function

$$G(\Omega) = e^{-2(\pi M\Omega)^2} . \tag{2.11}$$

The parameter M in (2.10) and (2.11) is the rms delay given by (2.9). The exponential delay power-density spectrum is given by

$$g(\xi) = \frac{1}{2M} e^{-2|\xi|/M} , \tag{2.12}$$

and the corresponding frequency correlation function is

$$G(\Omega) = (1 + 2(\pi M\Omega)^2)^{-1}. \tag{2.13}$$

The triangular delay spectrum, which was employed in [4] and [18] for the analysis of a slow-frequency-hopped FSK multiple-access system, is given by

$$g(\xi) = \begin{cases} \dfrac{T_0 - |\xi|}{T_0^2} ; & |\xi| \le T_0, \\ 0 ; & \text{otherwise} . \end{cases} \tag{2.14}$$

The frequency correlation function for the triangular spectrum is

$$G(\Omega) = \text{sinc}^2(\Omega T_0) , \tag{2.15}$$

where $\text{sinc}(x) = \sin(\pi x)/(\pi x)$; and the rms delay is given by $M = T_0/\sqrt{6}$. The rectangular delay power-density spectrum is given by

$$g(\xi) = \begin{cases} (2T_0)^{-1} ; & |\xi| \leq T_0 \\ 0 ; & \text{otherwise} , \end{cases} \tag{2.16}$$

with corresponding frequency correlation function

$$G(\Omega) = \text{sinc}(2\Omega T_0) , \tag{2.17}$$

where $M = T_0/\sqrt{3}$.

For a general frequency-selective channel, the detection of a given information bit may depend on a number of consecutive data pulses, because of intersymbol interference (ISI). Although the analysis presented below is easily extended to include more severe intersymbol interference, we assume as in [5,16,17] that the degree of frequency-selective fading is small enough that the intersymbol interference affects only adjacent data pulses; this is satisfied if $\rho(t-x,\xi) \approx 0$ for $|\xi| > T$ (cf. (2.4)). In this case, the channel is referred to as an adjacent-pulse-limited ISI channel. This assumption is made for two reasons. If the intersymbol interference is not limited to adjacent data pulses, it is much more difficult to formulate tractable expressions for the system error probability. Second, for all models of the delay power-density spectra considered here, the complementary assumption implies that the resulting average probability of error is unacceptably large.

Our assumption of adjacent-pulse-limited ISI places a restriction on the maximum value of the rms delay. In particular, if we require that at least 90% of the total energy of the delay spectrum lies within the range $[-T \leq \xi \leq T]$ for the Gaussian delay density, (i.e., if we require that in the absence of additive noise, less than 10% of the energy received in the interval $[(i-1)T, iT]$ is due to pulses transmitted outside the interval

[(i-2)T,(i+1)T]), then we must have

$$\mu = \frac{M}{T} < 0.43 \ .$$

where $\mu$ is the rms multipath spread. For the exponential delay power-density spectrum the requirement that 90% of the total energy of the delay spectrum is within the range $[-T \leq \xi \leq T]$ implies that the rms multipath spread satisfies

$$\mu = \frac{M}{T} < \frac{2}{\ln(.1)} \approx 0.62 \ .$$

In the case of a triangular delay spectrum, intersymbol interference is completely limited to adjacent pulses if

$$\mu^2 = \frac{T_0}{6T} \leq 1/6.$$

Finally, it is easy to see that intersymbol interference for the rectangular spectrum is limited to adjacent pulses if

$$\mu^2 = \frac{T_0}{3T} \leq 1/3 \ .$$

In the analysis that follows, we show that the "shape" of the delay power-density spectrum (as well as the rms multipath spread) can have considerable influence on the error probability of both differentially coherent and noncoherent communications.

# CHAPTER 3

## PERFORMANCE OF BINARY DPSK COMMUNICATIONS OVER FREQUENCY-SELECTIVE FADING CHANNELS

In this chapter, we consider the evaluation of the average probability of error for binary DPSK communications over wide-sense-stationary uncorrelated-scattering frequency-selective fading channels. In what follows, we primarily consider the performance of DPSK over WSSUS frequency-selective Rayleigh fading channels. It is in this case that the adverse effects of frequency-selective fading and the dependence of system performance on the channel delay power-density spectrum is most evident.

The dependence of the error probability for Rayleigh fading on the shape of the data-pulse waveform used as the DPSK signal has been considered in [5,16,17]. In particular, the rectangular pulse as well as the sine pulse, which is the basic pulse shape for minimum-shift-keying (MSK) modulation, is considered in [5] where the average probability of error is obtained for the Gaussian, exponential, triangular, and rectangular delay power-density spectrum models. The result for DPSK using the rectangular pulse for a Gaussian delay spectrum has been previously obtained by Bello and Nelin [17] and by Bailey and Lindenlaub [16]. In [16], the authors also consider the rectangular pulse and the raised-cosine-spectrum pulse for a rectangular delay power-density spectrum.

A number of conclusions may be drawn from these results:

i) For all models of delay power-density spectra considered, significant gains in performance can be achieved by proper choice of pulse shape.

ii) Closed-form expressions for the average probability of error can be unwieldy even for the simplest pulse shapes because of the quadratic nature of interference inherent in differential detection in a frequency-selective environment.

iii) Depending on the data pulse and the choice of normalization for multipath spread, the error probability can be very sensitive to the parameters of the fading channel, i.e., delay power-density spectrum.

The first observation indicates that the error probability of DPSK in frequency-selective fading channel can be substantially reduced by a judicious choice of pulse waveform. Unfortunately, the latter observations suggest that identification of a "good" pulse shape is, at best, analytically cumbersome and dependent on a number of channel and system parameters (as indicated by the complicated form of the results in [5,16,17]). Moreover, it is not necessarily true that analyses of this type provide a reasonable indication of the performance for a physical channel unless an exact mathematical description of the channel is available. This is especially unfortunate since a complete characterization may not be possible [13], and for many practical channels, the characteristics are not likely to remain constant during the time required for transmission of a long data sequence [9]. Hence, it is possible that several statistical models could be used to describe the same frequency-selective Rayleigh channel for repeated transmissions.

In this chapter, we show that the performance of DPSK communications over frequency-selective Rayleigh fading channels can be closely approximated in terms of one or two parameters which can be obtained from rms-type channel measurements. A technique for obtaining bounds on system performance in terms of the key channel parameters is described. We present a method for

approximating the performance of systems employing complicated pulse shapes and channels that are difficult to characterize fully. Finally, it is shown using the results of [19], that our results on bounds and approximations of the probability of error for Rayleigh channels can be applied to the more general case of frequency-selective Rician fading channels.

## 3.1 System Model

The system consists of an information source, a DPSK transmitter, and a differentially coherent receiver. The information to be transmitted is modeled as a sequence $(\bar{b}_i)$ of mutually independent random variables, each taking values 0 or 1 with equal probability. The binary data sequence $(b_i)$, with elements in $\{-1,1\}$, is formed by differentially encoding the information sequence $(\bar{b}_i)$. Thus, $(b_i)$ is a sequence of mutually independent random variables, each taking on the values -1 and +1 with equal probability. The data signal is given by

$$b(t) = b_i v(t-iT)$$

for each integer i. The data pulse-waveform v(t) is assumed to be time limited to the interval [0,T] such that

$$\frac{1}{T}\int_0^T v(t)^2\,dt = 1\ ;$$

thus for each integer i, the data signal is a positive or negative version of the basic pulse shape v(t). The transmitted signal $\tilde{s}(t)$ is given by (2.1) with s(t) defined by

$$s(t) = \sqrt{\frac{2E}{T}}\, b(t) \ , \tag{3.1}$$

where E is the energy per data bit of the transmitted signal.

In the present analysis, three examples of the pulse waveform v(t) are considered. These are the rectangular pulse

$$v(t) = p_T(t) \triangleq \begin{cases} 1, & 0 \le t < T \\ 0, & \text{otherwise} \ , \end{cases} \tag{3.2}$$

the sine pulse,

$$v(t) = \sqrt{2}\, \sin(\pi t/T) p_T(t) \ , \tag{3.3}$$

and the rectangular phase-coded pulse [26] given by

$$v(t) = \sum_{i=0}^{N-1} a_i\, p_{T_c}(t - iT_c) \tag{3.4}$$

for $0 \le t \le T$. The sequence $(a_i)$, referred to as the signature sequence, is a sequence of elements of $\{+1,-1\}$. The chip duration $T_c$ is related to T by $T = NT_c$ where N is the integer number of chips per data pulse. The sine pulse in (3.3) is the basic waveform used for minimum-shift-keying systems while the phase-coded pulse is referred to as the spectral-spreading signal in direct-sequence (DS) or code-division spread-spectrum multiple-access (SSMA) communications [26-29] and hybrid SFH/DS SSMA [4].

The DPSK receiver is the differentially coherent matched filter receiver shown in Fig. 3.1. At the end of the i-th data-pulse interval the receiver forms the decision statistic $Z_i$ represented (in terms of narrowband models) by

$$\begin{aligned} Z_i &= 2\mathrm{Re}\left[ 4 \int_{iT}^{(i+1)T} r(t)v^*(t)dt \int_{(i-1)T}^{iT} r^*(t)v(t)dt \right] , \\ &= UV^* + U^*V \end{aligned} \tag{3.5}$$

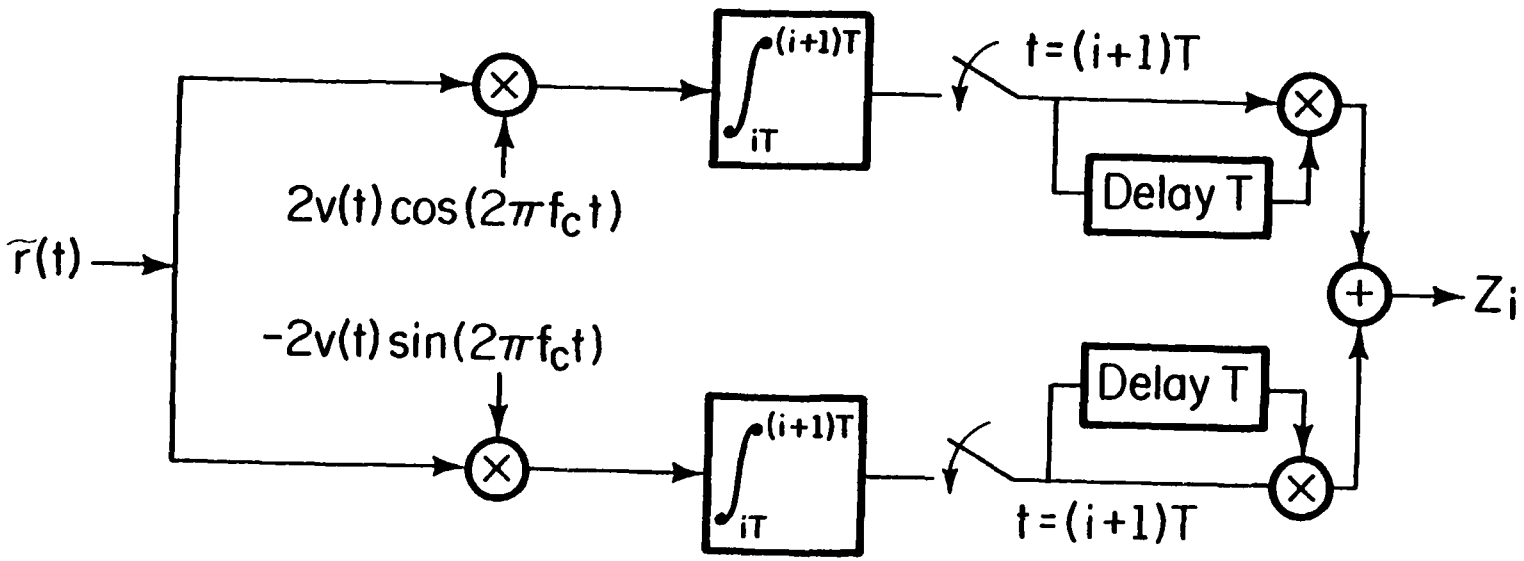


Figure 3.1. Differentially coherent matched filter receiver

where

$$U = 2 \int_{iT}^{(i+1)T} r(t)v^*(t)\, dt \tag{3.6a}$$

$$V = 2 \int_{(i-1)T}^{iT} r(t)v^*(t)\, dt\ . \tag{3.6b}$$

Notice from (3.5) that the statistic $Z_i$ is expressed as a quadratic form of complex Gaussian random variables U and V.

Under the assumption that $\rho(t-x,\xi) \approx 0;\ |\xi| > T$, i.e., adjacent-pulse-limited ISI, the output statistic $Z_i$ depends on at most four consecutive data bits represented by $\underline{b}_i = (b_{i-2}, b_{i-1}, b_i, b_{i+1})$ and the probability of error can be written in terms of probabilities conditioned on the event that certain sequences of data bits were transmitted, i.e.,

$$P_e = \frac{1}{16} \sum_{\underline{b}_i} P(\underline{b}_i)\ , \tag{3.7}$$

where $P(\underline{b}_i) = \Pr\{\text{error occurs}|\underline{b}_i \text{ transmitted}\}$. In [11,17] Bello and Nelin show that these conditional error probabilities are given by

$$P(\underline{b}_i) = (2 + \gamma(\underline{b}_i))^{-1}\ , \tag{3.8}$$

where $\gamma(\cdot)$ is the "equivalent" signal-to-noise ratio, which may be written in terms of the conditional moments $m_{XY}(\underline{b}_i) = E\{XY^*|\underline{b}_i\}$ of the random variables U and V as

$$\gamma(\underline{b}_i) = \begin{cases} \dfrac{2m_{UV}(\underline{b}_i)}{\sqrt{m_{UU}(\underline{b}_i)m_{VV}(\underline{b}_i)} - m_{UV}(\underline{b}_i)} & ;\ b_{i-1} = b_i \\ \dfrac{-2m_{UV}(\underline{b}_i)}{\sqrt{m_{UU}(\underline{b}_i)m_{VV}(\underline{b}_i)} + m_{UV}(\underline{b}_i)} & ;\ b_i \neq b_{i-1}\ . \end{cases} \tag{3.9}$$

Using (2.5) and (3.6), the necessary moments are written as

$$m_{UU}(\underline{b}_i) = 8\sigma^2 \int_{iT}^{(i+1)T} \int_{iT}^{(i+1)T} \int_{-T}^{T} \rho(t-x,\xi)s(t-\xi)v^*(t)s^*(x-\xi)v(x)\, d\xi dx dt + 8N_0T \tag{3.10a}$$

and

$$m_{UV}(\underline{b}_i) = 8\sigma^2 \int_{iT}^{(i+1)T} \int_{(i-1)T}^{iT} \int_{-T}^{T} \rho(t-x,\xi)s(t-\xi)v^*(t)s^*(x-\xi)v(x)\, d\xi dx dt. \tag{3.10b}$$

The moment $m_{VV}(\underline{b}_i)$ is defined similarly to $m_{UU}(\underline{b}_i)$ with the region of integration of the outer two integrals given by $[(i-1)T, iT]$, and $m_{VU}(\underline{b}_i) = m^*_{UV}(\underline{b}_i)$.

By substituting $g(\cdot)$ for $\rho(\cdot,\cdot)$ in (3.10) and using the assumption that $g$ is symmetric, the moments needed to evaluate $\gamma(\underline{b}_i)$ are found to be

$$m_{UU}(\underline{b}_i) = \frac{32\sigma^2E}{T}\left[\bar{\eta}_v + \eta_v + (b_{i-1}b_i + b_ib_{i+1})\eta'_v\right] + 8N_0T, \tag{3.11a}$$

$$m_{VV}(\underline{b}_i) = \frac{32\sigma^2E}{T}\left[\bar{\eta}_v + \eta_v + (b_{i-2}b_{i-1} + b_{i-1}b_i)\eta'_v\right] + 8N_0T, \tag{3.11b}$$

and

$$m_{UV}(\underline{b}_i) = \frac{16\sigma^2E}{T}\left[2b_ib_{i-1}\bar{\eta}_v + (b_{i-2}b_{i-1} + b_ib_{i+1})\eta_v + (2 + b_{i-2}b_i + b_{i-1}b_{i+1})\eta'_v\right], \tag{3.11c}$$

where

$$\bar{\eta}_v = \int_0^T g(\xi)\bar{R}_v^2(\xi)\, d\xi, \tag{3.12a}$$

$$\eta_v = \int_0^T g(\xi)R_v^2(\xi)\, d\xi, \tag{3.12b}$$

and

$$\eta'_v = \int_0^T g(\xi)\bar{R}_v(\xi)\, R_v(\xi)\, d\xi\,, \tag{3.12c}$$

where the parameters $\bar{R}_v(\xi)$ and $R_v(\xi)$ are defined in (3.14). By examining (3.9) and (3.11), it is easy to see that $\gamma(\underline{b}_i)$ exhibits certain symmetry relations in terms of the data pulse sequence $\underline{b}_i$. Making use of these properties, $P_e$ in (3.7) can be reduced to

$$P_e = \frac{1}{8}\,[P(-1,+1,-1,+1) + P(+1,+1,-1,-1) + 2P(-1,+1,-1,-1) + P(-1,+1,+1,-1) + P(+1,+1,+1,+1) + 2P(-1,+1,+1,+1)]. \quad (3.13)$$

The functions $\bar{R}_v(\cdot)$ and $R_v(\cdot)$ in (3.12), which are the usual continuous-time aperiodic autocorrelation functions [26,27] for time-limited signals, depend only on the pulse waveform v(t). They are defined by

$$\bar{R}_v(\xi) = \int_{\xi}^{T} v(t)\, v(t-\xi)\, dt \quad (3.14a)$$

and

$$R_v(\xi) = \int_{0}^{\xi} v(t)\, v(t+T-\xi)\, dt \quad (3.14b)$$

for $0 \le \xi \le T$. These functions are easily evaluated for the first two pulse shapes. They are found [27] to be

$$\bar{R}_v(\xi) = T - \xi \quad (3.15a)$$

and

$$R_v(\xi) = \xi \quad (3.15b)$$

for the rectangular pulse, and they are given by

$$\bar{R}_v(\xi) = (T-\xi)\cos(\pi\xi/T) + (T/\pi)\sin(\pi\xi/T) \quad (3.16a)$$

and

$$R_v(\xi) = -\xi\cos(\pi\xi/T) + (T/\pi)\sin(\pi\xi/T) \quad (3.16b)$$

for the sine pulse. The autocorrelation functions $\bar{R}_v(\cdot)$ and $R_v(\cdot)$ for the phase-coded pulse (3.4) are given for $0 \le kT_c \le \xi \le (k+1)T_c \le T$ by

$$\bar{R}_v(\xi) = C_a(k)((k+1)T_c - \xi) + C_a(k+1)(\xi - kT_c) \qquad (3.17a)$$

and

$$R_v(\xi) = C_a(N-k)((k+1)T_c - \xi) + C_a(N-k-1)(\xi - kT_c) , \qquad (3.17b)$$

where $C_a$ is the discrete aperiodic autocorrelation function for the sequence $(a_i)$ of length N defined in [26] by

$$C_a(k) = \begin{cases} \sum_{i=0}^{N-1-k} a_i a_{i+k}, & 0 \le k \le N-1 \\ \sum_{i=0}^{N-1+k} a_{i-k} a_i, & 1-N \le k \le 0 \\ 0, & |k| \ge N . \end{cases}$$

This function $C_a$ is considered in [26-29] and many of its properties are given in [30]. In what follows, it is shown that the performance of the phase-coded pulse depends on the correlation properties of the signature sequence $(a_i)$ as well as other system characteristics discussed earlier. Notice that the simple rectangular pulse (3.2) is obtained as a special case of (3.4) for any $N \ge 1$ by letting $a_i = +1$ for all $i \in \{0, \ldots, N-1\}$. We would also point out that the approximation [2,3] of the average error probability for SFH/SSMA in terms of the hopping pattern parameters and the probability of error given there are no hits does not generally apply to phase-coded pulse waveforms. Indeed, the principal reasons for considering this class of pulse shapes for coherent PSK systems include increased multiple-access capability [4,26-29] and immunity to the interference effects caused by multiple and/or diffuse

propagation paths [12,31]. Since, at present, there is no evidence to the contrary, one would expect similar gains to be realized in differentially coherent systems. Hence, a proper analysis of differentially coherent hybrid slow-frequency-hopped direct-sequence SSMA would be influenced by these characteristics.

Notice that the moments necessary to specify the average probability of error depend on the pulse shape and the delay power-density spectrum only through the integral expressions (3.12). Thus, the average probability of error is easily obtained once these three basic integrals are evaluated. In [5] closed-form expressions for the integrals in (3.12) are obtained for the rectangular and sine pulses, and for the four examples of delay spectra discussed in Chapter 2.

From (3.9) and (3.11) it is clear that the probability of error $P_e$ for a WSSUS frequency-selective fading channel depends on a number of system and channel parameters. In order to evaluate the effect of the fading process, it is instructive to first consider a limiting case in which the additive channel noise is neglected. In particular, Fig. 3.2 shows $P_e$ as a function of the signal-to-noise ratio $S = 2\sigma^2 E/N_0$, which is the ratio of the average energy per data pulse of the received signal to the real noise power spectral density $N_0/2$. The rectangular pulse waveform and the Gaussian model for the delay power-density spectrum with rms multipath spread $\mu = 0.05$ is assumed for this example. Also shown in Fig. 3.2 is $P_{ns}$, the error probability for DPSK in a <u>nonselective</u> Rayleigh fading channel, which is [6, Eq. 9-5-25],

$$P_{ns} = (2 + 4\sigma^2 E/N_0)^{-1} . \tag{3.18}$$

Notice that when the signal-to-noise ratio S is small, the average probability

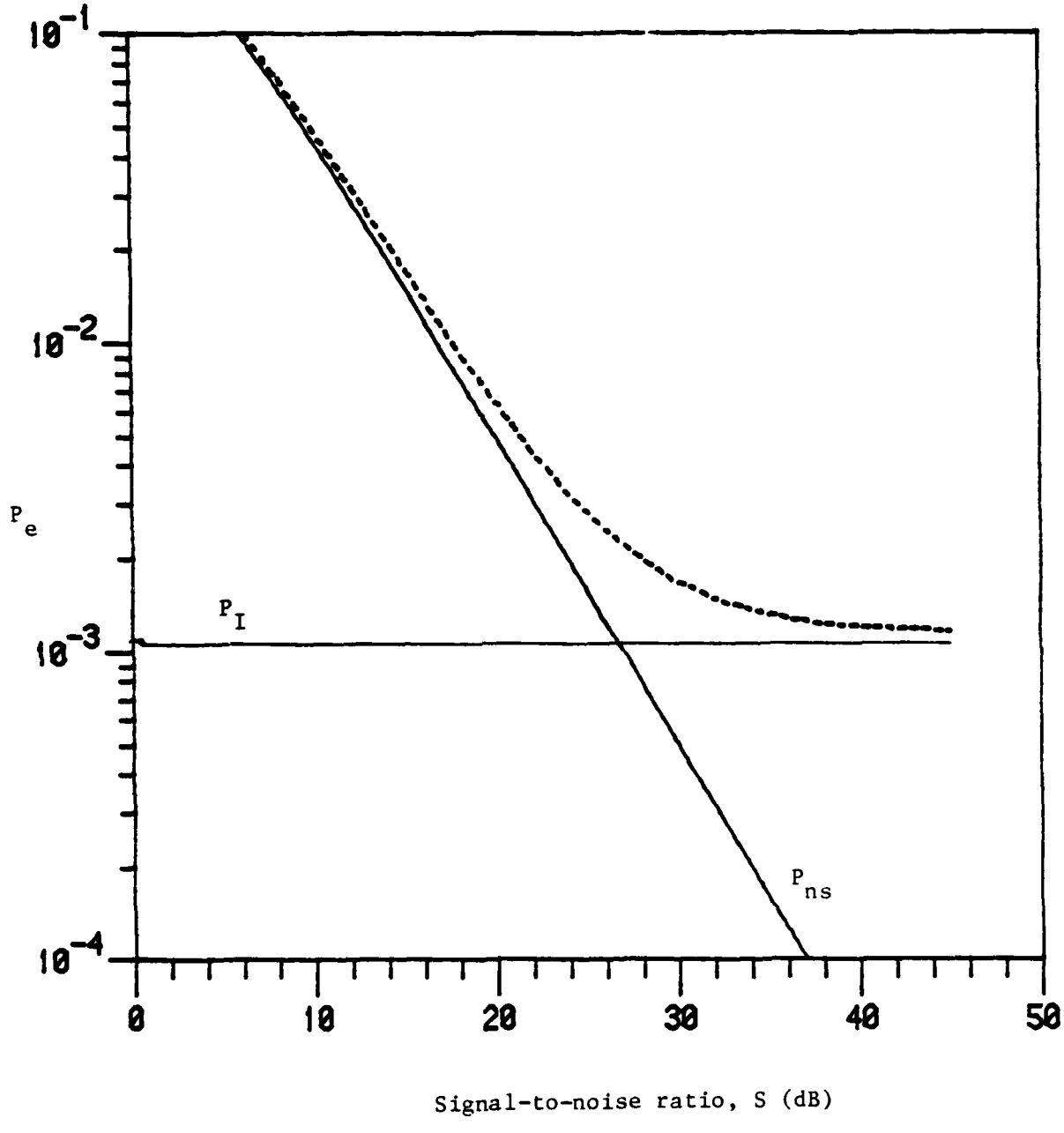


**Figure 3.2. $P_e$ vs. S for rectangular pulse DPSK and Gaussian delay power-density spectrum with $\mu = 0.05$**

of error is well approximated by $P_{ns}$. This is because at low signal-to-noise ratios, the decision errors are largely due to additive Gaussian noise rather than intersymbol interference.

For large signal-to-noise ratios, the errors caused by the effects of intersymbol interference dominate; the average error probability approaches a limiting error probability $P_I$ as $S \to \infty$. This limiting error probability is known as the irreducible error probability for the frequency-selective WSSUS Rayleigh fading channel [5,16,17]. For large signal-to-noise ratios, the irreducible error probability is a good (although pessimistic) estimate of the average probability of error. If $P_I$ and $P_{ns}$ are known, we can obtain a good approximation to the average probability of error for both large and small signal-to-noise ratios. Moreover, $P_I$ alone is a useful indication of performance for practical systems since it is a lower bound on $P_e$ for all signal-to-noise ratios and a good estimate of $P_e$ for high signal-to-noise ratios.

In [5] the results of numerical evaluations of $P_I \triangleq P_e\big|_{S \to \infty}$ are given for the rectangular and sine pulses and the four delay power-density spectra discussed above. The parameter d, given by

$$d = \frac{2}{T} \left\{ \int_{-\infty}^{\infty} \xi^2 g(\xi)\, d\xi \right\}^{1/2} , \tag{3.19}$$

is used as a basis for comparing the system performance for the various channel models. This parameter is just twice the rms multipath spread $\mu = M/T$ where M is the rms delay given by (2.9).

In Fig. 3.3, the irreducible error probabilities $P_I$ are shown as a function of the rms multipath spread $\mu$ for the various combinations of basic pulse shapes and delay power-density spectra mentioned above. The values of

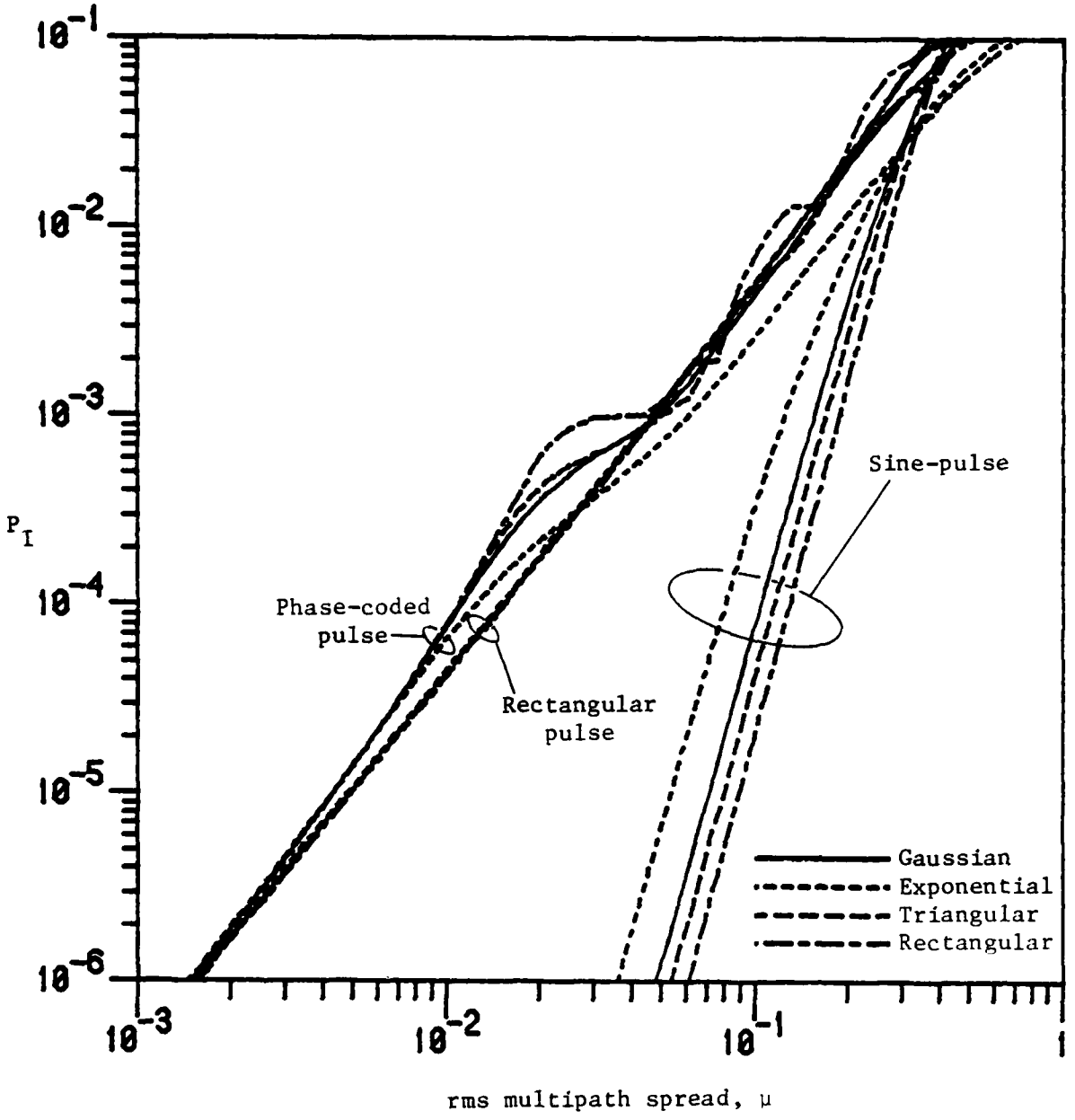


**Figure 3.3. Irreducible error probability vs. rms multipath spread**

$P_I$ for the phase-coded pulse are calculated by standard numerical integration techniques. The signature sequence used for this waveform is an m-sequence of length N = 31 in its characteristic phase (see definition and Fig. 7 in [32]). Unless stated otherwise, comparisons between irreducible error probabilities are always made with respect to a fixed value of rms multipath spread.

Notice that while the irreducible error probabilities for the rectangular and sine pulse are "well-behaved" functions of the rms multipath spread, the limiting error probability for the phase-coded pulse varies in a more erratic way making a relative evaluation of the effects of intersymbol interference difficult. In the next section, we show that such erratic behavior is characteristic of the irreducible error probability for phase-coded pulses when m-sequences (or any binary sequences that produce large time-bandwidth product signals) are used as signature sequences. These results do, however, indicate that rectangular pulse DPSK exhibits small variations in the irreducible error probability with respect to changes in the model for the delay power-density spectrum. In contrast, the irreducible error probabilities for systems employing the sine pulse and the phase-coded pulse vary by more than a factor of 10. In the next section, it is shown that this apparent insensitivity of the rectangular pulse to changes in the shape of the delay-spectrum is due primarily to the choice of delay-spread normalization rather than any inherent properties of the pulse itself. For example, if the normalization is defined in terms of the "1/e points" of the corresponding frequency correlation function $G(\Omega)$, as in [16,17], the irreducible error probabilities for the rectangular pulse vary by a factor of four. In the next section, we examine the implications of the choice of normalization on the evaluation of the irreducible and average error probabilities.

## 3.2 Performance Bounds and Approximations

In order to gain a better understanding of the relationships between data pulse shapes, models for the delay power-density spectrum, the signal-to-noise ratio, and other system design parameters, it is useful to examine the frequency-selective fading mechanism from a "cause-and-effect" point of view. In this section, we investigate the influence of the fading process on the average error probability by separately considering the effects of WSSUS frequency-selective fading in the time domain (or delay domain) and in the Fourier transform or frequency domain. It is true, of course, that these representations each merely describe the same fading mechanism from different points of view. However, the separate consideration of these two effects provides insight to the causes of degradation of system performance inherent in a frequency-selective environment. Moreover, investigating the fading characteristics in this way aids in the identification of the nature of the fundamental trade-offs between the key system parameters. In the remainder of this section, we first consider the characterization of frequency-selective fading in the delay domain and identify the key parameters for determining the effects of intersymbol interference. (In all that follows, we assume that the delay density $g(\xi)$ is symmetric.) We then focus on the frequency-domain characterization and identify the system parameters that provide an indication of performance degradation due to additive noise.

### 3.2.1 Effects of Intersymbol Interference: Characterization

Consider the detection of an information bit corresponding to the data-bit pair $(b_0,b_1)$. If we ignore the contributions of the desired signal as well as the additive noise and only consider the effects of intersymbol

interference resulting from positive (relative) propagation delays, the decision statistic $Z_1 = UV^* + U^*V$ with the random variables U and V given by

$$U = 2 \int_T^{2T} v(t-T) \int_0^T h(t-T,\xi) \sqrt{\frac{2E}{T}}\, b_0 v(t-\xi)\, d\xi dt \qquad (3.20a)$$

and

$$V = 2 \int_0^T v(t) \int_0^T h(t,\xi) \sqrt{\frac{2E}{T}}\, b_{-1} v(t+T-\xi)\, d\xi dt \ . \qquad (3.20b)$$

Using (2.4), (2.5) and (3.20), the moments necessary for the evaluation of the average probability of error are found as

$$m_{UU} = m_{VV} = \frac{16\sigma^2 E}{T}\, \eta_v \qquad (3.21a)$$

and

$$m_{UV} = \frac{16\sigma^2 E}{T}\, b_{-1} b_0\, \eta_v \ . \qquad (3.21b)$$

Under the assumption that the delay power-density spectrum $g(\xi)$ is symmetric, it is easy to see that identical expressions result from the consideration of the effects of intersymbol interference produced by negative values of relative delay (with a change of data-bit indices in (3.21b)). Alternatively, if we consider the matched filter output for both positive and negative relative delays when $\underline{b}_i = (+1,+1,+1,+1)$, the moments in (3.11) are found to be

$$m_{UU} = m_{VV} = m_{UV} = \frac{16\sigma^2 E}{T}\, 2[\bar{\eta}_v + \eta_v + 2\eta_v'] = \frac{16\sigma^2 E}{T} \cdot H_v \qquad (3.22)$$

so that in the absence of additive noise, (3.22) represents the total "power" at the filter output due to the transmitted signal with no data modulation. Thus, $2\eta_v/2(\bar{\eta}_v + \eta_v + 2\eta_v') = 2\eta_v/H_v$ represents the portion of filter output due to interfering signals relative to the <u>total</u> output. Hence, the parameter

$\eta_v/H_v$ provides a characterization of the effects of intersymbol interference on DPSK communications in frequency-selective fading.

From the discussion in Section 3.1 it is apparent that the parameter most indicative of the effects of intersymbol interference is the irreducible error probability $P_I$. Hence we would expect that if the delay-spread is normalized with respect to $2\eta_v/H_v$, the limiting error probability $P_I$ should exhibit minimal sensitivity to the actual shape of the delay power-density spectrum $g(\xi)$. In particular, notice that, under the assumption of adjacent-pulse-limited ISI, the rms multipath spread can be written as

$$\mu = \mu_r = \{ \frac{2}{H_r} \int_0^T g(\xi) R_r^2(\xi)\, d\xi \}^{1/2}$$

$$= \frac{1}{T} \{ 2\, \eta_r \}^{1/2} , \tag{3.23}$$

since $H_r = T^2$ for the rectangular pulse, where $R_r(\xi) = R_v(\xi)$ is given by (3.15). (The subscript "r" denotes the rectangular pulse.) Thus, it is not surprising that the normalized rms multipath spread $\mu_r$ provides an effective normalization of the various delay spectra for the rectangular pulse as suggested by the results in Fig. 3.3.

Similarly, we define the normalized rms multipath spread $\mu_s$ for the sine pulse by

$$\mu_s = \{ \frac{2}{H_s} \int_0^T g(\xi) R_s^2(\xi)\, d\xi \}^{1/2}$$

$$= \{ \frac{2}{H_s} \cdot \eta_s \}^{1/2} , \tag{3.24}$$

with $R_s(\xi) = R_v(\xi)$ given by (3.16b). In Table 3.1, numerical values of $H_s/T^2$ are listed for the four examples of delay power-density spectra discussed in

Table 3.1. $H_s/T^2$ for sine pulse DPSK with respect to the rms delay M

| M/T | Gauss | Exp | Tri | Rect |
|---|---|---|---|---|
| 0.005 | 1.0 | 1.0 | 1.0 | 1.0 |
| 0.01 | 0.999 | 0.999 | 0.999 | 0.999 |
| 0.05 | 0.9784 | 0.9796 | 0.9781 | 0.9778 |
| 0.1 | 0.9275 | 0.9356 | 0.9253 | 0.9223 |
| 0.5 | 0.6394 | 0.6813 | 0.6812 | 0.6304 |

Chapter 2 and various values of rms delay M. It is easy to see that $H_s/T^2 \geq 0.6$ for all values of rms delay, and that $H_s$ is not very sensitive to the shape of the delay spectra. Moreover, $H_s \cong T^2$ for all practical values of rms delay so that $\eta_s$ alone provides a good indication of the effects of intersymbol interference for the sine-pulse.

Finally, the normalized rms multipath spread $\mu_p$ for the phase-coded pulse is given by

$$\mu_p = \{ \frac{2}{H_p} \int_0^T g(\xi) R_p^2(\xi) \, d\xi \}^{1/2}$$

$$= \{ \frac{2}{H_p} \cdot \eta_p \}^{1/2} \tag{3.25}$$

with $R_p(\xi) = R_v(\xi)$ given by (3.17b). The values of $H_p/T^2$ for the m-sequence of length N = 31 are listed in Table 3.2 as a function of the rms delay M.

In contrast to the results for the rectangular and sine pulse, the parameter $H_p$ is very sensitive to the shape of the delay spectrum and can be much smaller than $T^2$ for relatively small values of rms delay. This is true for two reasons. The parameter $\bar{\eta}_p$ can be substantially smaller than the corresponding parameters for either the rectangular or sine pulse; this fact has profound implications on the performance of phase-coded pulse waveforms in the presence of additive noise. Using the properties of the discrete <u>periodic</u> autocorrelation function for m-sequences [30], it is easy to show that $\eta_p'$ given by (3.12c) is never positive. In fact, depending on the shape of the delay density, the negative contribution of $2\eta_p'$ can be nearly as large as the sum of $\bar{\eta}_p$ and $\eta_p$. This is in sharp contrast to the analogous situation for the rectangular and sine pulse where $\eta_v'$ is non-negative and generally much smaller than $\bar{\eta}_v$.

Table 3.2. $H_p/T^2$ for phase-coded pulse DPSK (N = 31) with respect to the rms delay M

| M/T | Gauss | Exp | Tri | Rect |
|---|---|---|---|---|
| 0.001 | 0.9446 | 0.9741 | 0.9488 | 0.9456 |
| 0.005 | 0.7703 | 0.7994 | 0.7643 | 0.7485 |
| 0.01 | 0.5917 | 0.6487 | 0.5798 | 0.5481 |
| 0.05 | 0.1636 | 0.2400 | 0.1598 | 0.1209 |
| 0.1 | 0.0835 | 0.1330 | 0.0831 | 0.0610 |
| 0.5 | 0.0199 | 0.0315 | 0.0547 | 0.0130 |

The negative contributions of $\eta_p'$ in the absence of data modulation can be viewed as intrasymbol interference which is characteristic of phase-coded pulses when m-sequences are used as signature sequences. While this characteristic is not exclusive to m-sequences, it is not generally true for other classes of binary sequences. Because of this intrasymbol interference, phase-coded pulses employing m-sequences are a particularly poor choice of pulse waveform.

In Figs. 3.4 and 3.5, the results of numerical evaluations of $P_I$ for the sine pulse (as a function of $\mu_s$) and the phase-coded pulse for N = 31 (as a function of $\mu_p$) are shown for the four models for the delay power-density spectra. For comparison, the irreducible error probabilities obtained by approximating the parameter $H_v$ as $T^2$ are also shown. By examining the results in Figs. 3.4 and 3.5 for the cases when the true value of $H_v$ is included in the computation, and when $H_v$ is approximated as $T^2$ (in which case $\mu_v = (2\eta_v)^{1/2}/T$), it is clear that this parameter is a significant factor only for phase-coded pulses. In fact, the error introduced by the approximation for the evaluation of the irreducible error probability for the sine-pulse is quite small. However, assuming $H_p \tilde{=} T^2$ for the evaluation of the irreducible error probability for a phase-coded pulse with N = 31 can produce a result in error by more than two orders of magnitude!

Notice that some of the irreducible error probabilities in Figs. 3.4 and 3.5 are shown for different ranges of normalized rms multipath spread for the cases where $H_v$ is approximated as $T^2$. This was necessary to ensure that the assumption of adjacent-pulse-limited ISI holds but is also indicative of the relative values of $\eta_v$ for different data-pulse shapes. That is, for a fixed channel model and fixed rms delay M, there is substantial variation between

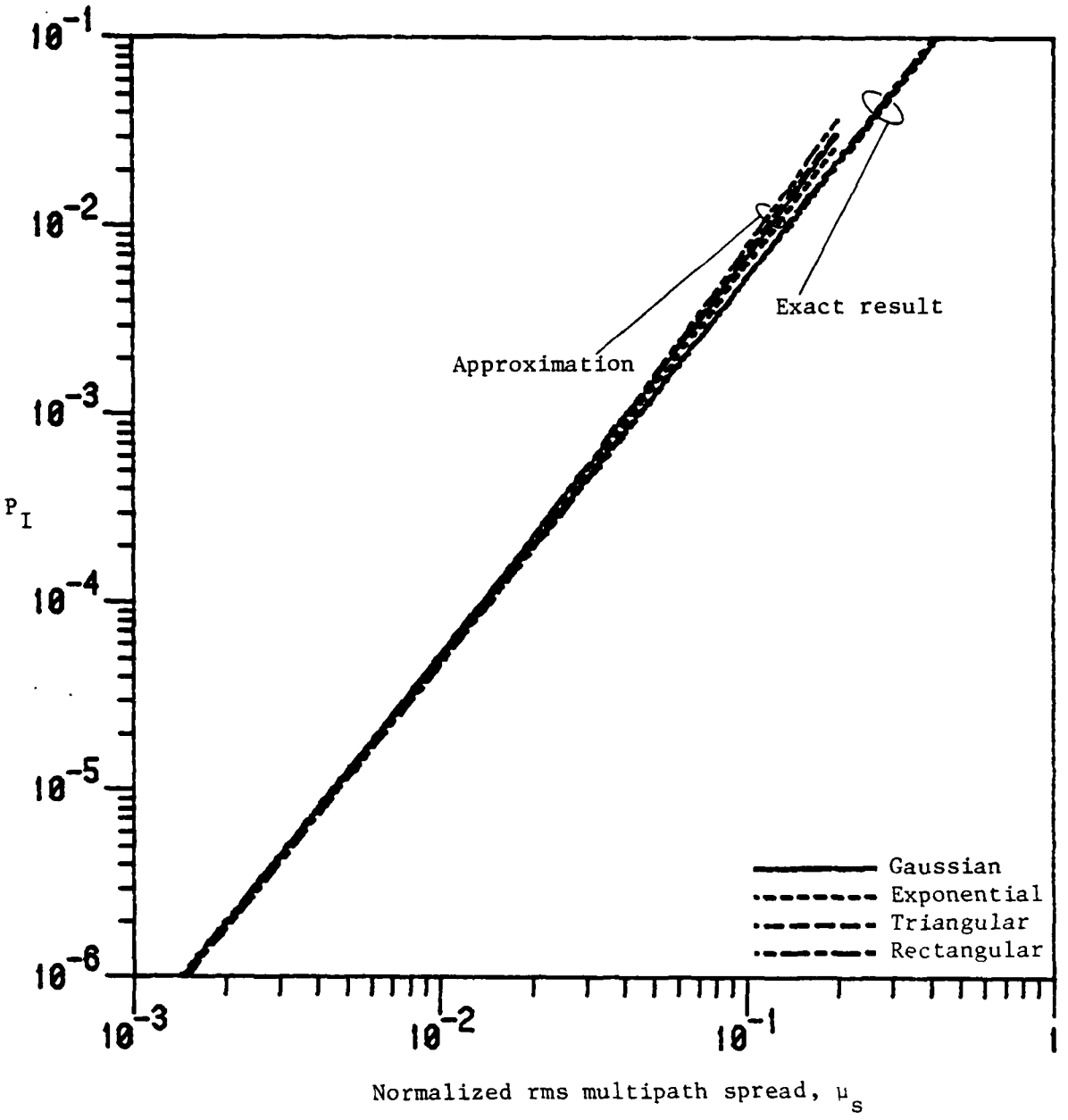


**Figure 3.4. Irreducible error probabilities for sine pulse DPSK vs. $\mu_s$**

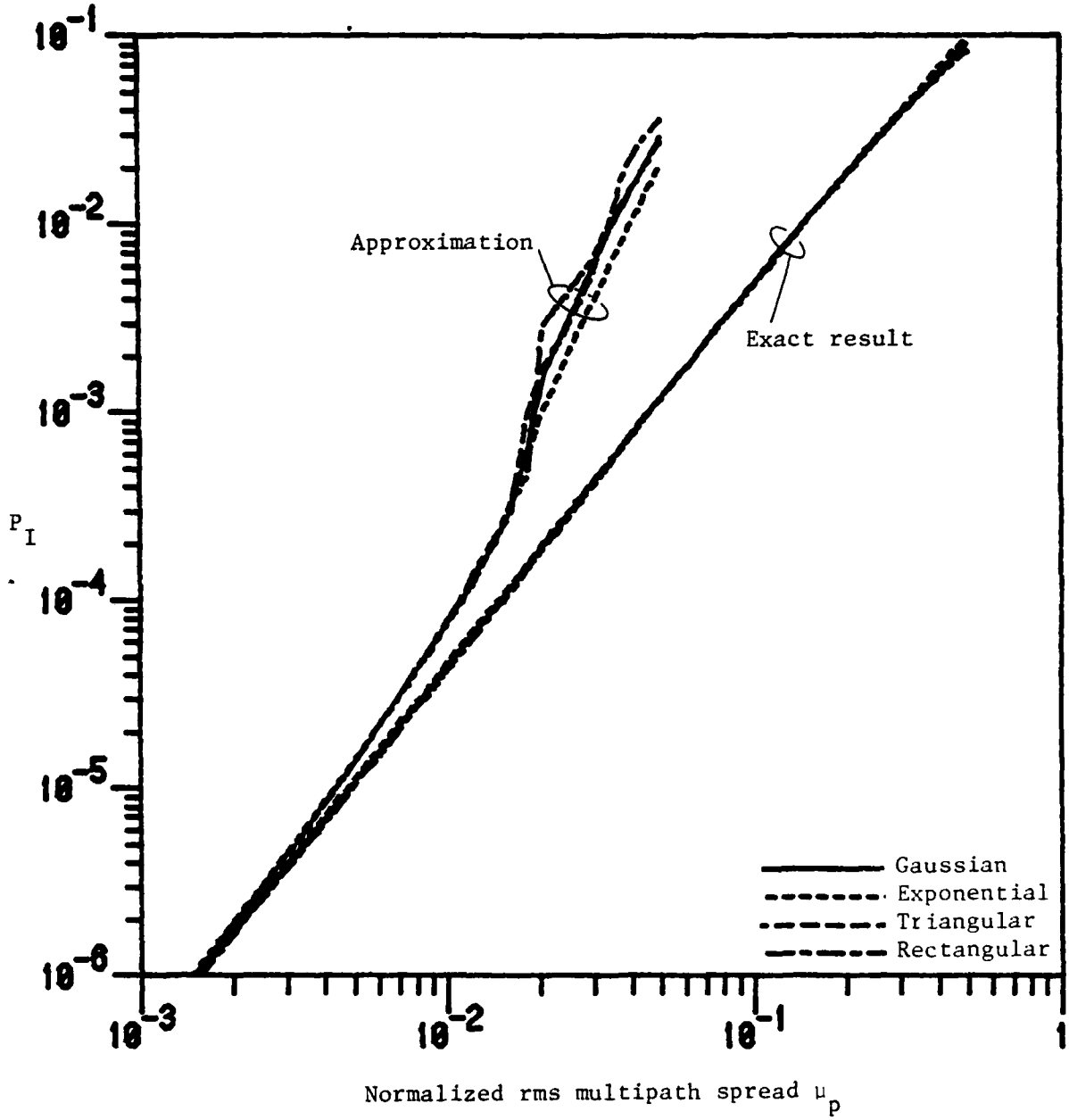


**Figure 3.5. Irreducible error probabilities for phase-coded pulse DPSK vs. $\mu_p$ for N = 31**

the values of $\eta_v$ for different pulse shapes. The roles of $H_v$ and $\eta_v$ in determining the normalized rms multipath spread is made apparent by examining the relationship between these parameters for different pulse shapes with a fixed channel model. The values of $(2\eta_v)^{1/2}/T$ for the Gaussian delay spectrum are given in Table 3.3 for the rectangular, sine, and phase-coded pulse shapes using characteristic m-sequences of lengths N = 7, 15, 31, and 63 given in [32, Fig. 7]. The values of the normalized rms multipath spread $\mu_v$ are listed in parentheses in Table 3.3. Notice that for large rms delays, the parameter $\eta_p$ for the phase-coded pulse can be much smaller than the corresponding parameter for the rectangular pulse. However, the values of normalized rms multipath spread for the phase-coded pulse can be significantly <u>larger</u> than the corresponding values for either the rectangular or sine pulse. Also, notice that both $\eta_p$ and $\mu_p$ seem to be independent of the sequence length N for any fixed value of rms delay. This is a bit surprising since it might be expected that the effects of intersymbol interference for phase-coded pulses employing m-sequences could be substantially reduced, for any rms delay, by simply using an m-sequence of greater length. Unfortunately, the results in Table 3.3 indicate that unless the sequences are carefully selected, increasing the sequence length can <u>increase</u> the sensitivity to delay spread, and that the phase-coded pulse is at least as vulnerable to the effects of intersymbol interference as the rectangular pulse.

The above results for the phase-coded pulse are a consequence of both the channel model we employ, (i.e., that of a continuous delay power-density spectrum), and the interaction between the data pulse correlation function $R_v(\xi)$ and the delay spectrum $g(\xi)$. In particular, for very small values of rms delay, the power spectrum of the delay is concentrated close to the origin

Table 3.3. $(2\eta_v)^{1/2}/T$ and (normalized rms multipath spread $\mu_v$) as a function of the rms delay M for the rectangular and sine pulses and for the phase-coded pulse with sequence lengths N = 7,15,31,63

| M/T | rect | sine | N = 7 | N = 15 | N = 31 | N = 63 |
|---|---|---|---|---|---|---|
| 0.01 | | | | | | |
| | (0.01) | (0.00001) | (0.01067) | (0.01139) | (0.01297) | (0.01639) |
| 0.05 | 0.05 | 0.0016 | 0.0496 | 0.0499 | 0.0191 | 0.0423 |
| | (0.05) | (0.00158) | (0.06874) | (0.08980) | (0.04728) | (0.14683) |
| 0.1 | 0.1 | 0.0119 | 0.0782 | 0.0929 | 0.0278 | 0.0495 |
| | (0.1) | (0.01235) | (0.13992) | (0.22867) | (0.09631) | (0.24218) |

so that the parameter $\mu_p$ depends most heavily on the portion of $R_p(\xi)$ that corresponds to very small values of $\xi$. From (3.17b) we see that, for values of $\xi$ in the range $[0,T_c]$, $|R_p(\xi)| = |R_r(\xi)| = \xi$. Unless the signature sequences are carefully chosen, this relationship can hold for several consecutive chip intervals. Thus, it is clear that for small values of rms delay, the normalized rms multipath spreads, and hence the irreducible error probabilities are nearly the same for the rectangular and phase-coded pulse shapes.

Finally, the results in Figs. 3.3-3.5 indicate that the irreducible error probability strongly depends on the normalized rms multipath spread $\mu_v$. From these results and the results in Table 3.3, one might erroneously conclude that the performance of the phase-coded pulse is approximated by the performance of the rectangular pulse. In what follows, we demonstrate that pulse shapes that produce similar <u>irreducible</u> error probabilities, do not necessarily exhibit similar performance for practical signal-to-noise ratios. These results do however show that the irreducible error probability, as a function of the normalized rms multipath spread, is insensitive to variations in the <u>shape</u> of the delay power-density spectrum. In fact, the maximum variation of $P_I$ for the pulse shapes evaluated in Figs. 3.3-3.5 is less than a factor of 1.2 for fixed normalized rms multipath spread. This latter observation indicates that the <u>limiting</u> error probability for a particular frequency-selective Rayleigh fading channel can be minimized by simply choosing a data pulse waveform which minimizes the normalized rms multipath spread (defined as in (3.23)-(3.25)) for the delay power-density spectrum of the fading channel.

### 3.2.2 Effects of Intersymbol Interference: Bounds

The relative insensitivity of the irreducible error probability to the shape of the delay spectrum for a fixed normalized rms multipath spread suggests the possibility of obtaining meaningful bounds on the probability of error. In this section we describe a method of obtaining bounds on $P_I$ for frequency-selective Rayleigh fading channels.

#### 3.2.2.1 Rectangular pulse

Under the assumption of adjacent-pulse-limited ISI, the functions defined by (3.12) can be written (for the rectangular pulse) as

$$\bar{\eta}_r = T^2/2 - 2Tf(g) + \mu_r^2/2 \ , \tag{3.26a}$$

$$\eta_r = \mu_r^2/2, \tag{3.26b}$$

and

$$\eta_r' = Tf(g) - \mu_r^2/2 \tag{3.26c}$$

with the normalized rms multipath spread $\mu_r$ given by (3.23) and where the functional f(g) is given by

$$f(g) = \int_0^T \xi \, g(\xi) \, d\xi \ . \tag{3.27}$$

Hence, for fixed $\mu_r$, the irreducible error probability is completely specified up to the determination of f(g). Equations (3.13) and (3.26) imply that the irreducible error probability is a continuous function of f(g) so that it is possible to characterize $P_I$ over the range of values taken on by the functional f(g). Thus, upper and lower bounds on $P_I$ can be obtained if the minimum and maximum values of f(g) can be found for a fixed normalized rms

multipath spread. The characterization of the variation of f(g) is accomplished through an application of a result due to Dubins [33].

Let M be the set of all non-negative measures m on the Borel sets of [0,T] such that m([0,T]) = 1/2. It can be shown [33] that the extreme points of M (denoted by ex M) are the point masses on [0,T] and that M is compact on the weak* topology [34]. If m $\in$ M, the hyperplane H defined by

$$\int_0^T x(t)\, m(dt) = c$$

for constant c is closed and bounded for x $\in$ C[0,T] [35]. Dubins' Theorem guarantees that every extreme point of M' $\triangleq$ {M$\cap$H} is a convex combination of at most two extreme points of M.

In terms of the present application, upper and lower bounds on $P_I$ can be obtained for each value of normalized rms multipath spread by finding the minimum and maximum values of

$$f(m) = \int_0^T \xi\, m(d\xi) \ , \tag{3.28}$$

for m $\in$ M subject to the constraint

$$T^{-2} \cdot \int_0^T \xi^2\, m(d\xi) = \mu_r^2/2, \tag{3.29}$$

where $m(d\xi) = g(\xi)d\xi$. Since the functional f in (3.27) is a continuous linear functional on m, it obtains its minimum value on an extreme point of M' = M$\cap$H. Hence, by Dubins' Theorem, the minimum of f is found by searching over all convex combinations of two point masses (impulse functions) in M' for the smallest value of f(m); i.e.,

$$f_{min} = \min\{\, f(m) : m \in \text{ex } M' \,\} \ .$$

This search in $[0,T]^2$ is easily implemented. In fact, for the rectangular pulse it can be shown that the pair $\{f_{min}, f_{max}\}$ is given by $\{\mu_r^2/2, \mu_r/2\}$ for $\mu_r < 1/2$. The resulting bounds for the irreducible error probability are then found by searching over the interval $[f_{min}, f_{max}]$ for the minimum and maximum values of $P_I$. It is necessary to carry out this final search since $P_I$ is not necessarily a monotonic function of f(g). In Fig. 3.6, the minimum and maximum irreducible error probabilities for the rectangular pulse are shown as a function of $\mu_r$. Notice that for a fixed value of $\mu_r$, the total variation from the minimum to the maximum value of $P_I$ is very small; the two bounds differ by a factor of less than 1.5.

3.2.2.2 Sine pulse

Using the fact that $H_s \cong T^2$, and assuming adjacent-pulse-limited ISI, we can write the functions in (3.12) for the sine pulse as

$$\bar{\eta}_s = T^2 f'(g) - 2Tf''(g) + \mu_s^2/2 , \tag{3.30a}$$

$$\eta_s = \mu_s^2/2, \tag{3.30b}$$

and

$$\eta_s' = Tf''(g) - \mu_s^2/2 \tag{3.30c}$$

with the normalized rms multipath spread $\mu_s$ given by (3.24) and where the functionals f'(g) and f''(g) are given by

$$f'(g) = \int_0^T \cos^2(\pi\xi/T)\, g(\xi)\, d\xi \tag{3.31a}$$

and

$$f''(g) = \int_0^T [-\xi\cos^2(\pi\xi/T) + T/\pi \sin(\pi\xi/T)\cos(\pi\xi/T)]\, g(\xi)\, d\xi . \tag{3.31b}$$

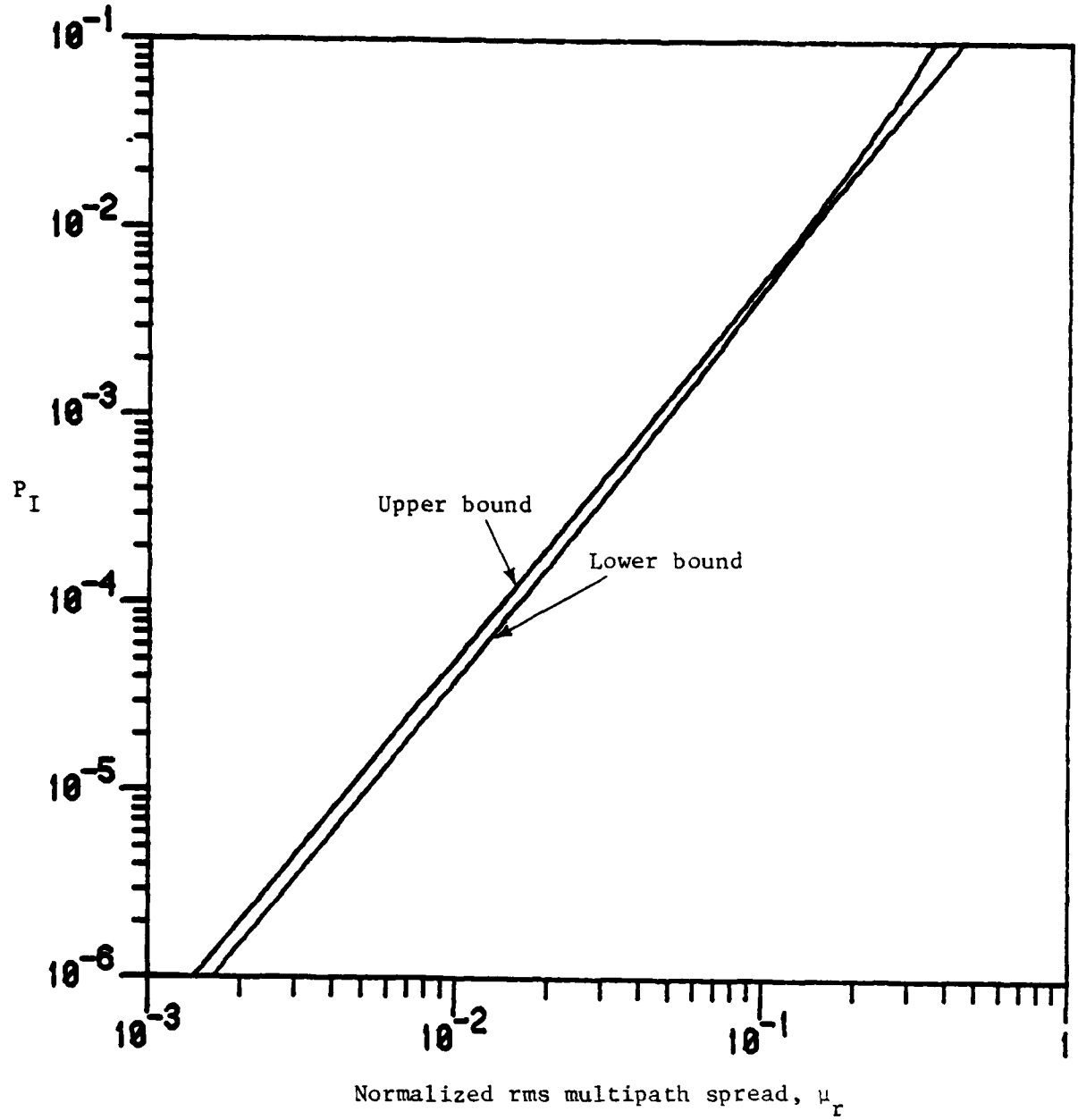


**Figure 3.6. Irreducible error probability bounds for rectangular pulse DPSK**

Thus, we may proceed as in the previous section where the constraint H is now given by

$$T^{-2}\cdot\int_0^T [-\xi\cos(\pi\xi/T) + T/\pi \sin(\pi\xi/T)]^2 \, g(\xi) \, d\xi = \mu_s^2/2, \qquad (3.32)$$

except that in this case the set $\{f'(m), f''(m);\ m \in \text{ex } M'\}$ is a region in $R^2$. Hence, the minimum and maximum <u>obtainable</u> error probabilities are found by searching over the convex region

$$Q = \text{co } \{(f'(m), f''(m)) : m \in \text{ex } M'\} \in R^2 ,$$

where co {S} denotes the convex hull of S. However, in order to avoid the task of completely characterizing Q, we perform the two-dimensional search for the minimum and maximum $P_I$ over the rectangular region

$$\bar{Q} = \{[f'_{min}, f'_{max}] \times [f''_{min}, f''_{max}]\} ,$$

which contains Q. The resulting bounds for the irreducible error probability for the sine-pulse are shown in Table 3.4 as a function of the normalized rms multipath spread $\mu_s$. Notice that even though we have "weakened" the bounds on $P_I$ by performing the search over $\bar{Q}$ rather than Q and assuming that $H_s = T^2$, the total variation between upper and lower bounds is still no larger than a factor of 4 (for fixed $\mu_s$).

### 3.2.2.3 <u>Phase-coded pulse</u>

Finally, we address the problem of obtaining bounds on $P_I$ for the phase-coded pulse, which is the most complicated of the three pulse shapes considered. Under the assumption of adjacent-pulse-limited ISI, the function $\eta_p$ can be written as

Table 3.4. Irreducible error probability bounds for sine pulse DPSK with respect to the normalized rms multipath spread $\mu_s$

| $\mu_s$ | Lower Bound | Upper Bound |
|---|---|---|
| 0.0005 | $0.8361 \cdot 10^{-7}$ | $1.2273 \cdot 10^{-7}$ |
| 0.001 | $3.7526 \cdot 10^{-7}$ | $5.2812 \cdot 10^{-7}$ |
| 0.005 | $1.0311 \cdot 10^{-5}$ | $1.4204 \cdot 10^{-5}$ |
| 0.01 | $4.1277 \cdot 10^{-5}$ | $6.1089 \cdot 10^{-5}$ |
| 0.05 | $1.0262 \cdot 10^{-3}$ | $2.4748 \cdot 10^{-3}$ |
| 0.1 | $0.4104 \cdot 10^{-2}$ | $1.6259 \cdot 10^{-2}$ |

$$\eta_p = \mu_p^2 H_p/2 \ . \tag{3.33}$$

Unfortunately, there is no obvious way to characterize the functions $\bar{\eta}_p$ and $\eta_p'$ in terms of the normalized rms multipath spread $\mu_p$ and a few linear functionals of g. Moreover, since $H_p$ strongly depends on the <u>shape</u> of the delay power-density spectrum and can, in fact, equal zero for certain examples of multipath delay spectra, there is not a clear relationship between $\mu_p$ and $\eta_p$ (as evidenced by the data in Table 3.3). Thus, a given value of normalized rms multipath spread does not necessarily correspond to a linear constraint on the set of delay power-density spectra. Alternatively, if we assume that $H_p \cong T^2$ and proceed as before, the resulting upper bound for the irreducible error probability is approximately 1/2.

However, if we make two additional assumptions concerning the characterization of the channel, both upper and lower bounds on the performance of phase-coded pulse DPSK can be obtained. We assume that a fraction of at least 1/2N of the total power of the delay spectrum lies in the range $[-T_c, T_c]$ where N is the length of the signature sequence. Second, we assume that the frequency-selective channel is represented by a specular multipath channel with paths corresponding to delays in the set $\{0, \pm T_c, \pm 2T_c, \cdots, \pm(N-1)T_c\}$ so that the delay power-density spectrum $g(\xi)$ is represented by a discrete density spectrum $g(kT_c)$. This model may, in a sense, be more appropriate for phase-coded pulse since systems employing phase-coded waveforms can resolve the multipath components of the delay spectrum for many channels of interest. We proceed by finding the minimum and maximum values of $\bar{\eta}_p$ and $\eta_p'$ under the constraint,

$$\frac{N^{-2}}{H_p} \sum_{k=0}^{N} C_a^2(N-k) \cdot g(kT_c) = \mu_p^2/2, \tag{3.34}$$

and performing the search for the minimum and maximum $P_I$ over the region

$$\bar{Q} = \{[\bar{\eta}_{p,min}, \bar{\eta}_{p,max}] \times [\eta'_{p,min}, \eta'_{p,max}] \times [\eta_{p,min}, \eta_{p,max}]\} ,$$

where $\bar{\eta}_{p,min} = 2\sigma^2 T^2/N$. The resulting bounds for the irreducible error probability for the phase-coded pulse are given in Tables 3.5 and 3.6, respectively, for m-sequences of length N = 7 and N = 31 discussed above.

Notice that there is almost no variation between upper and lower bounds, and that the bounds for the phase-coded pulses are very similar to those obtained for the rectangular and sine pulses. The small variation between the bounds in Tables 3.5 and 3.6 is partially a result of the first assumption; there is a path with non-zero energy corresponding to zero delay. However, the "closeness" of these bounds is primarily due to the fact that modeling the delay density as a discrete spectrum allows the effects of the parameter $H_p$ to be incorporated in the bounding procedure. (Recall that this parameter is a significant factor in determining the value of the normalized rms multipath spread.) In fact, it is easy to demonstrate that if we assume $H_p \cong T^2$, the resulting upper and lower bounds differ by a factor of N (the sequence length) for normalized rms multipath spreads of about 0.01.

Since the bounds in Tables 3.5 and 3.6 are obtained under assumptions that are more restrictive than those used to obtain the bounds for the other pulse shapes, it might be argued that the results for phase-coded pulses are of little consequence. However, it seems reasonable to assume that some portion of the received signal energy corresponds to zero (or near-zero) propagation delays, and that this portion is at least as large as the average of the energy received in any interval of width $T_c$. Since the upper bound on $P_I$ for phase-coded pulses can approach 1/2 if there is no signal component in

Table 3.5. Irreducible error probability bounds for N = 7 phase-coded pulse with respect to the normalized rms multipath spread $\mu_p$

| $\mu_p$ | Lower Bound | Upper Bound |
|---|---|---|
| 0.0005 | $1.1176 \cdot 10^{-7}$ | $1.3039 \cdot 10^{-7}$ |
| 0.001 | $4.9919 \cdot 10^{-7}$ | $5.1781 \cdot 10^{-7}$ |
| 0.005 | $1.2543 \cdot 10^{-5}$ | $1.2565 \cdot 10^{-5}$ |
| 0.01 | $4.9754 \cdot 10^{-5}$ | $5.0252 \cdot 10^{-5}$ |
| 0.05 | $1.1186 \cdot 10^{-3}$ | $1.4069 \cdot 10^{-3}$ |
| 0.1 | $3.3669 \cdot 10^{-3}$ | $7.3647 \cdot 10^{-3}$ |
| 0.5 | $3.7202 \cdot 10^{-2}$ | $2.5337 \cdot 10^{-1}$ |

Table 3.6. Irreducible error probability bounds for N = 31 phase-coded pulse with respect to the normalized rms multipath spread $\mu_p$

| $\mu_p$ | Lower Bound | Upper Bound |
|---|---|---|
| 0.0005 | $1.1176 \cdot 10^{-7}$ | $1.3039 \cdot 10^{-7}$ |
| 0.001 | $4.9919 \cdot 10^{-7}$ | $5.1781 \cdot 10^{-7}$ |
| 0.005 | $1.2267 \cdot 10^{-5}$ | $1.2850 \cdot 10^{-5}$ |
| 0.01 | $4.5614 \cdot 10^{-5}$ | $5.4812 \cdot 10^{-5}$ |
| 0.05 | $0.3679 \cdot 10^{-3}$ | $4.2587 \cdot 10^{-3}$ |
| 0.1 | $0.4683 \cdot 10^{-3}$ | $4.8358 \cdot 10^{-2}$ |
| 0.5 | $5.8824 \cdot 10^{-3}$ | $4.3373 \cdot 10^{-1}$ |

the range $[-T_c, T_c]$, this assumption can be viewed as a necessary condition for the operation of phase-coded pulse DPSK.

### 3.2.3 Effects of Additive Noise: Characterization

Consider the response of in-phase and quadrature correlation receivers matched to v(t) (and assumed synchronized in time) to a single transmitted data pulse signal

$$s(t) = \sqrt{\frac{2E}{T}}\, b_0 v(t) \; ; \; 0 \leq t < T \, ,$$

where E is the energy per data bit. In the absence of additive noise, the sum of the squares of the filter outputs is

$$s_{out} = \frac{16\sigma^2 E}{T} \int_{-\infty}^{\infty} g(\xi)\, \bar{R}_v^2(|\xi|)\, d\xi \qquad (3.35a)$$

$$= \frac{16\sigma^2 E}{T} \int_{-\infty}^{\infty} G(\Omega)\, \beta_v(\Omega)\, d\Omega \, , \qquad (3.35b)$$

by Rayleigh's theorem, where $\beta_v(\Omega)$ is the inverse Fourier transform of $\bar{R}_v^2(|\xi|)$. The corresponding output due to the additive white Gaussian noise with (two-sided) spectral intensity $N_0/2$ is $8N_0T$.

For a nonselective Rayleigh fading channel, $g(\xi) = \delta(\xi)$ so that the frequency correlation function $G(\Omega)$ is equal to unity across the band of interest. In this case, the signal-to-noise ratio (snr) at the output of the matched filter becomes

$$snr = \frac{2\sigma^2 E}{N_0} \, , \qquad (3.36)$$

since, by definition, $\bar{R}_v^2(0) = T^2$. Notice from (3.35) that the function $\beta_v(\Omega)$ can be viewed as a power-spectrum of the single-pulse, or "one-shot" matched filter output prior to sampling, in non-selective fading so that (3.35b) and

the resulting signal-to-noise ratio is maximized when the frequency correlation function $G(\Omega)$ is flat across the band.

In contrast, one of the essential characteristics of frequency-selective fading is the fact that the frequency correlation function $G(\Omega)$ is not flat but resembles the transfer function of a band-limited data channel. We point out that this is only a resemblance and not an equivalence. Rather, in the absence of additive noise, the function $G(\Omega)$ is a measure of the degree of statistical correlation between two received spectral components separated by $\Omega$ Hz. Thus, in the case of frequency-selective fading (3.35b) indicates, in a statistical sense, what fraction of the received power (due to a single pulse) is available at the output of the matched filter. This observation is made apparent in the resulting expression for the single-pulse signal-to-noise ratio for frequency-selective fading, given by

$$\text{snr} = \frac{2\sigma^2 E}{N_0 T^2} \int_{-\infty}^{\infty} G(\Omega)\ \beta_v(\Omega)\ d\Omega = \frac{2\sigma^2 E}{N_0 T^2} \int_{-\infty}^{\infty} g(\xi)\ \bar{R}_v^2(|\xi|)\ d\xi$$

$$= \frac{2\sigma^2 E}{N_0}\ 2\bar{\eta}_v/T^2 \quad , \tag{3.37}$$

which implies that $\bar{\eta}_v$ is the key parameter in determining the signal-to-noise ratio for single-pulse matched filter detection. Notice that if we neglect the effects of intersymbol interference on the error probability in frequency-selective fading so that both $\eta_v$ and $\eta_v'$ (cf. (3.12)) are taken to be zero, the average error probability (3.7) becomes

$$P_e = \left[\ 2 + \frac{4\sigma^2 E}{N_0} \cdot \frac{2\bar{\eta}_v}{T^2}\ \right]^{-1} . \tag{3.38}$$

The results in Section 3.1 demonstrate that for small signal-to-noise ratios, the average error probability for frequency-selective Rayleigh fading is well approximated by $P_{ns} = (2 + 4\sigma^2 E/N_0)^{-1}$, which is the probability of error for non-selective fading. While this approximation is valid independent of data-pulse shape, the above discussion implies that (3.38) is a much better approximation of the error probability for small signal-to-noise ratios than $P_{ns}$. In fact, for a given pulse shape, the asymptotic error probability for small signal-to-noise ratios is given by (3.38). Moreover, for all examples of data-pulse shape and delay density considered here, (3.38) may be taken as a lower bound for the average probability of error for all values of snr. Hence, the parameter $\bar{\eta}_v$ in some sense determines the position of the "inverse-linear" lower bound on the error probability as a function of signal-to-noise ratio $S = 2\sigma^2 E/N_0$.

The differences between the signal-to-noise ratios in (3.36) and (3.38) are probably not a major concern for signals with relatively small time-bandwidth products, viz. the rectangular and sine pulses. However, for large time-bandwidth product pulses, such as the phase-coded pulse with moderately large N, this factor becomes significant and plays a central role in the choice of pulse shape. For a channel with Gaussian delay power-density spectrum, the values of the parameter $\bar{\eta}_v/T^2$ are given in Table 3.7 for the rectangular and sine pulse shapes, and for the phase-coded pulse shapes using the m-sequences of length N = 7, 15, 31, and 63 discussed above. The results in Table 3.7 show that for small to moderate values of M/T, a large percentage of the received signal power is utilized by the matched filter detector for both the rectangular and sine pulses for this channel. If M/T = 0.1, for example, the matched filter output for the rectangular and the sine pulse

Table 3.7. Values of $\bar{\eta}_v/T^2$ in terms of the rms delay M for the rectangular and sine pulses and for the phase-coded pulse with sequence lengths N = 7,15,31,63

| M/T | rect | sine | N = 7 | N = 15 | N = 31 | N = 63 |
|---|---|---|---|---|---|---|
| 0.05 | 0.4614 | 0.4886 | 0.2419 | 0.1634 | 0.0844 | 0.0424 |
| 0.1 | 0.4252 | 0.4594 | 0.1453 | 0.0878 | 0.0436 | 0.0217 |
| 0.5 | 0.2246 | 0.2124 | 0.0437 | 0.0208 | 0.0106 | 0.0049 |

represents about 85% and 91% of the total received signal power, respectively. In comparison, only about 9% and 5% of the received signal power is utilized for matched filter detection of the phase-coded pulse for N = 31 and N = 63.

In contrast to the analogous results for the normalized rms multipath spread, the parameters $\bar{\eta}_p$ for phase-coded pulses uniformly exhibit a strong dependence on the sequence length. It can be shown that, for a large class of channel models and typical sequence lengths N, the parameter $\bar{\eta}_p$ is closely approximated by k/N where k depends on the channel. For the above example, this constant is approximately 2.62, 1.35, and 0.33 for M/T equal to 0.05, 0.1, and 0.5, respectively. The low signal-to-noise ratio asymptotic error probability (3.38) becomes

$$P_e \approx \left[ 2 + \frac{4\sigma^2 E}{N_0} \cdot \frac{2k}{N} \right]^{-1} \tag{3.39}$$

for the phase-coded pulse with sequence length N.

In the previous section, it was demonstrated that the phase-coded pulse waveform is at least as susceptible to the effects of intersymbol interference as the rectangular pulse. Thus, phase-coded pulses provide little potential for improvement in the limiting error probability. Moreover, when coupled with the data in Table 3.7, these results indicate that the average error probabilities for the phase-coded pulse are relatively large for all practical values of $S = 2\sigma^2 E/N_0$. For example, from Table 3.7 for M/T = 0.05 and N = 63, we see that for fixed error probability, the additional signal-to-noise ratio required for the phase-coded pulse relative to the rectangular pulse is about 0.4614/0.0424 or 10.37 dB.

The relationships between irreducible error probabilities, available signal power, and system error performance can be seen by examining Fig. 3.7.

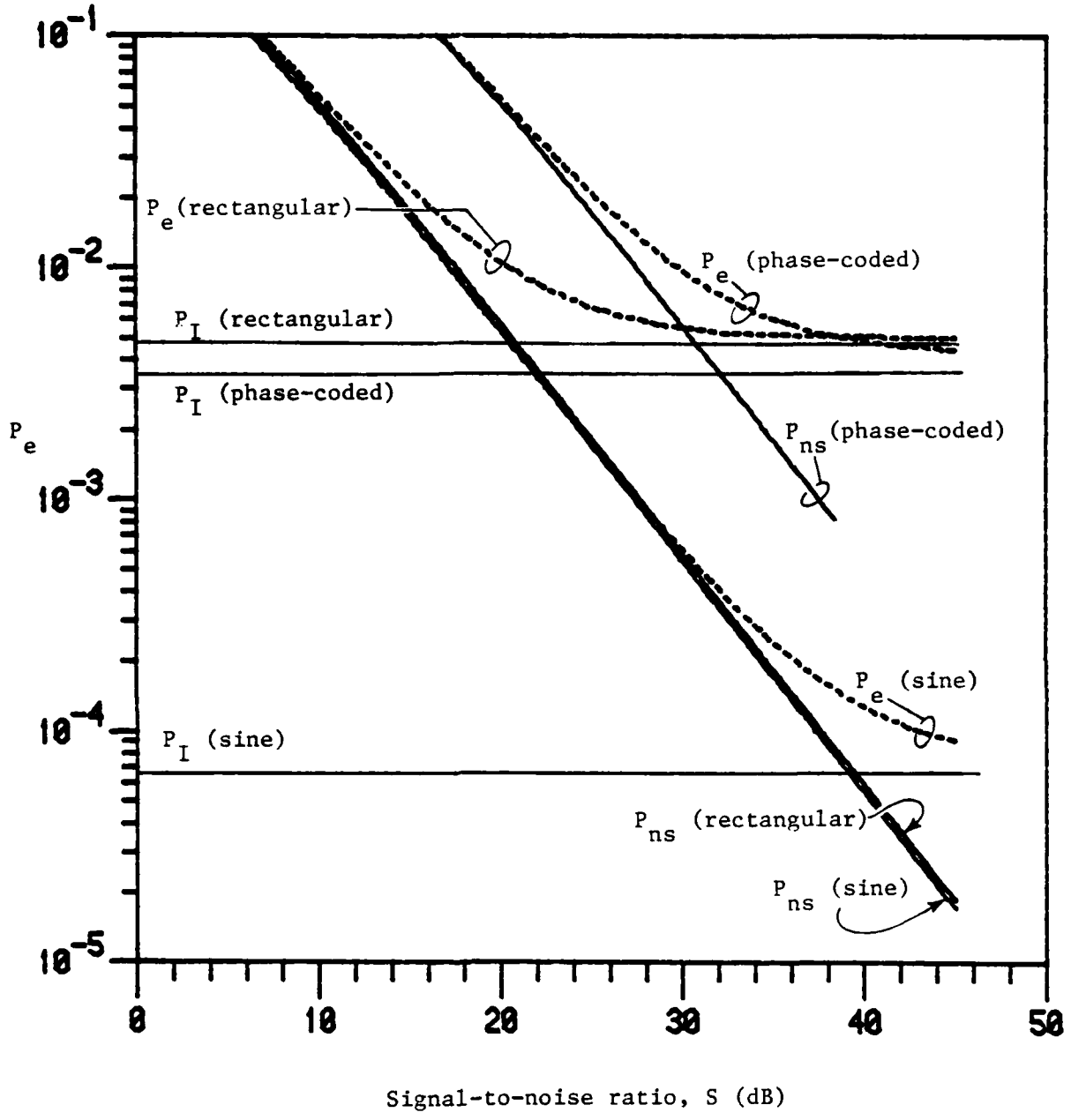


**Figure 3.7. Average error probability for rectangular, sine and phase-coded pulse using an m-sequence of length N = 31 for a Gaussian delay spectrum with $\mu = 0.1$**

The average probability of error is given as a function of $S = 2\sigma^2 E/N_0$ for the rectangular, sine, and phase-coded pulse (N = 31) for the Gaussian delay power-density spectrum with rms delay M = T/10. The low signal-to-noise ratio asymptote given by (3.38) and the irreducible error probabilities (which appear as horizontal asymptotes) are shown for each pulse. Notice that while the limiting error probability for the phase-coded pulse with N = 31 is roughly equivalent to that of the rectangular pulse, the actual error probability for the phase-coded pulse is higher than for the rectangular pulse for values of signal-to-noise ratio less than 35 dB. Also, notice that the sine pulse exhibits the best performance of the four pulse shapes considered for the entire range of signal-to-noise ratios. These results are in agreement with the data presented in Tables 3.3 and 3.7 which show that the normalized rms multipath spread $\mu_s$ for the sine pulse is significantly smaller than the corresponding parameter for the rectangular pulse. Moreover, the parameter $\bar{\eta}_v$, which is related to the utilizable signal power, is largest for the sine pulse while the corresponding parameter for the phase-coded pulse indicates severe performance degradation in the presence of additive noise.

Finally, we point out that the performance of phase-coded pulse DPSK in Rayleigh fading is related to previous results concerning the performance of coherent spread-spectrum communications. In particular, the results in [26] and [31] demonstrate that the effects of interference caused by multiple propagation paths for relative delays in the range $[-T+T_c, T-T_c]$ can be substantially reduced by the choice of the signature sequence. More importantly, it is shown that the spread-spectrum receiver (which is essentially a coherent matched filter) severely discriminates against signals with propagation delays outside the range $[-T_c, T_c]$. This property is

generally desirable for communications in a multipath environment when there is at least one relatively strong path. However, it is precisely this property that degrades the error probability of spread-spectrum communications in a frequency-selective Rayleigh fading channel.

## 3.3 Performance Approximations for Other DPSK Systems

In the previous section it was demonstrated that bounds on the error probability of DPSK in a WSSUS frequency-selective Rayleigh fading environment can be obtained when the channel delay spectrum is normalized with respect to the autocorrelation function of the specified data-pulse shape. The resulting bounds show that the limiting error probability is relatively insensitive to variations of the channel delay power-density spectrum (for fixed normalized rms multipath spread).

The bounds on system performance represent useful results since the limits on the effects of frequency-selectivity on DPSK communications have not been previously characterized. Moreover, the closeness of these bounds imply that it is not necessary to fully characterize the channel in order to obtain an accurate estimate of system performance. This is of considerable importance, since in practice it is difficult to precisely describe the fading process [13].

Another implication of the above results is that it may be possible to estimate the average probability of error of a proposed system from the tabulated error probabilities in Section 3.2. In particular, Figs. 3.3 and 3.4 indicate that the irreducible error probability for the rectangular pulse as a function of the normalized rms multipath spread $\mu_r$ closely approximates the irreducible error probability for the sine-pulse as a function of $\mu_s$.

Similarly, Figs. 3.3 and 3.4 indicate that the irreducible error probability for the rectangular pulse as a function of $\mu_r$ closely approximates the irreducible error probability for the phase-coded pulse as a function of $\mu_p$. In Fig. 3.8, the irreducible error probabilities for the rectangular pulse, the sine pulse, and the phase-coded pulse (N = 31) are shown as a function of their respective normalized multipath spreads, $\mu_v$. The results in Figs. 3.3-3.5 indicate that there is little to be gained by considering more than one delay power-density spectrum. Hence, for this example we have represented the fading channel by a Gaussian delay power-density spectrum.

The results in Section 3.2 and Fig. 3.8 indicate that there is essentially a <u>single</u> relationship (represented by Fig. 3.8) between the irreducible error probability $P_I$ and the normalized rms multipath spread $\mu_v$ for DPSK in frequency-selective Rayleigh fading. We make the following observation concerning this result: The data in Fig. 3.8 in some sense represents the irreducible error probability as a function of $\mu_v$ for a generic (time-limited) data-pulse waveform v(t). Hence, the limiting error probability for a particular Rayleigh fading channel and a particular time-limited data-pulse waveform u(t) (say) can be closely approximated by means of a <u>single</u> rms-type [13] channel parameter,

$$\mu_u = \left\{ \frac{2}{H_u} \cdot \int_0^T g(\xi) R_u^2(\xi)\, d\xi \right\}^{1/2} = \left\{ \frac{1}{H_u} \cdot \int_{-T}^{T} g(\xi) R_u^2(|\xi|)\, d\xi \right\}^{1/2}$$

$$= \left\{ \frac{1}{H_u} \cdot \int_{-\infty}^{\infty} g(\xi) R_u^2(|\xi|)\, d\xi \right\}^{1/2} \qquad (3.40)$$

with the autocorrelation function $R_u^2(\xi)$ defined by (3.14). Of course, the last equality in (3.40) follows only if the adjacent-pulse-limited ISI assumption holds. (However, the data presented in Section 3.2 indicates that

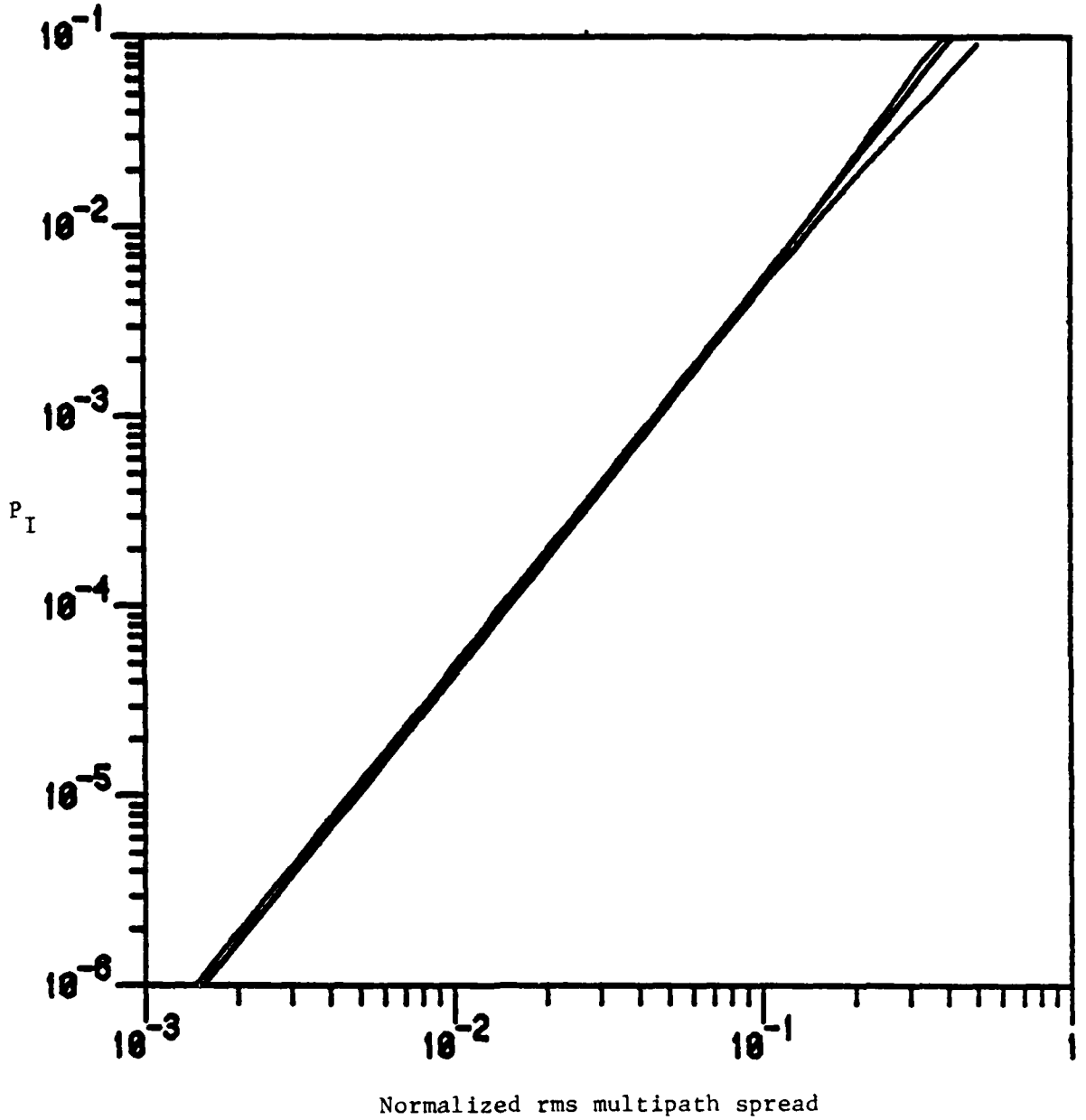


**Figure 3.8. Irreducible error probabilities as a function of the normalized rms multipath spread $\mu_v$**

this must be the case if the performance is to be acceptable at all.) The resulting approximation for the irreducible error probability is found as the corresponding value of $P_I$ in Fig. 3.8.

For small time-bandwidth product pulse shapes, a good estimate of the average error probability as a function of the signal-to-noise ratio S is realized as a curve which lies above $P_{ns}$ in (3.18) and $P_I$ (calculated from (3.40)) and which asymptotically approaches $P_{ns}$ and $P_I$ for extreme values of the signal-to-noise ratio. If it is also possible to measure the quantity

$$2\bar{\eta}_u/T^2 = \int_{-\infty}^{\infty} g(\xi)\ \bar{R}_u^2(|\xi|)\ d\xi = \int_{-\infty}^{\infty} G(\Omega)\ \beta_u(\Omega)\ d\Omega\ , \qquad (3.41)$$

then a more accurate approximation (especially for large time-bandwidth pulse shapes) can be found as above by replacing $P_{ns}$ by the low signal-to-noise ratio asymptote given in (3.38) for the parameter $\bar{\eta}_u$ calculated from (3.41).

There may, of course, exist design situations for which an approximation of error performance is unacceptable for a system evaluation. In these situations, it may be necessary to construct and test the proposed system or obtain a more complete characterization of the channel. However, the approximations discussed above could be of significant utility in the consideration of DPSK systems employing complicated pulse shapes and in applications to fading channels which are difficult to fully characterize. For example, if phase-coded pulse waveforms are under consideration as candidates for the pulse shape, these approximations may be useful in the selection of signature sequences, as well as in the comparative system evaluations which would provide insight into the potential benefits of hybrid frequency-hopping/direct-sequence systems versus simple frequency-hopped systems employing DPSK modulation.

## 3.4 Applications to Frequency-Selective Rician Channels

In the analysis of the preceding sections, we have assumed that the response of the fading channel to a deterministic input signal s(t) is represented by a zero-mean complex Gaussian random variable (i.e., Rayleigh fading). There are, however, situations where the fading channel is more accurately modeled as Rician. This channel model arises when the received signal contains a nonfaded specular component as well as a Rayleigh faded component.

The narrowband model for the received signal in the case of Rician fading is given by (2.3) with the parameter $\alpha > 0$ representing the strength of the specular component. As in the case of Rayleigh fading, the decision statistic $Z_i$ in (3.5) can be written as a quadratic form of Gaussian random variables U and V. The resulting conditional probability of error, given a particular sequence of data bits $(\underline{b}_i)$ is transmitted, is related to the probability distribution of the ratio of Chi-square variables, each having two degrees of freedom; the non-centrality parameters depend on the characteristics of the system. Expressions for the conditional error probabilities are derived in [19] and [36], where in each case the result is obtained through the inversion of the characteristic function of Hermitian quadratic form of complex Gaussian random variables [37] by means of a double integral evaluated by Price [38].

Results of previous investigations of the performance of digital communications over Rician fading channels indicate that the error probability is upper and lower bounded by the corresponding results for the Rayleigh channel (no specular component) and the additive white Gaussian noise channel (no fading), respectively. In the remainder of this section, we show that the

average probability of error for DPSK in Rician fading is completely determined by the parameter $\alpha$ in (2.3) and the parameters necessary for the evaluation of the error probability for Rayleigh fading considered in the previous sections. Thus, the results for Rayleigh fading, which are essentially the results for the "worst-case" Rician channel, are also useful in determining the error performance in the more general Rician case.

It can be shown that the conditional error probabilities for the Rician channel depend on the characterization of the Rayleigh faded portion of the received signal only through the parameters $\bar{\eta}_v$, $\eta_v$, and $\eta_v'$ defined in (3.12) and discussed in Section 3.1. In particular, assuming without loss of generality that $b_{i-1} = b_i$ for the transmitted signal s(t) given by (3.1), the conditional error probability [19] can be written as

$$P(\underline{b}_i) = Q(\sqrt{A(\underline{b}_i)}, \sqrt{B(\underline{b}_i)}) - \left[ \frac{\sqrt{m_{UU}(\underline{b}_i)m_{VV}(\underline{b}_i)} + m_{UV}(\underline{b}_i)}{2\sqrt{m_{UU}(\underline{b}_i)m_{VV}(\underline{b}_i)}} \right] \cdot \exp\left[ - \frac{A(\underline{b}_i)+B(\underline{b}_i)}{2} \right] \cdot I_0(\sqrt{A(\underline{b}_i)B(\underline{b}_i)}) , \quad (3.42)$$

where $Q(\cdot,\cdot)$ is Marcum's Q function [6], and $I_0(x)$ is the modified Bessel function of the first kind of order zero and argument x. The parameters $A(\underline{b}_i)$ and $B(\underline{b}_i)$ in (3.42), which are related to the non-centrality parameters of the corresponding Chi-square variates, are given by

$$A(\underline{b}_i) = \frac{4\alpha^2 ET}{m_{UU}(\underline{b}_i)m_{VV}(\underline{b}_i)} \left[ m_{UU}(\underline{b}_i)+m_{VV}(\underline{b}_i) - 2(b_i b_{i-1}) \sqrt{m_{UU}(\underline{b}_i)m_{VV}(\underline{b}_i)} \right] \quad (3.43a)$$

and

$$B(\underline{b}_i) = \frac{4\alpha^2 ET}{m_{UU}(\underline{b}_i)m_{VV}(\underline{b}_i)} \left[ m_{UU}(\underline{b}_i)+m_{VV}(\underline{b}_i) + 2(b_i b_{i-1}) \sqrt{m_{UU}(\underline{b}_i)m_{VV}(\underline{b}_i)} \right]. \quad (3.43b)$$

The moments, $m_{XY}(\underline{b}_i)$ in (3.43) are the central moments of the random variables U and V defined as

$$m_{XY}(\underline{b}_i) = E\{(X - E[X|\underline{b}_i])\cdot(Y - E[Y|\underline{b}_i])^* | \underline{b}_i\} .$$

Using (2.3) and (3.6) for the signal defined by (3.1), we see that $E\{U\} = \alpha\sqrt{8ET}\cdot b_i$ and $E\{V\} = \alpha\sqrt{8ET}\cdot b_{i-1}$ so that the moments in (3.43) are precisely the same as those defined in (3.10) for the analysis of Rayleigh fading channels.

It is easy to see that (3.42) reduces to the error probability expressions for Rayleigh fading (see (3.8) and (3.9)) when $\alpha = 0$. In fact, if $\alpha = 0$, then $A(\underline{b}_i) = B(\underline{b}_i) = 0$, and (3.42) becomes

$$P(\underline{b}_i) = \frac{\sqrt{m_{UU}(\underline{b}_i)m_{VV}(\underline{b}_i)} + m_{UV}(\underline{b}_i)}{2\sqrt{m_{UU}(\underline{b}_i)m_{VV}(\underline{b}_i)}} , \qquad (3.44)$$

since $Q(0,0) = I_0(0) = 1$, which is identical to (3.8) for the case $b_{i-1} = b_i$. Alternatively, if there is no faded component in the received signal, then $2\sigma^2 = 0$ (cf. (2.4)) so that the moments in (3.43) become

$$m_{UU} = m_{VV} = 8N_0T$$

and

$$m_{UV} = 0.$$

If $b_{i-1} = b_i$, then $A(\underline{b}_i) = 0$, and $B(\underline{b}_i) = 2\alpha^2E/N_0$ and (3.42) becomes

$$P(\underline{b}_i) = \frac{1}{2}\exp\left[ - \frac{\alpha^2E}{N_0} \right] ,$$

(since $Q(0,x) = \exp(-x/2)$ [6]), which is the average error probability of DPSK for the additive white Gaussian noise channel.

# CHAPTER 4

## PERFORMANCE OF BINARY FSK COMMUNICATIONS OVER FREQUENCY-SELECTIVE FADING CHANNELS

In this chapter, we consider the evaluation of the average probability of error for binary FSK communications over WSSUS fading channels. As in Chapter 3, the analysis is first carried out for the case of Rayleigh fading channels (i.e., with the channel response given by (2.3) for $\alpha = 0$). It is then shown that the error probability for the more general Rician channel is completely specified in terms of the key system parameters used in the performance evaluation for Rayleigh fading.

Previous results on the performance of FSK in frequency-selective fading include those found in [2,17,18]. In [17], Bello and Nelin consider the performance of FSK where the frequency separation between the two signals is assumed to be an integer multiple of 1/2T. The channel is modeled as a Rayleigh fading channel with a Gaussian delay power-density spectrum. The degree of frequency-selectivity is defined as the distance between the 1/e points of the frequency correlation function $G(\Omega)$. It is shown that the system error performance depends on the relative phases as well as the frequency separation of the two transmitted signals. The authors claim that FSK is generally less sensitive to the effects of frequency-selective fading than rectangular pulse DPSK. The authors also state that for large signal-to-noise ratios, FSK produces lower error rates than rectangular pulse DPSK for channels which are highly selective. However, these claims are not supported by the numerical results for the irreducible error probability in [16] which differ from the results in [17] by an order of magnitude.

In [2] and [18], the performance of FH/FSK for Rician fading channels is considered for a triangular delay power-density spectrum model. However, in both cases the authors assume that the two FSK signals are orthogonal at the receiver. In Section 4.2, we show that this is equivalent to assuming that the frequency separation between the FSK tones is infinite.

In this chapter, the effect of frequency-selective fading on the performance of noncoherently-detected FSK is investigated for a number of signaling formats. The parameters that characterize the effects of intersymbol interference and additive channel noise are identified. It is shown that the performance of FSK communications over frequency-selective Rayleigh fading channels can be well approximated in terms of these key parameters which are related to rms-type channel measurements. The results for FSK are compared to the results for DPSK in Chapter 3. It is found that the error performance of these two systems depends on a number of common factors and can be quite similar in some cases. The technique for obtaining bounds on the irreducible error probability for DPSK is applied to the analysis of FSK. Finally, we consider the approximation of the performance of other FSK systems in terms of the key system parameters.

## 4.1 System Model

The information source for the FSK transmitter is modeled as a sequence $(\bar{b}_i)$ of mutually independent random variables, each taking on values in the set {0,1} with equal probability. The binary data sequence $(b_i)$ is given by the mapping

$$b_i = (-1)^{\bar{b}_i}$$

from {0,1} to {-1,1} for each integer i. Using the narrowband signal models discussed in Chapter 2, the transmitted signal s(t) is defined by

$$s(t) = \sqrt{\frac{2E}{T}}\, v(t-iT)e^{-j[b_i \pi h t/T + \theta(i,b_i)]} \qquad (4.1)$$

for $t \in [iT,(i+1)T]$ for each integer i. The real-valued waveform v(t) is assumed to be time limited to the interval [0,T] such that

$$\frac{1}{T}\int_0^T v(t)^2\, dt = 1,$$

so that E is the energy per data bit.

The parameter h in (4.1) is known as the deviation ratio or <u>modulation index</u> of the FSK signal set [39] and is related to the frequency deviation $f_d$ from the carrier frequency $f_c$ (which, of course does not appear in the narrowband signal representation) by $h = 2f_dT$. The two transmitted signals are referred to as the <u>mark signal</u> and the <u>space signal</u>. We follow the convention in [39] by denoting the signal transmitted at frequency $f_c - f_d$ as the mark signal and the signal transmitted at frequency $f_c + f_d$ as the space signal. From (4.1) we see that the mark signal corresponds to the case when $b_i = -1$ (i.e., $\bar{b}_i = 1$), and the space signal is transmitted when $b_i = 1$ (i.e., $\bar{b}_i = 0$). The phase angle $\theta(i,b_i)$, which depends on both the value of the i-th data bit and the interval in which it is transmitted, represents the phase of the transmitted signal s(t) at time t = 0.

Depending on the method used to generate the transmitted signal, the phase angles $\theta(i,-1)$ and $\theta(i,+1)$, corresponding to the mark and space signals, respectively, may be related or may be modeled as statistically independent random variables. For example, if the transmitted signal is obtained by switching between two uncoupled oscillators, the two phase angles are modeled

as independent random variables uniformly distributed on $[0,2\pi]$. Alternatively, if the transmitted signal is a continuous-phase FSK (CPFSK) signal, then the phase angles are related by $\theta(i,+1) = \theta(i+1,-1) + 2\pi hi$. We assume in any case that no abrupt phase transition occurs between two consecutive data-pulse intervals if the two corresponding data bits are identical. That is, we assume that $\theta(i,+1) = \theta(i+1,+1)$ and that $\theta(i,-1) = \theta(i+1,-1)$.

By using narrowband signal models to represent the signals in the FSK system, we have removed the dependence of the orthogonality of the two transmitted signals on the carrier frequency $f_c$. Rather, the two signals are said to be orthogonal if and only if

$$\int_0^T v^2(t)e^{-j[2\pi ht/T + \theta(0,+1)-\theta(0,-1)]}\,dt = \int_0^T v^2(t)e^{-j[2\pi ht/T]}\,dt = 0 .$$

Unless stated otherwise, "orthogonality" is used to describe the relationship of the mark and space signals at the transmitter. Hence, for narrowband signal models, the orthogonality (or lack of orthogonality) between the mark and space signals is completely determined by the pulse waveform $v(t)$ and the modulation index $h$. This is equivalent to the assumption that both $f_c$ and $h$ are integer valued, or that $(f_cT - h) \gg 1$.

The FSK receiver is modeled as the noncoherent matched filter receiver shown in Fig. 4.1, which is discussed in [39]. During each time interval, $[iT,(i+1)T]$, the receiver forms the decision statistic $Z_i$ represented by

$$Z_i = 4\left| \int_{iT}^{(i+1)T} r(t)v^*(t)e^{j\pi t/T}\,dt \right|^2 - 4\left| \int_{iT}^{(i+1)T} r(t)v^*(t)e^{-j\pi t/T}\,dt \right|^2$$

$$= |U|^2 - |V|^2 , \qquad (4.2)$$

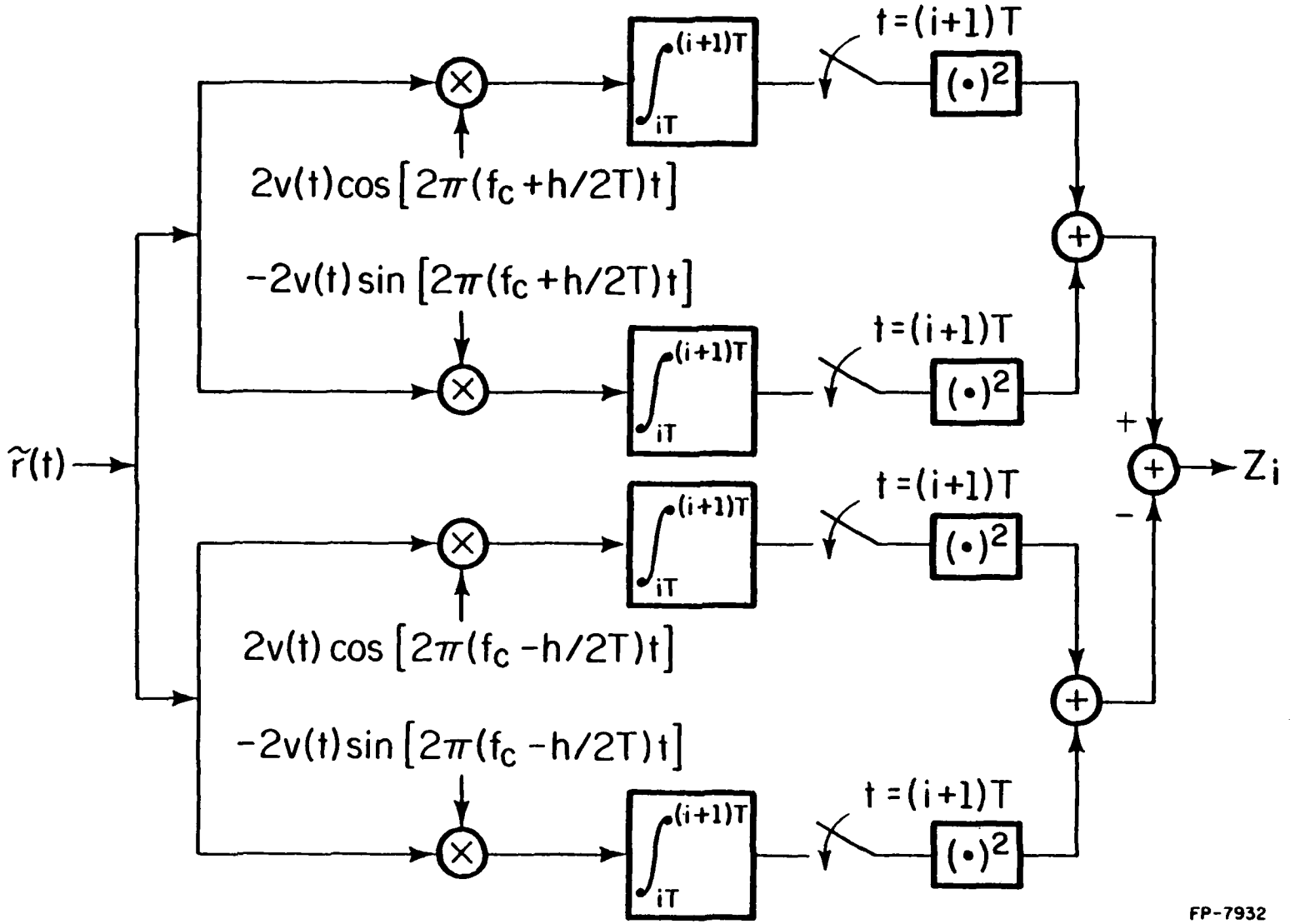


Figure 4.1. Noncoherent matched filter receiver

where

$$U = 2 \int_{iT}^{(i+1)T} r(t)v^*(t)e^{j\pi th/T}\, dt \ , \tag{4.3a}$$

and

$$V = 2 \int_{iT}^{(i+1)T} r(t)v^*(t)e^{-j\pi th/T}\, dt \ . \tag{4.3b}$$

From (4.2) we see that the decision statistic for the i-th data bit is a quadratic form of complex Gaussian random variables U and V.

Under the assumption that $\rho(t-x,\xi) \approx 0$; $|\xi| > T$, (i.e., adjacent-pulse-limited ISI), the output statistic $Z_i$ depends on at most three consecutive data bits represented by $\underline{b}_i = (b_{i-1}, b_i, b_{i+1})$. The probability of error can be written as the average of probabilities, each conditioned on the event that one of the eight possible sequences of data bits are transmitted, i.e.,

$$P_e = \frac{1}{8} \sum_{\underline{b}_i} P(\underline{b}_i) \ , \tag{4.4}$$

where $P(\underline{b}_i) = \Pr\{\text{error occurs}|\underline{b}_i \text{ transmitted}\}$. In [11,17], Bello and Nelin show that the conditional error probabilities are given by

$$P(\underline{b}_i) = (2 + \gamma(\underline{b}_i))^{-1} \ , \tag{4.5}$$

where the "equivalent" signal-to-noise ratio $\gamma(\cdot)$ may be written as

$$\gamma(\underline{b}_i) = \frac{2|(m_{UU}(\underline{b}_i) - m_{VV}(\underline{b}_i))|}{\sqrt{(m_{UU}(\underline{b}_i) + m_{VV}(\underline{b}_i))^2 - 4|m_{UV}(\underline{b}_i)|^2} - |(m_{UU}(\underline{b}_i) - m_{VV}(\underline{b}_i))|} \ ; \tag{4.6}$$

a function of the moments $m_{XY}(\underline{b}_i) = E\{XY^*|\underline{b}_i\}$ of the random variables U and V.

Using (2.5) and (4.3), the moments in (4.6) are found to be

$$m_{UU}(\underline{b}_i) = 8\sigma^2 \int_{iT}^{(i+1)T} \int_{iT}^{(i+1)T} \int_{-T}^{T} \rho(t-x,\xi)s(t-\xi)v^*(t)e^{j\pi th/T} \cdot s^*(x-\xi)v(x)e^{-j\pi xh/T}\, d\xi dx dt + 8N_0T, \quad (4.7a)$$

$$m_{VV}(\underline{b}_i) = 8\sigma^2 \int_{iT}^{(i+1)T} \int_{iT}^{(i+1)T} \int_{-T}^{T} \rho(t-x,\xi)s(t-\xi)v^*(t)e^{-j\pi xh/T} \cdot s^*(x-\xi)v(x)e^{j\pi th/T}\, d\xi dx dt + 8N_0T, \quad (4.7b)$$

and

$$m_{UV}(\underline{b}_i) = 8\sigma^2 \int_{iT}^{(i+1)T} \int_{iT}^{(i+1)T} \int_{-T}^{T} \rho(t-x,\xi)s(t-\xi)v^*(t)e^{j\pi th/T} \cdot s^*(x-\xi)v(x)e^{j\pi xh/T}\, d\xi dx dt + 8N_0 \int_0^T v(t)v^*(t)e^{j2\pi th/T}\, dt. \quad (4.7c)$$

By substituting $g(\cdot)$ for $\rho(\cdot,\cdot)$ in (4.7), we see that the moments needed to evaluate $\gamma(\underline{b}_i)$ and hence $P_e$ can be written as

$$m_{UU}(\underline{b}_i) = \frac{16\sigma^2 E}{T} \int_0^T g(\xi) \cdot \Big[ 2|\bar{R}_v(h,b_i,\xi)|^2 + |R_v(h,b_{i-1},\xi)|^2 + |R_v(h,b_{i+1},\xi)|^2 + 2\mathrm{Re}\{e^{-j[\theta_T(i,\underline{b}_i)-(b_i-b_{i-1})\pi h\xi/T]} \cdot \bar{R}_v(h,b_i,\xi) \cdot R_v^*(h,b_{i-1},\xi) + 2\mathrm{Re}\{e^{j[\theta_T(i+1,\underline{b}_i)+(b_{i+1}-1)\pi h]} \cdot \bar{R}_v(h,b_i,\xi) \cdot R_v^*(h,b_{i+1},\xi) \Big]\, d\xi + 8N_0T, \quad (4.8a)$$

$$m_{VV}(\underline{b}_i) = \frac{16\sigma^2 E}{T}\int_0^T g(\xi)\cdot\Big[\ 2|\bar{R}_v^*(h,-b_i,\xi)|^2 + |R_v^*(h,-b_{i-1},\xi)|^2 + |R_v^*(h,-b_{i+1},\xi)|^2$$

$$+ 2\mathrm{Re}\{e^{-j[\theta_T(i,\underline{b}_i)-(b_i-b_{i-1})\pi h\xi/T]}\cdot\bar{R}_v^*(h,-b_i,\xi)\cdot R_v(h,-b_{i-1},\xi)$$

$$+ 2\mathrm{Re}\{e^{j[\theta_T(i+1,\underline{b}_i)+(b_{i+1}+1)\pi h]}\cdot\bar{R}_v^*(h,-b_i,\xi)\cdot R_v(h,-b_{i+1},\xi)\ \Big]\,d\xi$$

$$+ 8N_0T, \qquad (4.8b)$$

and

$$m_{UV}(\underline{b}_i) = \frac{16\sigma^2 E}{T}\int_0^T g(\xi)\cdot\Big[\ (1+e^{-j2\pi h\xi/T})\cdot\bar{R}_v(h,b_i,\xi)\cdot\bar{R}_v(h,-b_i,\xi)$$

$$+ R_v(h,b_{i-1},\xi)\cdot R_v(h,-b_{i-1},\xi) + e^{-j2\pi h(\xi-T)/T}\cdot R_v(h,b_{i+1},\xi)\cdot R_v(h,-b_{i+1},\xi)$$

$$+ e^{j[\theta_T(i,\underline{b}_i)-(b_i-b_{i-1})\pi h\xi/T]}\cdot R_v(h,b_{i-1},\xi)\cdot\bar{R}_v(h,-b_i,\xi)$$

$$+ e^{-j[\theta_T(i,\underline{b}_i)-(b_i-b_{i-1})\pi h\xi/T]}\cdot\bar{R}_v(h,b_i,\xi)\cdot R_v(h,-b_{i-1},\xi)$$

$$+ e^{-j[\theta_T(i+1,\underline{b}_i)+2\pi h\xi/T+\pi h(b_{i+1}-1)]}\cdot R_v(h,b_{i+1},\xi)\cdot\bar{R}_v(h,-b_i,\xi)$$

$$+ e^{j[\theta_T(i+1,\underline{b}_i)-2\pi h\xi/T+\pi h(b_{i-1}+1)]}\cdot\bar{R}_v(h,b_i,\xi)\cdot R_v(h,-b_{i+1},\xi)\ \Big]\,d\xi$$

$$+ 8N_0\int_0^T v(t)v^*(t)e^{j2\pi th/T}\,dt\ . \qquad (4.8c)$$

The phase transitions, $\theta_T(i,\underline{b}_i)$, which denote the <u>differences</u> between the phases of the mark and space signals at time t = 0 is given by

$$\theta_T(i,\underline{b}_i) = \begin{cases} \theta(i,b_i) - \theta(i-1,b_{i-1}) & ;\ b_i \neq b_{i-1} \\ 0 & ;\ b_i = b_{i-1}\ . \end{cases} \qquad (4.9)$$

The correlation functions $\bar{R}_v(h,b_i,\xi)$ and $R_v(h,b_i,\xi)$ in (4.8) are defined by

$$\bar{R}_v(h,b_i,\xi) = \int_{\xi}^{T} v(t)\, v(t-\xi)\, e^{j\pi h t(1-b_i)/T}\, dt \qquad (4.10a)$$

and

$$R_v(h,b_i,\xi) = \int_{0}^{\xi} v(t)\, v(t+T-\xi)\, e^{j\pi h t(1-b_i)/T}\, dt \qquad (4.10b)$$

for $0 \leq \xi \leq T$. Notice that $\bar{R}_v(h,b_i,\xi)$ and $R_v(h,b_i,\xi)$ are related to the aperiodic autocorrelation functions defined by (3.10a) and (3.10b). In fact, using (3.10a) and (4.10a), it is easy to see that $\bar{R}_v(h,1,\xi) = \bar{R}_v(\xi)$. Similarly, from (3.10b) and (4.10b) we have that $R_v(h,1,\xi) = R_v(\xi)$. In contrast, the functions $\bar{R}_v(h,-1,\xi)$ and $R_v(h,-1,\xi)$ are, in general, complex-valued functions that depend on the modulation index h as well as the waveform v(t). Unfortunately, it is difficult to express the result of these integrals in compact form for arbitrary modulation index. Finally, notice that the function $\bar{R}_v(h,-1,0)$ is simply a measure of the orthogonality of the two FSK signals.

Using (4.6), (4.8), and the fact that we consider only binary symmetric signal sets (cf. (4.1)), it can be shown that $\gamma(\underline{b}_i) = \gamma(-\underline{b}_i)$. This property, along with (4.4), implies that $P_e$ in (4.5) can be reduced to

$$P_e = \frac{1}{4}\,[P(-1,+1,-1) + P(+1,+1,-1) + P(-1,+1,+1) + P(+1,+1,+1)], \qquad (4.11)$$

so that we need only consider the case when a space signal is transmitted during the i-th data-bit interval.

In the present analysis, we consider a number of examples of binary FSK signal formats. Within the class of CPFSK signals, we consider modulation indices h = 1/2, 1, 2, and 10 for a rectangular waveform v(t). The example of rectangular pulse FSK for h = 10 is considered as an approximation to the case of "infinite" frequency separation between the two FSK tones. Notice that the CPFSK signal with h = 1/2 produces what is known as a minimum-shift-keyed

or MSK signal [39]. Of course, it is not common practice to consider the performance of MSK signals for noncoherent detection since MSK signals do not comprise an orthogonal signal set. By examining $\bar{R}_r(h,-1,0)$ in (4.10a), it is easy to see that h = 1 is the smallest modulation index producing an orthogonal signal set for the rectangular pulse. We include the case of h = 1/2 as an example in order to gain a better understanding of the role of the modulation index in determining the performance of noncoherent FSK in the presence of frequency-selective fading. Since we assume that knowledge of the phase of the transmitted signal is unavailable to the receiver, the phase transitions for MSK signals are related by $\theta_T(i,\underline{b}_i) = 0$ and $\theta_T(i+1,\underline{b}_i) = \pi$ or equivalently, $\theta_T(i,\underline{b}_i) = \pi$ and $\theta_T(i+1,\underline{b}_i) = 0$ for differing consecutive data bits.

Other examples of FSK signals considered include those generated by phase-coded waveforms defined by (3.4). The signature sequences for this pulse waveform are the m-sequences discussed in Chapter 3. Notice that for the phase-coded pulse, the orthogonality of the transmitted signals depends only on the modulation index h so long as the pulse waveform is composed of a sequence of rectangular pulses. In this case, $\bar{R}_p(h,-1,0) = \bar{R}_r(h,-1,0)$, where the subscripts "p" and "r" denote the phase-coded pulse and the rectangular pulse, respectively. Hence, h = 1 is the smallest modulation index for which the phase-coded pulse signals are orthogonal. However, for fixed modulation index, the spectral spreading effect of the direct-sequence waveform causes significantly more overlap of the spectra of the mark and space signals than for the rectangular pulse. For a given sequence length N, we can specify a set of orthogonal phase-coded pulse signals with roughly the same degree of spectral overlap as rectangular pulse FSK with h = 1 by letting h = N for

phase-coded pulse signals. In what follows, we consider examples of phase-coded pulse FSK where the modulation index is taken as the sequence length, i.e., h = N, as well as examples with h = 1.

In Fig. 4.2, the results of the numerical evaluation of the average error probability of CPFSK with modulation index h = 1 are shown as a function of the signal-to-noise ratio $S = 2\sigma^2 E/N_0$ for a Gaussian delay spectrum with rms multipath spread $\mu = 0.05$. The probability of error for orthogonal FSK in non-selective Rayleigh fading, given by

$$P_{ns} = (2 + 2\sigma^2 E/N_0)^{-1} , \tag{4.12}$$

is also shown. From Fig. 4.2 we see that for small signal-to-noise ratios, the average error probability is largely determined by the value of $P_{ns}$. As the signal-to-noise ratio becomes large, the effects of intersymbol interference become more significant and the average error probability asymptotically approaches the irreducible error probability for FSK in frequency-selective fading defined by $P_I \triangleq P_e|_{S \to \infty}$. The results in Fig. 4.2 imply that $P_I$ (shown as a horizontal asymptote) is a key performance parameter for the design and evaluation of practical systems.

The irreducible error probabilities $P_I$ for several examples of FSK signal sets and the four examples of delay spectra given in Chapter 2 are shown in Figs. 4.3 and 4.4 as a function of the rms multipath spread $\mu = M/T$. In all cases, the results are obtained using standard numerical integration techniques. In Fig. 4.3, the results are shown for rectangular pulse CPFSK with modulation indices h = 1/2 and 1, and for rectangular pulse FSK with h = 1 and $\theta_T(i,-1) = \theta_T(i+1,-1) = \theta_T = \pi$, where $\theta_T$ denotes the common phase transition. Notice that for modulation index h = 1, the irreducible error

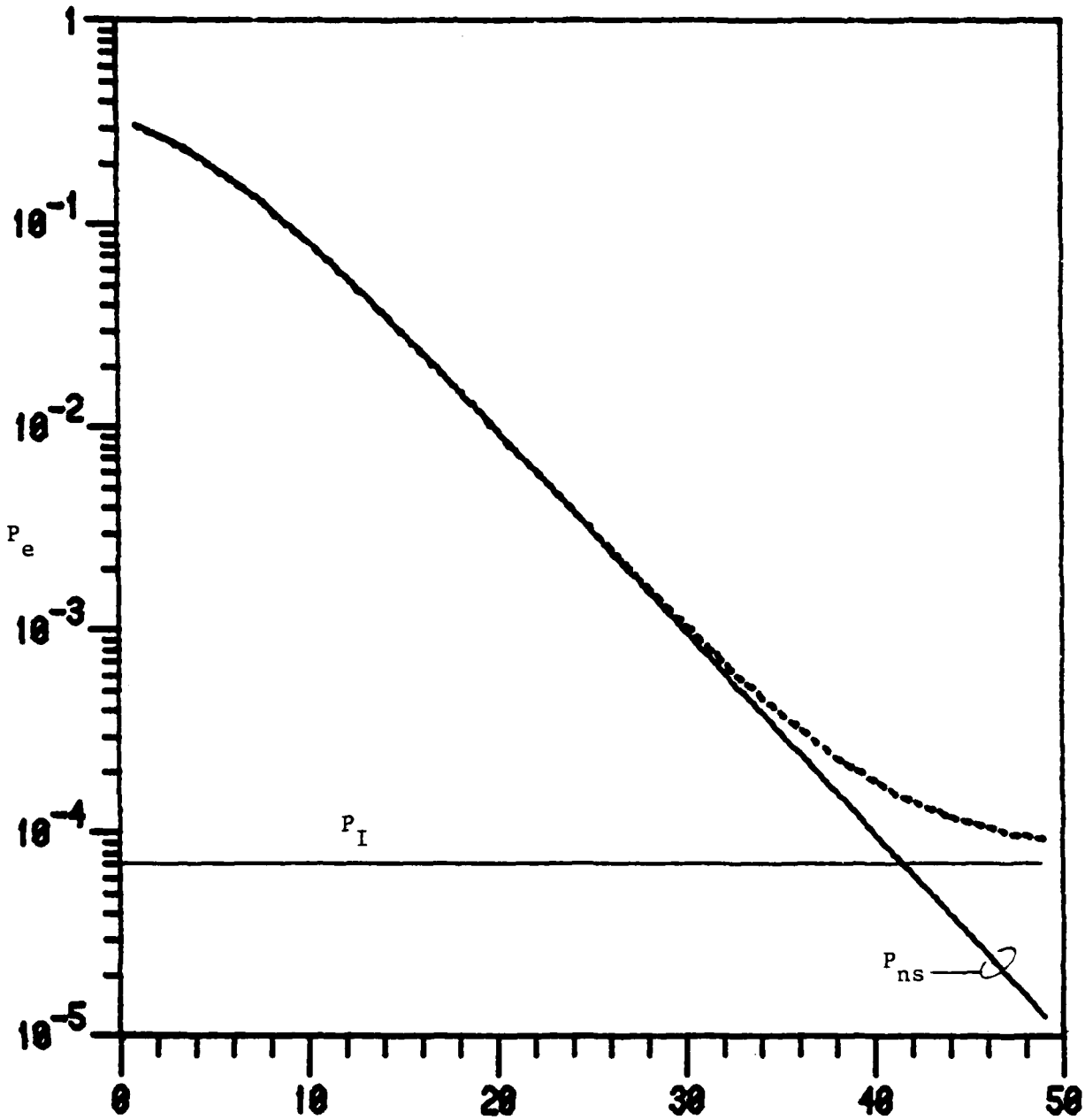


Figure 4.2. $P_e$ vs. S for rectangular pulse FSK and Gaussian delay power-density spectrum with $\mu = 0.05$

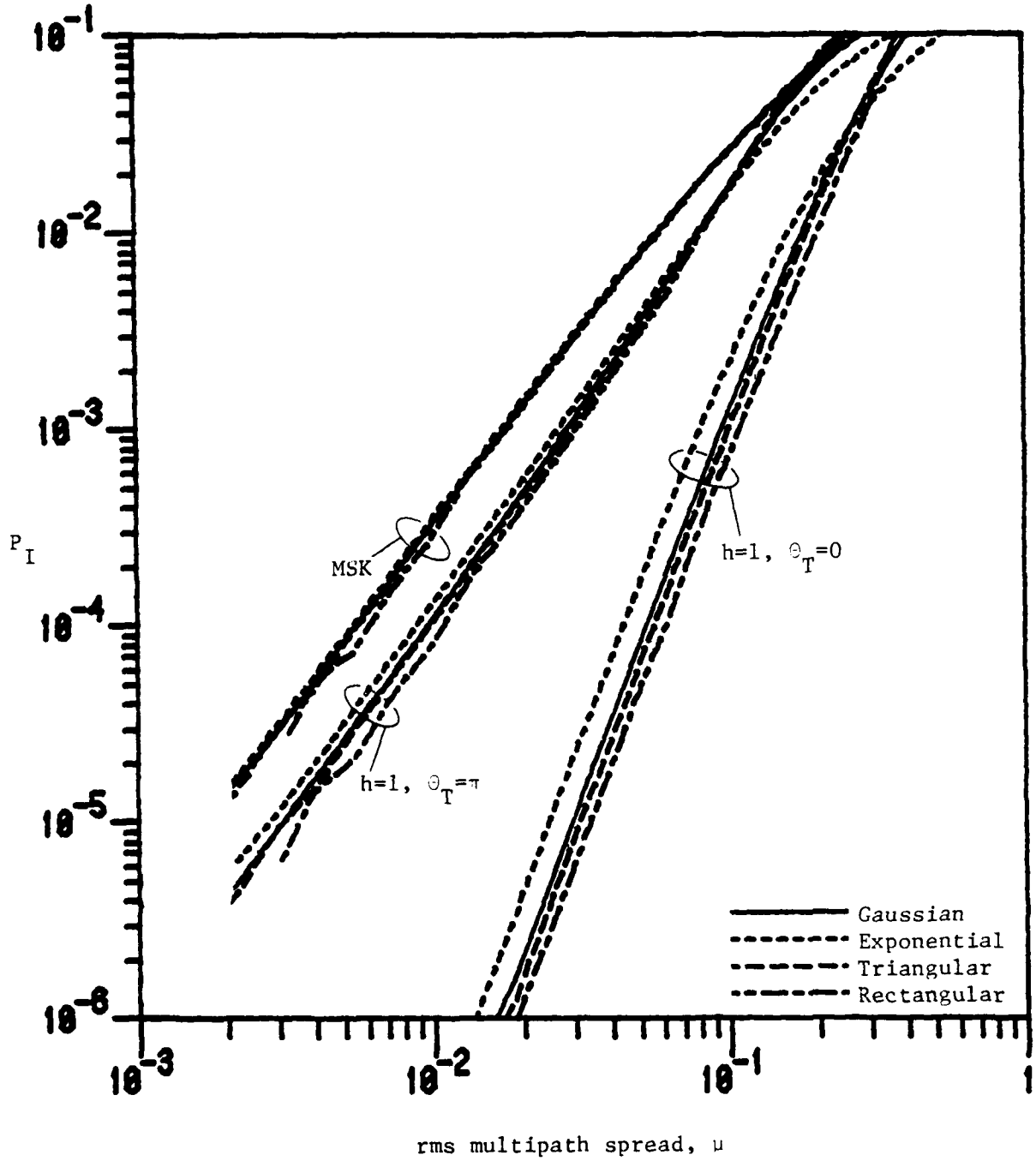


**Figure 4.3. Irreducible error probability for MSK and rectangular pulse FSK with h = 1, and $\Theta_T$ = 0, π vs. rms multipath spread**

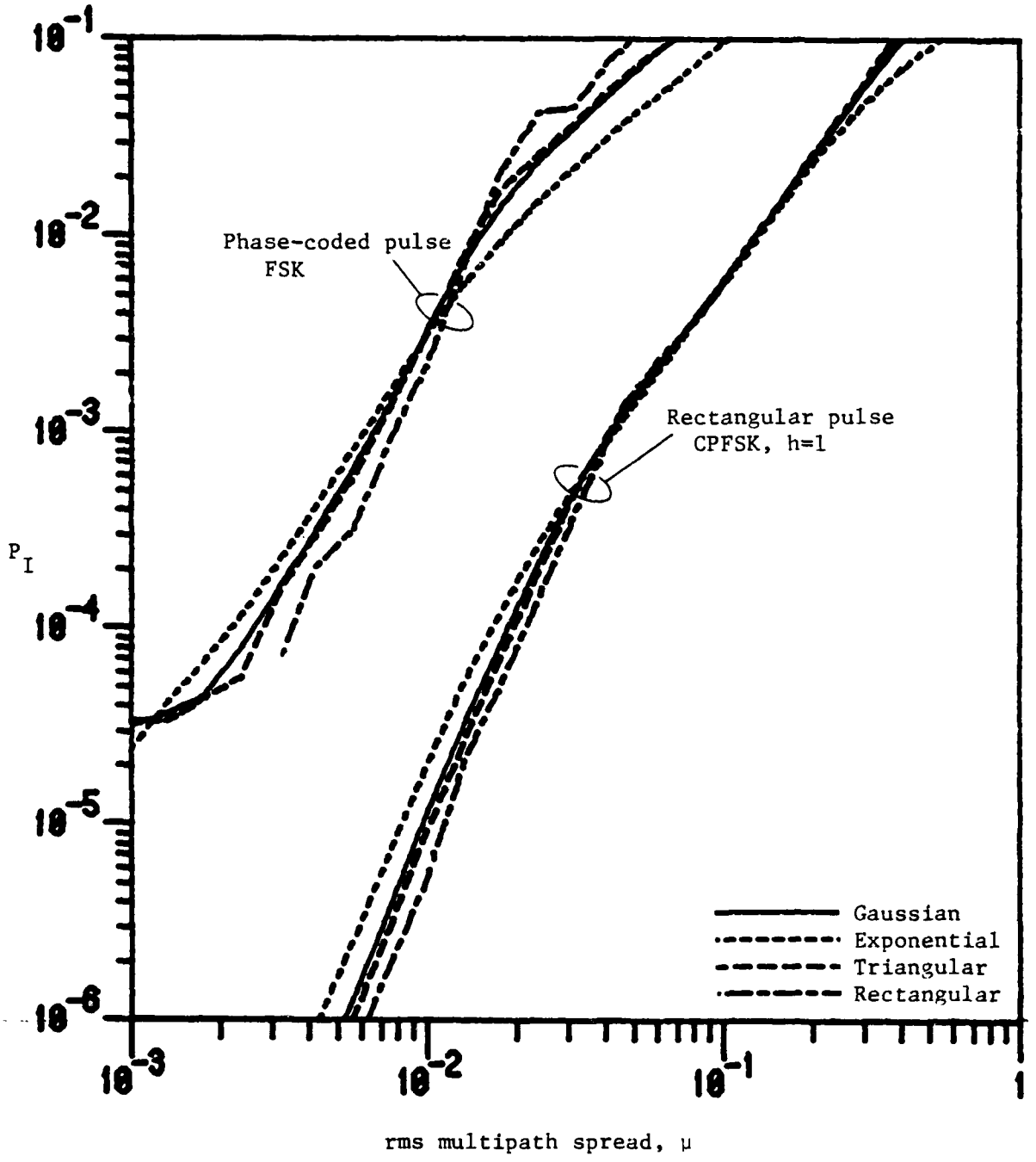


**Figure 4.4. Irreducible error probabilities for phase-coded pulse FSK with N = 31, h = 1 and rectangular pulse FSK with h = 10 vs. rms multipath spread**

probabilities exhibit significant sensitivity to the shape of the delay density. However, the variations caused by changes in the shape of the delay density are small compared to the variations between the examples for $\theta_T = 0$ and $\theta_T = \pi$. The results in Fig. 4.3 for the two examples of CPFSK (i.e., h = 1/2 and h = 1) seem to indicate that the irreducible error probability is also sensitive to small changes in the modulation index. However, in Section 4.2 it is shown that the larger values of $P_I$ for CPFSK with h = 1/2 (MSK) are primarily due to orthogonality considerations rather than the effects of intersymbol interference.

In Fig. 4.4, the irreducible error probabilities for rectangular pulse CPFSK with h = 10 and phase-coded pulse FSK with h = 1 and signature sequence length N = 31 with $\theta_T = 0$ are shown. For this example of rectangular pulse CPFSK, we see that the irreducible error probability is not sensitive to changes in the shape of the delay density for large values of rms multipath spread. Also notice that the irreducible error probability for phase-coded FSK exhibits the same erratic behavior as the results for phase-coded DPSK.

## 4.2 Performance Bounds and Approximations

In this section, the relationships between irreducible error probability, intersymbol interference, and signal orthogonality are explored by first characterizing the frequency-selective fading mechanism in the delay domain. The results for FSK are compared to the analogous results for DPSK in Chapter 3. We show that, in some cases, the limiting error performance of FSK is dependent on parameters that are closely related to the key parameters for DPSK. We then focus on the frequency-domain characterization of the fading channel and identify the system parameters which provide an indication of

average error probability with respect to the degree of frequency-selectivity and the degradation due to additive noise.

### 4.2.1 Effects of Intersymbol Interference: Characterization

Consider the effects of the interference from the signal corresponding to $b_{-1}$ on the detection process for the signal corresponding to $b_0 = +1$. If we consider the portions of the received signal corresponding to positive propagation delays only, the decision statistic in (4.2) is given by $Z_0 = |U|^2 - |V|^2$ with the random variables U and V given by

$$U = \sqrt{\frac{8E}{T}} \int_0^T v^*(t) e^{j\pi th/T} \int_0^T h(t,\xi) \cdot \left[ v(t-\xi) e^{-j\pi h(t-\xi)/T} + v(t+T-\xi) e^{-j[b_{-1}\pi h(t-\xi)/T + \Theta(-1,b_{-1})]} \right] d\xi dt \quad (4.13a)$$

and

$$V = \sqrt{\frac{8E}{T}} \int_0^T v^*(t) e^{-j\pi th/T} \int_0^T h(t-T,\xi) \left[ v(t-\xi) e^{-j\pi h(t-\xi)/T} + v(t+T-\xi) e^{-j[b_{-1}\pi h(t-\xi)/T + \Theta(-1,b_{-1})]} \right] d\xi dt. \quad (4.13b)$$

Using (2.4), (2.5) and (4.7), the moments $m_{UU}$ and $m_{VV}$ are found to be

$$m_{UU} = \frac{16\sigma^2 E}{T} \int_0^T g(\xi) \cdot \left[ |\bar{R}_v(h,1,\xi)|^2 + |R_v(h,b_{-1},\xi)|^2 + 2\mathrm{Re}\{ e^{-j[\Theta_T(0,\underline{b}_0) - (1-b_{-1})\pi h\xi/T]} \cdot \bar{R}_v(h,1,\xi) \cdot R_v^*(h,b_{-1},\xi) \} \right] d\xi \quad (4.14a)$$

and

$$m_{VV} = \frac{16\sigma^2 E}{T} \int_0^T g(\xi) \cdot \left[ |\bar{R}_v^*(h,-1,\xi)|^2 + |R_v^*(h,-b_{-1},\xi)|^2 + 2\mathrm{Re}\{ e^{-j[\Theta_T(0,\underline{b}_0) - (1-b_{-1})\pi h\xi/T]} \cdot \bar{R}_v^*(h,-1,\xi) \cdot R_v(h,-b_{-1},\xi) \} \right] d\xi. \quad (4.14b)$$

In view of the complicated form of (4.14a) and (4.14b), it is useful to consider the evaluation of these moments for specific examples of signaling formats. In particular, for the case when the modulation index h is integer-valued and v(t) is the rectangular pulse given by (3.2), the autocorrelation functions in (4.10) are given simply as

$$\bar{R}(h,b,\xi) = \begin{cases} T - \xi & ; \ b = 1 \\ -\xi e^{j\pi h\xi/T} \cdot \mathrm{sinc}(h\xi/T) & ; \ b = -1 \end{cases} \tag{4.15a}$$

and

$$R(h,b,\xi) = \begin{cases} \xi & ; \ b = 1 \\ \xi e^{j\pi h\xi/T} \cdot \mathrm{sinc}(h\xi/T) & ; \ b = -1 \ , \end{cases} \tag{4.15b}$$

where $\mathrm{sinc}(x) = \sin(\pi x)/(\pi x)$. The bracketed terms appearing in (4.14) depend only on the transition phase $\theta_T(0,\underline{b}_0)$ and the functions in (4.15). For this example, the terms appearing in the expression for $m_{UU}$ are given by

$$T^2, \qquad \text{if } b_{-1} = 1, \tag{4.16a}$$

and

$$(T-\xi)^2 + \xi^2 \mathrm{sinc}^2(h\xi/T) + 2(T-\xi)\xi\cos(\theta_T(0,b_0)-\pi h\xi/T)\,\mathrm{sinc}(h\xi/T), \qquad \text{if } b_{-1} = -1. \tag{4.16b}$$

Similarly, the bracketed terms for $m_{VV}$ in (4.14b) become

$$0, \qquad \text{if } b_{-1} = 1 \tag{4.17a}$$

and

$$\xi^2 + \xi^2 \mathrm{sinc}^2(h\xi/T) - 2\xi\cos(\Theta_T(0,b_0) - \pi h\xi/T)\xi\,\mathrm{sinc}(h\xi/T), \text{ if } b_{-1} = -1. \quad (4.17b)$$

Under the assumption that the delay power-density spectrum $g(\xi)$ is symmetric, it is easy to see that similar expressions result from the consideration of the signal components corresponding to negative delays and the effects of the signal corresponding to $b_{i+1}$.

By examining (4.16) and the expression for $Z_i$ in (4.2), we can interpret $m_{UU}$ as the average "power" in the desired signal component of the received signal when a space signal is transmitted. Similarly, $m_{VV}$ represents the average power in the interfering (undesired) component of the received signal. (The roles of $m_{UU}$ and $m_{VV}$ are simply reversed if the desired signal happens to be a mark signal.) Notice that (4.17a) indicates that no intersymbol interference is produced by the successive transmission of $(b_{-1},b_0)$ if $b_{-1} = b_0$, while if $b_{-1} = -b_0$, the intersymbol interference produced by the data pulse preceding $b_0$ is given by the integral of (4.17b).

Now consider the output of the matched filters for both positive and negative delays for the transmitted sequence $\underline{b}_i = (+1,+1,+1)$ in the absence of additive noise. For the rectangular pulse waveform and integer-valued modulation index, we see from (4.7), (4.16), and (4.17) that the moments $m_{UU}$, $m_{VV}$, and $m_{UV}$ are given by

$$m_{UU}(+1,+1,+1) = \frac{16\sigma^2 E}{T}\int_0^T g(\xi)\cdot[\,2T^2]\,d\xi = 32\sigma^2 ET, \quad (4.18a)$$

$$m_{VV}(+1,+1,+1) = 0, \quad (4.18b)$$

and

$$m_{UV}(+1,+1,+1) = 0\ . \quad (4.18c)$$

Hence, the total average power at the output of the space signal filter in the absence of data modulation is given by (4.18a) as $32\sigma^2 ET$. Using (4.18a) and (4.17b), we see that the portion of detector output due to interfering signals relative to the <u>total</u> output is

$$\frac{m_{VV}(-1,+1,-1)}{m_{UU}(+1,+1,+1)} = T^{-2}\cdot\int_0^T g(\xi)\left[\,\xi^2 + \xi^2\,\mathrm{sinc}^2(h\xi/T)\right.$$

$$\left.-\xi[\cos(\theta_T(0,b_0)-\pi h\xi/T)+\cos(\theta_T(1,b_1)-\pi h\xi/T)]\xi\,\mathrm{sinc}(h\xi/T)\,\right]d\xi\ . \quad (4.19)$$

From the discussion above, we conclude that the effects of intersymbol interference are well characterized by

$$\mu_v(h,\theta) = \sqrt{\frac{m_{VV}(-1,+1,-1)}{m_{UU}(+1,+1,+1)}}\ , \quad (4.20)$$

which we take as the definition of the <u>normalized rms multipath spread</u> for FSK communications in frequency-selective fading. From (4.19) it is clear that $\mu_v(h,\theta)$ in (4.20) depends on the phase transitions $\theta_T(i,\underline{b}_i)$ as well as the modulation index h.

If it is assumed that the delay power-density spectrum $g(\xi)$ is a unimodal function, (4.19) provides a means to predict the role of the modulation index and the phase transitions in determining the effects of intersymbol interference. A positive, real-valued function f(x) is said to be unimodal if f is non-increasing for increasing $|x|$. For example, the four models of delay spectra discussed in Chapter 2 are unimodal functions. If $g(\xi)$ is unimodal and h is integer valued, it is easy to show, using (4.19), that the sensitivity to the effects of intersymbol interference is <u>minimized</u> if the common phase transition $\theta_T = 0$ (i.e., CPFSK). Similarly, (4.19) indicates that the effects of intersymbol interference are <u>maximized</u> when $\theta_T = \pi$, which

is the limiting case of phase-discontinuous FSK. These results are in agreement with the irreducible error probabilities shown in Fig. 4.3 for the rectangular pulse with h = 1. For this example, the assumptions $\theta_T = 0$ and $\theta_T = \pi$ produce limiting error probabilities that can differ by more than an order of magnitude. From this discussion, it is also clear that, for unimodal delay densities and integer-valued modulation indices, the irreducible error probability for random phases must lie between the values of $P_I$ for $\theta_T = 0$ and $\theta_T = \pi$.

As the modulation index increases, (4.19) indicates that the normalized rms multipath spread becomes less dependent on the phase transition $\theta_T$. In fact, it is easy to show that for increasing h, the normalized rms multipath spread given by (4.20) approaches

$$\mu_v(\infty,0) = \left[ 2T^{-2}\int_0^T g(\xi)\cdot\xi^2 \, d\xi \right]^{1/2} = M/T, \tag{4.21}$$

where M is the rms delay defined in (2.3). We conclude that for large modulation index and fixed rms delay, the irreducible error probability as a function of M/T becomes independent of the shape of the delay density as well as the phase transition $\theta_T$.

Now suppose that the modulation index is some fixed integer. If $g(\xi)$ is unimodal, then for large values of rms delay, the value of $\mu_v(h,\theta)$ is dominated by $2TM^2 = 2T^2\mu_v(\infty,0)$, which corresponds to the integral of the $\xi^2$ term in (4.19). This may be seen by noting that the integral of the sinusoidal terms in (4.19) becomes small for increasingly wide delay spectra. Alternatively, as the rms delay (and hence the first term in (4.19)) becomes small, the sinusoidal terms become significant so that $\mu_v(h,\theta)$ is influenced by the shape of the delay density as well as the phase transition $\theta_T$. The

irreducible error probabilities in Fig. 4.4 for h = 10 provide a good example of the behavior of systems with large modulation indices. Notice that $P_I$ for this example depends on the shape of the delay spectrum only for rms delays less than 0.01.

We next examine the characteristics of the parameters discussed above for an example of non-orthogonal signals. In particular, for rectangular pulse CPFSK with h = 1/2 (i.e., MSK), $m_{UU}(+1,+1,+1) = 32\sigma^2 ET$ as before. However, the normalized rms multipath spread is given by

$$\mu_v^2(h,\cdot) = T^{-2}\int_0^T g(\xi)\left(\xi^2+\left[\frac{\cos(\pi\xi/2T)}{\pi/2T}\right]^2-2\xi\cos(\pi/2+\pi\xi/2T)\left[\frac{\cos(\pi\xi/2T)}{\pi/2T}\right]\right)d\xi. \quad (4.22)$$

By comparing (4.22) and (4.19), we see that if the delay density is unimodal, MSK is considerably more sensitive to the effects of intersymbol interference than signals with integer-valued modulation index. It can be shown that this increased sensitivity is partly due to the lack of orthogonality between the two MSK signals. Notice that, in the absence of additive noise, (4.8b) becomes

$$m_{VV} = \frac{32\sigma^2 E}{T}\int_0^T g(\xi)\left(\left[\frac{\cos(\pi\xi/2T)}{\pi/2T}\right]^2+\xi^2\,\mathrm{sinc}^2(\xi/2T)\right)d\xi = 32\sigma^2 ET\cdot\left[\frac{4}{\pi^2}\right] \quad (4.23)$$

for $\underline{b}_i = (+1,+1,+1)$. Equation (4.23) implies that if three consecutive space signals are transmitted, the output of the mark signal filter is more than half that of the space filter, a property which holds even for nonfading channels. In comparison, recall from (4.18b) that for integer-valued modulation index, $m_{VV}(+1,+1,+1) = 0$. This result and the data presented in Fig. 3.3 suggest that MSK signals are of little interest for noncoherent detection, especially for applications to frequency-selective fading channels.

In Table 4.1, numerical values of the normalized rms multipath spread defined by (4.20) are shown as a function of the rms delay M for the Gaussian delay power-density spectrum. The results are listed for signals with modulation indices h = 1, 2, and 10, for $\Theta_T = 0$ (CPFSK) and $\Theta_T = \pi$. Notice that in the case of CPFSK, there is substantial variation between the normalized rms multipath spreads for different modulation indices. In fact, for very small values of rms delay, this variation is nearly equal to h. Also notice that in all cases, the difference between the values of normalized rms multipath spread for $\Theta_T = 0$ and $\Theta_T = \pi$ are very large. It is also interesting to note that for the case when $\Theta_T = \pi$, there is almost no variation for different modulation indices. Numerical evaluations of the normalized rms multipath spread for MSK signals revealed that this parameter ranges between 0.64 for M/T = 0.001 and 0.82 for M/T = 0.5, indicating that the parameter $\mu_v(h,\Theta_T)$ is not a useful measure of the effects of intersymbol interference for this case.

For the consideration of phase-coded pulses, it is much more difficult to derive analytical expressions which provide insight to the character of the normalized rms multipath spread $\mu_v(h,\theta)$. Alteratively, consider the moment $m_{UU}$ in (4.7) for the phase-coded pulse with modulation index h = N, where N is the sequence length. If we neglect the terms corresponding to the additive noise, $m_{UU}(+1,+1,+1)$ is given by

$$m_{UU} = \frac{16\sigma^2 E}{T} \int_0^T g(\xi) \cdot 2[\bar{R}_p^2(h,1,\xi) + R_p^2(h,1,\xi) + 2\bar{R}_p(h,1,\xi) R_p(h,1,\xi)]\, d\xi. \qquad (4.24)$$

Recall that $\bar{R}_p(h,1,\xi)$ and $R_p(h,1,\xi)$ are given by $\bar{R}_p(\xi)$ and $R_p(\xi)$, respectively, where these latter functions are the autocorrelation functions given by (3.10) for the analysis of DPSK. Hence, in the absence of data

Table 4.1. Normalized rms multipath spread $\mu_v(h,\theta_T)$ as a function of the rms delay M for rectangular pulse FSK with $\theta_T = 0$ and $(\theta_T = \pi)$

| M/T | h = 1 | h = 2 | h = 10 |
|---|---|---|---|
| 0.001 | $7.4081 \cdot 10^{-6}$<br>$(2.3915 \cdot 10^{-3})$ | $1.4814 \cdot 10^{-5}$<br>$(2.3914 \cdot 10^{-3})$ | $7.4049 \cdot 10^{-5}$<br>$(2.3896 \cdot 10^{-3})$ |
| 0.005 | $1.3602 \cdot 10^{-4}$<br>$(9.9984 \cdot 10^{-3})$ | $2.7192 \cdot 10^{-4}$<br>$(9.9938 \cdot 10^{-3})$ | $1.3419 \cdot 10^{-3}$<br>$(9.8481 \cdot 10^{-3})$ |
| 0.01 | $5.4384 \cdot 10^{-4}$<br>$(1.9988 \cdot 10^{-2})$ | $1.0859 \cdot 10^{-3}$<br>$(1.9950 \cdot 10^{-2})$ | $5.1151 \cdot 10^{-3}$<br>$(1.8839 \cdot 10^{-2})$ |
| 0.05 | $1.0001 \cdot 10^{-2}$<br>$(9.8481 \cdot 10^{-2})$ | $2.5776 \cdot 10^{-2}$<br>$(9.4197 \cdot 10^{-2})$ | $5.4470 \cdot 10^{-2}$<br>$(5.5126 \cdot 10^{-2})$ |
| 0.1 | $5.0002 \cdot 10^{-2}$<br>$(1.8839 \cdot 10^{-1})$ | $8.6507 \cdot 10^{-2}$<br>$(1.6123 \cdot 10^{-1})$ | $1.0250 \cdot 10^{-1}$<br>$(1.0250 \cdot 10^{-1})$ |
| 0.5 | $5.0000 \cdot 10^{-1}$<br>$(4.8907 \cdot 10^{-1})$ | $4.5710 \cdot 10^{-1}$<br>$(4.5099 \cdot 10^{-1})$ | $4.4052 \cdot 10^{-1}$<br>$(4.4026 \cdot 10^{-1})$ |

modulation, the average power at the output of the space signal filter is given by $16\sigma^2 EH_p/T$, where the parameter $H_p$ is defined by the relation (3.22). The values of $H_p/T^2$ for an m-sequence of length N = 31 are listed in Table 3.1 for a Gaussian delay density as a function of the rms delay M.

In Table 4.2, the values of the $\mu_p(h,\theta)$ with h = N are shown for phase-coded pulses with sequence lengths N = 7 and 31. Also listed in Table 4.2 are the values of $\mu_p(h,\theta)$ for modulation index h = 1 (shown in parentheses). In each case the results are obtained for $\theta_T = 0$. Surprisingly, these results indicate that the normalized rms multipath spreads are generally smaller for h = 1 than for h = N. From the similarity of the results for h = N and h = 1, we conclude that the sensitivity to the effects of intersymbol interference is largely determined by the autocorrelation properties of the phase-coded pulse waveform rather than the value of the modulation index. From this we might also assume that the normalized rms multipath spread is relatively independent of the phase transition $\theta_T$. The evaluation of $\mu_p(h,\theta_T)$ with $\theta_T = \pi$ for the cases listed in Table 4.2 shows that $\mu_p(h,\pi)$ differs from the values listed in Table 4.2 by at most a factor of two. Also notice that there is no clear dependence of $\mu_v(h,\theta_T)$ on the sequence length, N. Finally, we point out that in comparison to the corresponding results for phase-coded DPSK listed in Table 3.3, it is clear that phase-coded pulse FSK is, in general, much more sensitive to the effects of intersymbol interference.

The discussion leading to the expression for $m_{UV}$ in (4.18c) also provides an interesting interpretation of the role of this parameter in determining the performance of FSK. Recall from Chapter 2 that the rms delay M is related to the bandwidth of the frequency correlation function $G(\Omega)$. For small rms delays (large frequency-correlation bandwidths), there is significant

Table 4.2. Normalized rms multipath spread $\mu_v(h,0)$ as a function of the rms delay M for phase-coded pulse FSK for N = 7,31 with h = N and (h = 1)

| M/T | N = 7 | N = 31 |
|---|---|---|
| 0.001 | $9.6176 \cdot 10^{-3}$ ($3.3950 \cdot 10^{-3}$) | $3.8895 \cdot 10^{-2}$ ($4.4933 \cdot 10^{-3}$) |
| 0.005 | $4.1005 \cdot 10^{-2}$ ($1.4575 \cdot 10^{-2}$) | $1.6159 \cdot 10^{-1}$ ($2.0919 \cdot 10^{-2}$) |
| 0.01 | $8.2911 \cdot 10^{-2}$ ($3.0111 \cdot 10^{-2}$) | $2.7283 \cdot 10^{-1}$ ($4.7569 \cdot 10^{-2}$) |
| 0.05 | $3.1451 \cdot 10^{-1}$ ($1.9762 \cdot 10^{-1}$) | $3.8556 \cdot 10^{-1}$ ($2.5002 \cdot 10^{-1}$) |
| 0.1 | $4.0232 \cdot 10^{-1}$ ($3.9451 \cdot 10^{-1}$) | $4.0257 \cdot 10^{-1}$ ($4.3055 \cdot 10^{-1}$) |
| 0.5 | $7.0356 \cdot 10^{-1}$ ($8.3483 \cdot 10^{-1}$) | $6.9406 \cdot 10^{-1}$ ($9.2494 \cdot 10^{-1}$) |

correlation between the fading processes acting on the two signals. The parameter that characterizes the relationship between the effect of frequency correlation and the orthogonality of the transmitted signals is $m_{UV}(+1,+1,+1)$, (or more precisely, $m_{UV}(+1,+1,+1)/m_{UU}(+1,+1,+1)$). For the rectangular pulse waveform and integer-valued modulation index, we see from (4.18c) that $m_{UV}/m_{UU} = 0$. In contrast, it is easy to see from (4.7c), that for MSK signals,

$$m_{UV}(+1,+1,+1)/m_{UU}(+1,+1,+1) = \frac{T^{-2}}{2}\int_0^T g(\xi)\cdot\left[\frac{2jT^2}{\pi}\right] d\xi \ , \qquad (4.25)$$

which not only shows that the received signals are highly correlated but also shows that the value of the correlation is independent of both g and M. Notice that the square of the magnitude of (4.25) corresponds to the result in (4.24), confirming that the lack of orthogonality of MSK signals is a significant factor in determining resulting error probability for both selective and nonselective fading channels. Finally, we point out that the close relationship between the values of $m_{UV}(+1,+1,+1)$ and $m_{VV}(+1,+1,+1)$ for the rectangular pulse waveform does not hold for phase-coded pulse waveforms. In fact, for N = 31 and Gaussian delay density with M/T = 0.001, numerical evaluations of these parameters reveal that $m_{UV} \tilde{=} m_{VV}/10$ and $m_{UV} \tilde{=} m_{VV}/100$ for h = 31 and h = 1, respectively.

The discussion leading to the definition of the normalized rms multipath spread in (4.20) and the results in Tables 4.1 and 4.2 suggest that the normalized rms multipath spread is a good indicator of the effects of intersymbol interference for both rectangular pulse and phase-coded pulse with integer-valued modulation index. Since the irreducible error probability is the performance parameter most dependent on the effects of intersymbol

interference, we expect that if the delay spread is normalized with respect to $\mu_v(h,\theta_T)$, $P_I$ should exhibit minimal sensitivity to either the signal format or the shape of the delay power-density spectrum $g(\xi)$. Numerical evaluations of $P_I$ as a function of the normalized rms multipath spread show that of all examples of pulse waveform, modulation index, and delay density considered, the cases exhibiting the most variation are rectangular pulse waveforms with h = 1 for $\theta_T = 0$ and $\theta_T = \pi$. The irreducible error probabilities for these two cases are shown in Fig. 4.5 as a function of $\mu_r(h,\theta_T)$ for the Gaussian, exponential, and triangular delay densities. Notice that even for these extreme cases the maximum variation for fixed normalized rms multipath spread is less than a factor of 1.4. These results show that the limiting error probability is almost completely determined by the normalized rms multipath spread $\mu_v(h,\theta_T)$ defined in (4.20).

Before concluding the discussion on the characterization of the effects of intersymbol interference, it is interesting to draw comparisons between the normalized rms multipath spread parameters for DPSK and FSK. In particular, notice from (3.23) and (4.21), that for large h, the parameter $\mu_v(h,\theta) = \mu_r$ which is the normalized rms multipath spread for rectangular pulse DPSK. Thus, for fixed rms delay M and sufficiently large modulation index, the irreducible error probability for rectangular pulse DPSK is a good approximation for $P_I$ for FSK.

Next, notice that the parameter $\mu_s$ for sine pulse DPSK is given by

$$\int_0^T g(\xi)\left[\xi^2\cos^2(\pi\xi/T) + 2\xi^2\mathrm{sinc}^2(\xi/T) - 2\xi^2\cos(\pi\xi/T)\mathrm{sinc}(\xi/T)\right]d\xi \ . \quad (4.26)$$

For the case when the phase transition $\theta_T = 0$, (4.20) becomes (except for a constant factor),

AD-A142 427 PERFORMANCE OF DIGITAL COMMUNICATIONS OVER SELECTIVE FADING CHANNELS(U) ILLINOIS UNIV AT URBANA COORDINATED SCIENCE LAB F D GARBER SEP 83 R-998 N00014-79-C-0424 2/2

UNCLASSIFIED F/G 17/2.1 NL

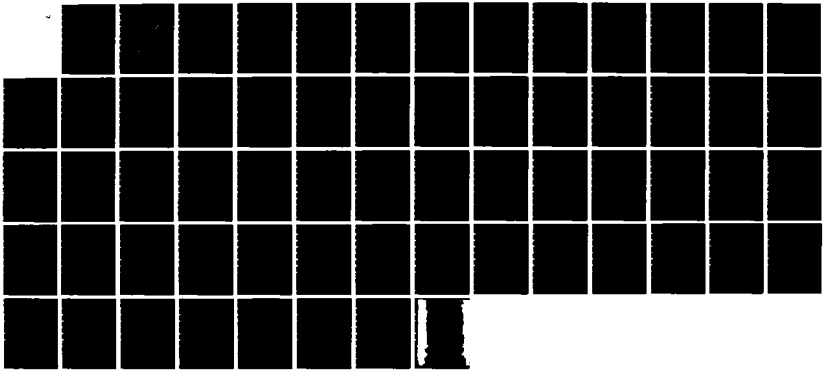

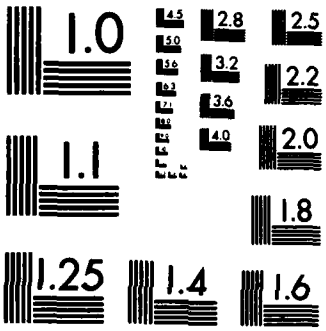

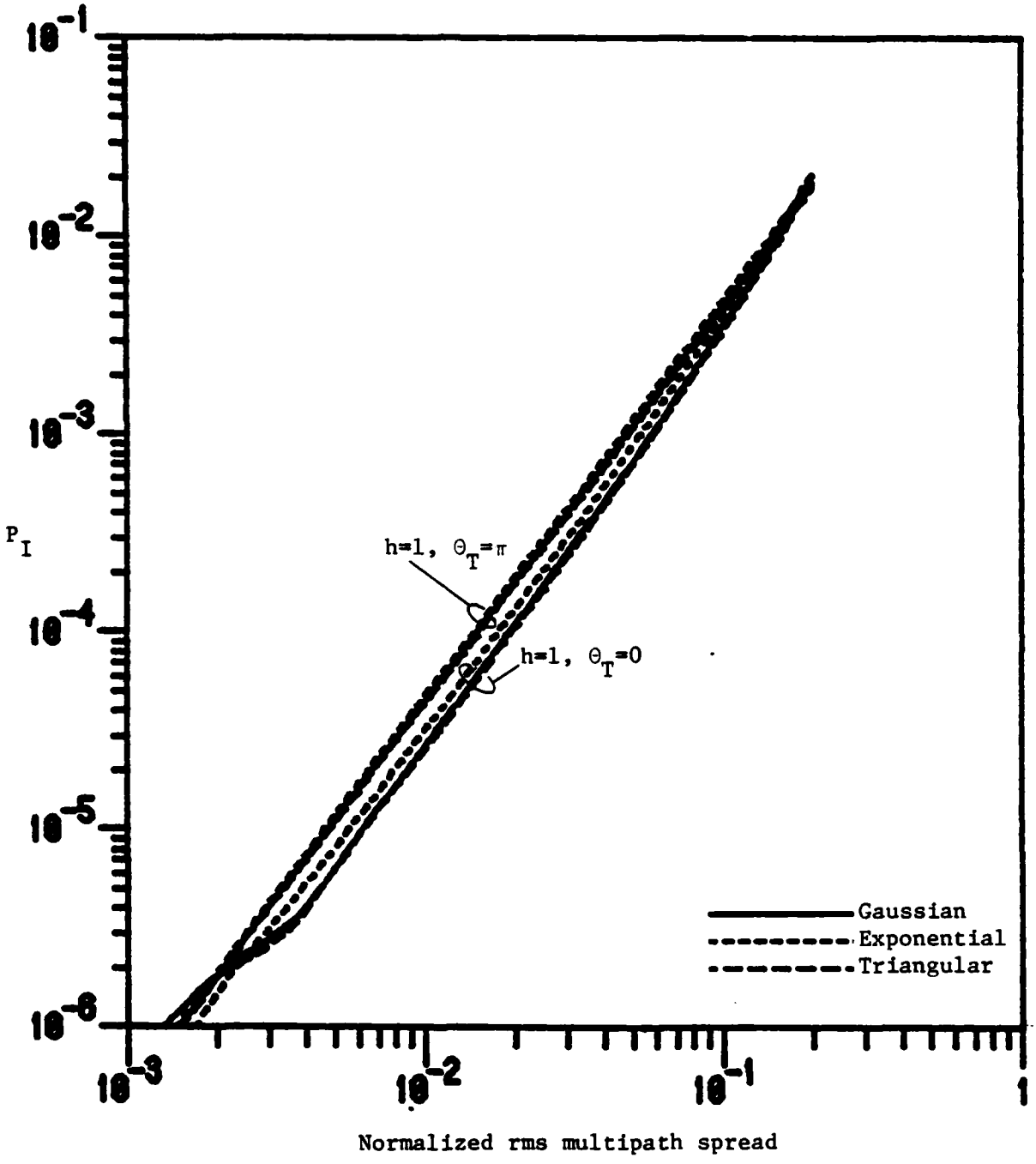


**Figure 4.5. Irreducible error probabilities for rectangular pulse FSK with h = 1 vs. $\mu_p(h,\Theta_T)$ for $\Theta_T = \pi$ and $\Theta_T = 0$**

$$\int_0^T g(\xi) \left[\xi^2 + 2\xi^2 \mathrm{sinc}^2(\xi/T) - 2\xi^2 \cos(\pi\xi/T)\mathrm{sinc}(\xi/T)\right] d\xi. \qquad (4.27)$$

Hence, we see that sine-pulse DSPK is considerably less sensitive to intersymbol interference effects than FSK for any integer-valued modulation index, even for the minimizing case of phase transition, $\theta_T = 0$.

### 4.2.2 Effects of Intersymbol Interference: Bounds

As in the consideration of DPSK in Chapter 3, the insensitivity of the irreducible error probability for FSK as a function of the normalized rms multipath spread suggests the possibility of obtaining useful bounds on the probability of error with respect to the parameters of the fading channel. In this section, the method of obtaining bounds on the irreducible error probability for DPSK communications in a frequency-selective Rayleigh fading environment is applied to the evaluation of $P_I$ for FSK.

It is clear from the definition of $\mu_v(h,\theta_T)$ in (4.20) and the discussion above that the normalized rms multipath spread is dependent on the phases $\theta_T(i,-1)$ and $\theta_T(i+1,-1)$. However, the results in the previous section indicate that $\theta_T(i,-1) = \theta_T(i+1,-1) = \theta_T = 0$ and $\theta_T(i,-1) = \theta_T(i+1,-1) = \theta_T = \pi$ in some sense represent limiting cases in terms of the normalized rms multipath spread. In what follows, the bounds for the irreducible error probability are considered for these cases only. The resulting bounds for these cases are representative of, if not limits for, the results for other choices of phases.

#### 4.2.2.1 Rectangular pulse

Under the assumption of adjacent-pulse-limited ISI, the moments defined in (4.7) can be written (for integer-valued modulation index) as

$$m_{UU}(\underline{b}_i) = 16\sigma^2 E/T \cdot \left[ 2T^2 + (I\{b_{i-1}=-1\} + I\{b_{i+1}=-1\}) f'(g) \right] , \tag{4.28a}$$

$$m_{VV}(\underline{b}_i) = 16\sigma^2 E/T \cdot \left[ (I\{b_{i-1}=-1\} + I\{b_{i+1}=-1\}) \cdot T^2 \mu_v^2(h,\theta_T) \right] , \tag{4.28b}$$

and

$$m_{UV}(\underline{b}_i) = 16\sigma^2 E/T \cdot \left[ I\{b_{i-1}=-1\} \cdot f''^*(g) + I\{b_{i+1}=-1\} f''(g) \right] , \tag{4.28c}$$

where the normalized rms multipath spread $\mu_v(h,\theta_T)$ is given by (4.20), and $I\{\cdot\}$ is the indicator function. The functionals $f'(g)$ and $f''(g)$ in (4.28) are given by

$$f'(g) = \int_0^T g(\xi) \left[ \xi^2 - 2\xi T + \xi^2 \mathrm{sinc}^2(\xi/T) + 2(T-\xi)\xi^2 \cos(\pi\xi/T + \theta_T) \mathrm{sinc}(\xi/T) \right] d\xi , \tag{4.29}$$

and

$$f''(g) = \int_0^T g(\xi) \left[ 2(\xi - T)\xi e^{j(\pi h \xi/T)} \cdot \mathrm{sinc}(\xi/T) + \cos(\theta_T)(T-\xi)\xi^2 \cdot \mathrm{sinc}(\xi/T) - \xi^2 \cos(\theta_T) \mathrm{sinc}^2(\xi/T) \right] d\xi . \tag{4.30}$$

Thus we may proceed as in Chapter 3 by characterizing the functions $f'(g)$ and $f''(g)$ for delay spectra $g(\xi)$ satisfying the constraint, given by

$$T^{-2} \int_0^T g(\xi) \left[ \xi^2 + \xi^2 \mathrm{sinc}^2(\xi/T) - 2\xi^2 \cos(\theta_T - \pi\xi/T) \mathrm{sinc}(\xi/T) \right] d\xi = \mu_v^2(h,\theta_T) . \tag{4.31}$$

Notice that $f''$ is, in general, a complex-valued function of $g$. From (4.5) and (4.6) we see that the average probability of error depends on the moment $m_{UV}(\underline{b}_i)$ only through its magnitude. Hence, in order to obtain bounds for the

error probability, it is necessary to characterize the range of values of $|f''(g)|$ for g satisfying (4.31). Recall from Chapter 3 that the minimum and maximum values of a continuous linear functional are found by searching over the set of extremal g. Since $|f''(g)|$ represents a non-linear functional of g, this technique cannot be directly applied to find the minimum and maximum of $|f''|$. However, it can be shown, through an application of the triangle inequality, that the maximum of $|f''(g)|$ for g satisfying (4.31) is obtained for some extreme g. The characterization of the possible values of $|f''|$ is completed by assuming that the minimum of $|f''(g)|$ is zero. Also, notice that if $b_{i-1} = b_{i+1} = -1$, $m_{UV}$ depends only on $f'' + f''^{*} = 2Re\{f''\}$ so that the problem of a non-linear functional does not arise in this case. The resulting bounds for the limiting error probability are found by searching over the volume

$$\bar{Q} = \{ [f'_{min}, f'_{max}] \times [0, |f''|_{max}] \times [2Re\{f''\}_{min}, 2Re\{f''\}_{max}] \}.$$

Numerical evaluations of the resulting bounds for the irreducible error probability reveal that the maximum variation between the upper and lower bounds for fixed $\mu_r(h,\theta_T)$ occurs for the case $h = 1$ and $\theta_T = 0$. The results for this case are shown in Fig. 4.6 as a function of $\mu_r(1,0)$. Notice that the maximum variation for this example is still less than a factor of 3. We point out that the bounds in Fig. 4.6 not only represent the case of the maximum variation, but also represent upper and lower bounds for all examples of rectangular pulse waveforms considered. That is, the bounds for rectangular pulse FSK, with modulation indices h = 1, 2, and 10 for the cases $\theta_T = 0$ and $\theta_T = \pi$, all lie between the bounds shown in Fig. 4.6.

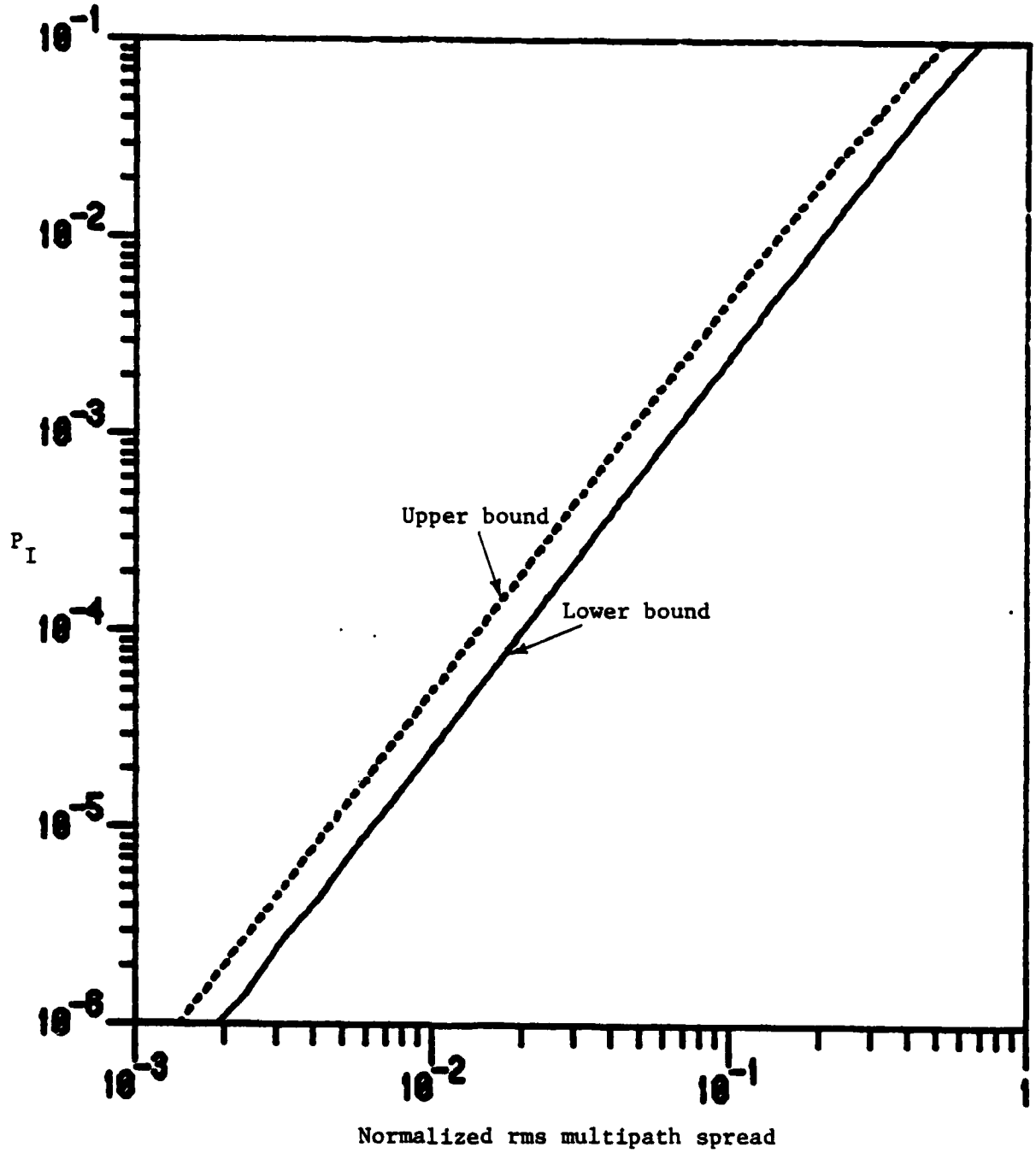


**Figure 4.6. Irreducible error probability bounds for rectangular pulse FSK with h = 1, and $\Theta_T = 0$**

4.2.2.2 Phase-coded pulse

The task of obtaining bounds for the irreducible error probability for phase-coded pulse FSK is more difficult than for DPSK since $P_I$ for FSK depends on essentially twice as many parameters (a number of which are complex valued) as the limiting error probability for DPSK. Under the assumption of adjacent-pulse-limited ISI, the function $m_{VV}(-1,+1,-1)$ can be written as

$$m_{VV}(-1,+1,-1) = \mu_p^2(h,\theta_T)H_p \ . \tag{4.32}$$

As in the case for phase-coded pulse DPSK, there is no obvious way to characterize the moments $m_{UU}(\underline{b}_i)$, $m_{VV}(\underline{b}_i)$, and $m_{UV}(\underline{b}_i)$ in terms of the normalized rms multipath spread $\mu_p(h,\cdot)$ and a few linear functionals of $g$. Also, we have seen that $m_{UU}(+1,+1,+1)$, which is closely related to the parameter $H_p$ defined in (3.22) is dependent on the shape of the delay power-density spectrum. Moreover, unless the rms delay is zero, both $m_{UV}(+1,+1,+1)$ and $m_{VV}(+1,+1,+1)$ can be significant in the determination of the irreducible error probability.

However, representative bounds on the irreducible error probability can be obtained by assuming a specular multipath model for the fading channel, as in Chapter 3, with a sampling epoch chosen so that a path with average power of at least $1/2N$ of the total power of the delay spectrum corresponds to a zero relative delay. We proceed by using the model for the discrete density spectrum $g(kT_c)$ and rewriting the equivalent signal-to-noise ratio $\gamma(\underline{b}_i)$ in (4.6) as

$$\frac{2|m_{UU}(\underline{b}_i)-m_{VV}(\underline{b}_i)|}{\sqrt{(m_{UU}(\underline{b}_i)-m_{VV}(\underline{b}_i))^2 + 4[m_{UU}(\underline{b}_i)m_{VV}(\underline{b}_i)-|m_{UV}(\underline{b}_i)|^2]} - |m_{UU}(\underline{b}_i)-m_{VV}(\underline{b}_i)|} \ . \tag{4.33}$$

The bounds for the irreducible error probability are found by characterizing the minimum and maximum values of the parameters $(m_{UU}(\underline{b}_i)-m_{VV}(\underline{b}_i))$ and $(m_{UU}(\underline{b}_i)m_{VV}(\underline{b}_i)-|m_{UV}(\underline{b}_i)|^2)$ for each combination of the interfering data bits $(b_{i-1}$ and $b_{i+1})$ under the constraint

$$m_{VV}(-1,+1,-1) = \mu_p^2(h,\theta_T)H_p \ .$$

Using the assumed symmetry properties of the delay spectrum $g(kT_c)$, the search for the minimum and maximum irreducible error probability can be reduced to the six-dimensional search over the limiting values of the two functions described above for the cases $b_{i-1}=b_{i+1}=1$, $b_{i-1}=b_{i+1}=-1$, and $b_{i-1}=-b_{i+1}$. The resulting bounds for the irreducible error probability of phase-coded pulse waveforms are given in Tables 4.3 and 4.4, respectively, for m-sequences of length N = 7 and N = 31 discussed above. Notice that the variation between upper and lower bounds is not large, and that the bounds for the phase-coded pulse are very similar to those obtained for the rectangular pulse above.

### 4.2.3 Effects of Additive Noise: Characterization

Consider the response of the space and mark filters (producing the sampled outputs U and V) to a single transmitted data pulse signal,

$$s(t) = \sqrt{\frac{2E}{T}}\ v(t)e^{-jb_0\pi ht/T} \ ; \ 0 \le t \le T \ ,$$

where E is the energy per data bit. In the absence of additive noise and assuming a space signal is sent, the second moments of the outputs of the space and mark filters are given by

$$m_{UU} = \frac{16\sigma^2E}{T}\int_{-\infty}^{\infty} g(\xi)\ |\bar{R}_v(h,1,|\xi|)|^2\ d\xi$$

$$= \frac{16\sigma^2E}{T}\int_{-\infty}^{\infty} G(\Omega)\ [|V(\Omega)|^2 \circledcirc |V(\Omega)|^2]\ d\Omega \ , \qquad (4.34a)$$

Table 4.3. Irreducible error probability bounds for N = 7 phase-coded pulse FSK with respect to the normalized rms multipath spread $\mu_p(h,\theta)$, for h = 7, and $\theta_T = 0$

| $\mu_p(h,\theta)$ | Lower Bound | Upper Bound |
|---|---|---|
| 0.0005 | $1.2499 \cdot 10^{-7}$ | $1.2504 \cdot 10^{-7}$ |
| 0.001 | $4.9999 \cdot 10^{-7}$ | $5.0060 \cdot 10^{-7}$ |
| 0.005 | $1.2499 \cdot 10^{-5}$ | $1.2887 \cdot 10^{-5}$ |
| 0.01 | $4.9998 \cdot 10^{-5}$ | $5.6829 \cdot 10^{-5}$ |
| 0.05 | $1.2488 \cdot 10^{-3}$ | $4.9551 \cdot 10^{-3}$ |

Table 4.4. Irreducible error probability bounds for N = 31 phase-coded pulse with respect to the normalized rms multipath spread $\mu_p(h,\theta)$, for h = 31, and $\theta_T = 0$

| $\mu_p(h,\theta)$ | Lower Bound | Upper Bound |
|---|---|---|
| 0.0005 | $1.2499 \cdot 10^{-7}$ | $1.4131 \cdot 10^{-7}$ |
| 0.001 | $4.9999 \cdot 10^{-7}$ | $9.2896 \cdot 10^{-7}$ |
| 0.005 | $1.2499 \cdot 10^{-5}$ | $4.4880 \cdot 10^{-5}$ |

and

$$m_{VV} = \frac{16\sigma^2 E}{T} \int_{-\infty}^{\infty} g(\xi) \; |\bar{R}_v(h,-1,|\xi|)|^2 \; d\xi$$

$$= \frac{16\sigma^2 E}{T} \int_{-\infty}^{\infty} G(\Omega) \; [V(\Omega-2\pi h/T)V^*(\Omega) \circledast V^*(\Omega-2\pi h/T)V(\Omega)] \; d\Omega \; , \quad (4.34b)$$

where $V(\Omega)$ is the inverse Fourier transform of the basic pulse shape $v(t)$, and $\circledast$ denotes convolution. Notice that (4.34a) represents a measure of the common spectra between the data pulse waveform and the frequency correlation function $G(\Omega)$. Similarly, (4.34b) represents a measure of the common spectra of $v(t)$, a frequency shifted version of $v(t)$, and the correlation function $G(\Omega)$. The corresponding output of each filter due to the (real) additive white Gaussian noise with (two-sided) spectral intensity $N_0/2$ is $8N_0T$.

For a nonselective Rayleigh fading channel, the signal-to-noise ratio at the output of the space filter becomes

$$snr = \frac{2\sigma^2 E}{N_0} \; , \quad (4.35)$$

since, from (4.10a), $\bar{R}_v^2(h,1,0) = T^2$. Thus, it is easy to see that the one-shot signal-to-noise ratio at the output of the space signal filter is maximized when the rms delay spread is zero. In the case of frequency-selective fading, the signal-to-noise ratio at the output of the desired signal filter is

$$snr = \frac{2\sigma^2 E}{N_0 T^2} \int_{-\infty}^{\infty} g(\xi) \; \bar{R}_v^2(h,1,|\xi|) \; d\xi \; = \frac{2\sigma^2 E}{N_0} \; 2\bar{\eta}_v/T^2 \; . \quad (4.36)$$

Recall from (4.10a) and (3.14a), that $\bar{R}_v^2(h,1,\xi) = \bar{R}_v^2(\xi)$, so that $\bar{\eta}_v$ defined in (3.12a) for the consideration of DPSK communications is also the key parameter in determining the signal-to-noise ratio for the space signal filter for

single-pulse matched filter detection. If we neglect the effects of intersymbol interference and assume that the modulation index is sufficiently large that the signal components of both $m_{VV}$ and $m_{UV}$ are approximately zero, the average error probability (4.5) becomes

$$P_e = \left[ 2 + \frac{2\sigma^2 E}{N_0} \cdot \frac{2\bar{\eta}_v}{T^2} \right]^{-1} , \tag{4.37}$$

which is identical to (3.38) except for a factor of two appearing in the signal-to-noise ratio.

The results in Section 4.1 (see Fig. 4.2) demonstrate that for rectangular pulse FSK with integer-valued modulation index, the low signal-to-noise ratio average error probability in frequency-selective Rayleigh fading is well approximated by $P_{ns} = (2 + 2\sigma^2 E/N_0)^{-1}$ which is the probability of error for orthogonal FSK in non-selective fading. While it is not surprising that $P_{ns}$ represents a lower bound for the average error probability, it might not have been anticipated that this performance parameter for orthogonal signals would provide an adequate low signal-to-noise ratio approximation of $P_e$ for selective fading. In particular, notice from (4.35) that even in the case when a single data pulse is transmitted, the relative delays introduced by the frequency-selective channel produce non-zero outputs in both filters. Thus, in general, the transmission of a space signal also produces an output due to this signal at the mark signal filter. However, it can be shown that $P_{ns}$ is an accurate low signal-to-noise ratio approximation of the average probability of error in selective fading for rectangular pulse FSK for any integer-valued modulation index h.

The discussion above indicates that the low signal-to-noise ratio error probability is largely determined by the output due to the desired signal at

the filter matched to that signal, which in turn, depends only on the parameter $\bar{\eta}_v$. Thus, we expect that for a given pulse shape, the asymptotic error probability for small signal-to-noise ratios is well approximated by (4.37) which is independent of the modulation index h. Numerical evaluations of the average error probability in (4.4) and $P_e$ defined in (4.37) show that this is the case for both rectangular pulse and phase-coded pulse FSK, for all combinations of delay spectra, modulation indices and phase transitions considered. In fact, the average probability of error for phase-coded pulse FSK is both well approximated by (4.37) for small values of signal-to-noise ratio and lower bounded by (4.37) for all values of snr. Hence, just as for DPSK, the parameter $\bar{\eta}_v$ determines the position of the "inverse-linear" lower bound on FSK error probability as a function of signal-to-noise ratio $S = 2\sigma^2 E/N_0$. Of course, the factor of two (or 3 dB) difference between (4.37) for FSK and (3.38) for DPSK reflects the disadvantage of noncoherent versus differentially coherent detection in Rayleigh fading channels.

In Table 3.7 of Section 3.2, the values of $\bar{\eta}_v/T^2$ are listed for the rectangular pulse, and for the phase-coded pulse using the m-sequences of length N = 7, 15, 31, and 63 for a Gaussian delay power-density spectrum. It can be shown that for phase-coded pulse FSK,

$$P_e \approx \left[ 2 + \frac{2\sigma^2 E}{N_0} \cdot \frac{2k}{N} \right]^{-1} , \tag{4.38}$$

independent of the modulation index h, where N is the length of the signature sequence and the constant k depends on the channel. Moreover, the discussion in Section 3.2 concerning the performance degradation of the phase-coded pulse relative to the rectangular pulse for DPSK applies to the consideration of phase-coded pulse versus rectangular pulse FSK. In particular, Table 3.7

shows that for a Gaussian delay density with M/T = 0.1, the additional signal-to-noise ratio requirement for phase-coded pulse FSK relative to rectangular pulse FSK for fixed error probability is about 5 dB and 9 dB for sequence lengths N = 7 and N = 31, respectively.

In Figure 4.7, the average error probability for several examples of FSK signalling formats is shown as a function of the signal-to-noise ratio, S. For comparison with the results for DPSK in Figure 3.7, the results are shown for rectangular pulse FSK with modulation indices h = 1, and 10 ($\Theta_T = 0$) and phase-coded pulse FSK (N = h = 31, $\Theta_T = 0$) for the Gaussian delay power-density spectrum with rms delay M = T/10. Also shown are the low signal-to-noise ratio asymptotes given by (4.37), and the irreducible error probabilities which appear as horizontal asymptotes. (The low signal-to-noise ratio error probability given by (4.37) is identical for both examples of rectangular pulse FSK). Notice that in contrast to the results for DPSK in Section 3.2, the limiting error probability for the phase-coded pulse is considerably larger than that of either example of rectangular pulse FSK. Also notice that the rectangular pulse with h = 1 exhibits the best performance of the three FSK signals considered for the entire range of signal-to-noise ratios. These results are in agreement with the discussion leading to (4.37) which shows that the phase-coded pulse experiences severe performance degradation in the presence of additive noise; and the data presented in Tables 4.1 and 4.2 which show that the normalized rms multipath spread $\mu_v(h,\Theta_T)$ for rectangular pulse FSK (with modulation index h = 1, and phase transition $\Theta_T = 0$) is significantly smaller than the corresponding parameter for phase-coded pulse FSK.

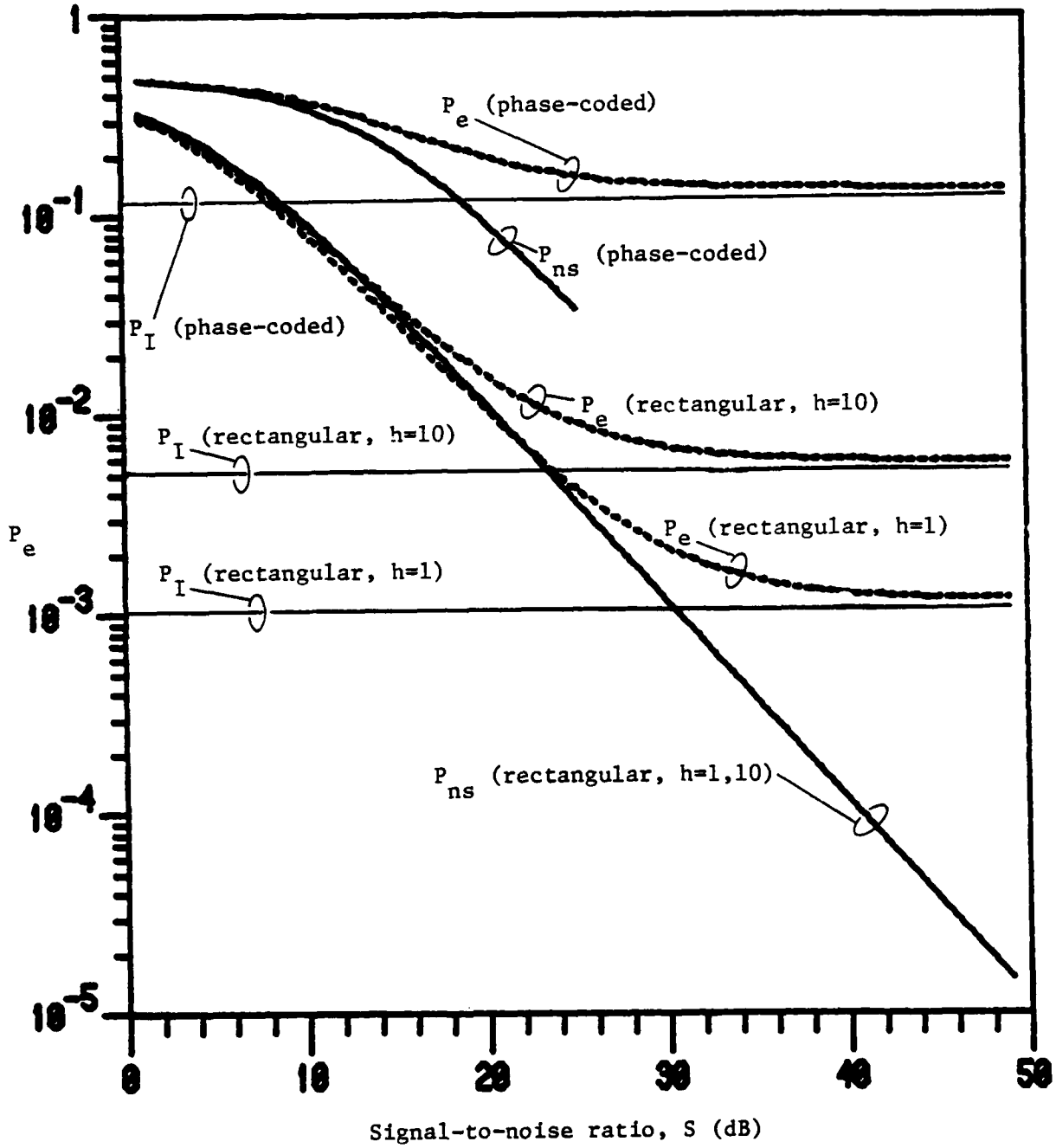


**Figure 4.7. Average error probability for rectangular pulse FSK (h = 1, 10, and $\theta_T = 0$) and phase-coded pulse FSK (N = h = 31, and $\theta_T = 0$)**

## 4.3 Performance Approximations for Other FSK Systems

In Section 4.2 it was shown that meaningful bounds for the irreducible error probability of FSK in a WSSUS frequency-selective Rayleigh fading channel can be obtained under assumptions that correspond to the characteristics of many practical systems [16,17]. These bounds demonstrate that the normalized rms multipath spread $\mu_v(h,\theta_T)$ defined in (4.20) is the key parameter in determining the limiting error probability for FSK systems. Moreover, the closeness of these bounds (for fixed normalized rms multipath spread) indicates that it is sufficient to specify only this parameter in order to obtain an accurate estimate of the irreducible error probability for a particular fading channel and FSK signalling format.

Since in many practical systems, the limiting error probability is of primary concern in the evaluation of system performance, the bounds in Section 4.2 represent a characterization of the limits of the effects of frequency-selectivity on FSK communications for a wide variety of signalling formats and frequency-selective fading channel models. As in the case of DPSK in Section 3.3, these results also imply that if it is possible to measure the normalized rms multipath spread parameter for a proposed FSK system, then we can obtain an estimate of the average probability of error for this system from the error probabilities in listed in Section 4.2.

In particular, it was shown in Section 4.2 that the irreducible error probability as a function of the normalized rms multipath spread for rectangular pulse FSK for any integer-valued modulation index and any phase transition is bounded by the results presented in Fig. 4.5. Also, comparing the results in Tables 4.3 and 4.4 with Fig. 4.5, we see that the irreducible

error probability for phase-coded pulse FSK as a function of $\mu_p(h,\theta_T)$ closely approximates the irreducible error probability for rectangular pulse FSK as a function of $\mu_r(h,\theta_T)$. Hence, the results presented in Fig. 4.5 represent what is essentially a single relationship between the irreducible error probability $P_I$ and the normalized rms multipath spread $\mu_v(h,\theta_T)$ for FSK in a frequency-selective Rayleigh fading environment. Thus, we can take the data in Fig. 4.5 as representing the irreducible error probability as a function of $\mu_v(h,\theta_T)$ for a generic FSK signalling format with time-limited data-pulse waveform v(t). The limiting error probability for a particular FSK system may be approximated by means of a <u>single</u> channel measurement,

$$\mu_v(h,\theta) = \sqrt{\frac{m_{VV}(-1,+1,-1)}{m_{UU}(+1,+1,+1)}} \; . \tag{4.39}$$

Using this measurement, the resulting approximation for the irreducible error probability is found as the corresponding value of $P_I$ in Fig. 4.5.

Notice that this performance parameter is more complicated than the corresponding result in (3.40) for DPSK. Unfortunately, it is not clear that a less complicated form of channel measurement would provide information that is adequate for determining the limiting error probability. However, for the special case of rectangular pulse FSK, the results in the previous section indicate that an accurate estimate can be obtained from a less complicated channel measurement. In particular, for rectangular pulse waveforms, $m_{UU}(+1,+1,+1)$ is independent of the modulation index h and the phase transition $\theta_T$ (cf. (4.18a)). If, in addition, the modulation index is large, the channel may be characterized by measuring the value of

$$\mu_v(\infty,0) = \left[ T^{-2}\int_{-T}^{T} g(\xi)\cdot\xi^2 \, d\xi \right]^{1/2} , \tag{4.40}$$

which is equal to both the normalized rms multipath spread for rectangular pulse DPSK and the multipath spread $\mu = M/T$. For rectangular pulse FSK with smaller modulation index where the phase transitions are modeled as uniformly distributed random variables, (4.19) and the results in Table 4.1 indicate that (4.40) also gives a reasonable estimate of the limiting error probability for this case.

A good estimate of the average error probability for small time-bandwidth product pulse shapes is realized as a curve lying above $P_{ns}$ in (4.12) and $P_I$ calculated from (4.40) and the data in Fig. 4.6 which asymptotically approaches $P_{ns}$ and $P_I$ for extreme values of the signal-to-noise ratio. For large time-bandwidth pulse shapes, a more accurate approximation may be obtained by additionally measuring the quantity

$$2\bar{\eta}_u/T^2 = \int_{-\infty}^{\infty} g(\xi)\ \bar{R}_v^2(h,1,|\xi|)\ d\xi = \int_{-\infty}^{\infty} g(\xi)\ \bar{R}_v^2(|\xi|)\ d\xi\ , \qquad (4.41)$$

and replacing $P_{ns}$ by the low signal-to-noise ratio asymptote given in (4.37).

If, in the absence of a complete channel characterization, it is possible to obtain close estimates of the parameters discussed above, these approximations could be used in the preliminary evaluation of FSK systems employing complicated signals. Alternatively, if a fairly accurate model for the delay power-density spectrum can be obtained, the definition of the normalized rms multipath spread (4.20), the data in Fig. 4.5, and the expression for the low signal-to-noise ratio error probability in (4.37) may be used for comparative evaluations of FSK signalling formats and data-pulse shapes.

Finally, we point out the several basic similarities between the above results for the approximations of FSK and the approximations for DPSK

discussed in Section 3.2. In particular, the low signal-to-noise ratio asymptotic error probabilities for any particular data-pulse shape are identical for DPSK (3.38) and FSK (4.37) except for a factor of two increase in effective noise power for FSK. Also, the normalized rms multipath spread for rectangular pulse DPSK is similar to the normalized rms multipath spread for rectangular pulse FSK, especially for large modulation indices. The relationship between the low signal-to-noise ratio performance of the two systems might have been predicted by noting that DPSK can be viewed as a form of binary orthogonal signalling with signal duration 2T. In contrast, the relative effects of intersymbol interference on the two binary orthogonal signalling systems do not appear to be related to the basic similarities between system models. In particular, it is not immediately apparent that rectangular pulse FSK exhibits the same sensitivity to intersymbol interference as rectangular pulse DPSK only for very large modulation indices. Nor was it expected, prior to the development in Section 4.2, that it is possible to choose a time-limited pulse waveform for DPSK (sine-pulse) that produces lower error probabilities than any standard (i.e., rectangular pulse) form of FSK communications over the same fading channel.

## 4.4 Applications to Frequency-Selective Rician Channels

In this section it is shown, in a development that closely parallels Section 3.4, that when the received signal contains a nonfaded specular component as well as a Rayleigh faded component, the average error probability depends on the same key parameters identified in the preceding sections of this chapter. With the parameter $\alpha > 0$ in (2.3) representing the strength of the specular component, the decision statistic $Z_i$ in (4.2) is a quadratic form

of (nonzero mean) Gaussian random variables U and V. As in the analogous situation for DPSK communications, the probability of error, given a particular sequence of data bits $(\underline{b}_i)$ is transmitted, is given by a value of the probability distribution of the ratio of Chi-square variables with non-centrality parameters dependent on the characteristics of the FSK system. In the remainder of this section, we show that the average probability of error for FSK in Rician fading is completely determined by the parameter $\alpha$ in (2.3) and the moments $m_{UU}(\underline{b}_i)$, $m_{VV}(\underline{b}_i)$, and $m_{UV}(\underline{b}_i)$ defined in (4.7) for the evaluation of the error probability for Rayleigh fading channels.

In particular if we assume, without loss of generality, that $b_i = 1$ in (4.1), so that a space signal is transmitted during the i-th signalling interval, the conditional error probability [19] can be written as

$$P(\underline{b}_i) = Q(\sqrt{A(\underline{b}_i)}\ , \sqrt{B(\underline{b}_i)})$$

$$- \left[\frac{\sqrt{(m_{UU}(\underline{b}_i)+m_{VV}(\underline{b}_i))^2 - 4|m_{UV}(\underline{b}_i)|^2} + |m_{UU}(\underline{b}_i)-m_{VV}(\underline{b}_i)|}{2\sqrt{(m_{UU}(\underline{b}_i)+m_{VV}(\underline{b}_i))^2 - 4|m_{UV}(\underline{b}_i)|^2}}\right]$$

$$\cdot \exp\left[-\frac{A(\underline{b}_i)+B(\underline{b}_i)}{2}\right] \cdot I_0\left(\sqrt{A(\underline{b}_i)B(\underline{b}_i)}\right), \qquad (4.42)$$

where $Q(\cdot,\cdot)$ is Marcum's Q function, and $I_0(x)$ is the modified Bessel function. The parameters $A(\underline{b}_i)$ and $B(\underline{b}_i)$ in (4.42) are given by

$$A(\underline{b}_i) = 8\alpha^2 ET \cdot \left[\frac{m_{UU}(\underline{b}_i) + m_{VV}(\underline{b}_i) - \sqrt{(m_{UU}(\underline{b}_i)+m_{VV}(\underline{b}_i))^2 - 4|m_{UV}(\underline{b}_i)|^2}}{\sqrt{(m_{UU}(\underline{b}_i)+m_{VV}(\underline{b}_i))^2 - 4|m_{UV}(\underline{b}_i)|^2}}\right] \qquad (4.43a)$$

and

$$B(\underline{b}_i) = 8\alpha^2 ET \cdot \left[\frac{m_{UU}(\underline{b}_i) + m_{VV}(\underline{b}_i) + \sqrt{(m_{UU}(\underline{b}_i)+m_{VV}(\underline{b}_i))^2 - 4|m_{UV}(\underline{b}_i)|^2}}{\sqrt{(m_{UU}(\underline{b}_i)+m_{VV}(\underline{b}_i))^2 - 4|m_{UV}(\underline{b}_i)|^2}}\right]. \qquad (4.43b)$$

The moments, $m_{XY}(\underline{b}_i)$ in (4.43) are the central moments of the random variables U and V defined in Chapter 3. Using (2.3) and (4.3) for the signal defined by (4.1) and assuming a space signal is sent, we see that $E\{U\} = \alpha\sqrt{8ET}$ and $E\{V\} = 0$ so that the moments in (4.43) are precisely the same as those defined in (4.7) for the analysis of Rayleigh fading channels.

It is easy to see that (4.42) reduces to the error probability expressions for Rayleigh fading (see (4.6) and (4.8)) when $\alpha = 0$. In this case, $A(\underline{b}_i) = B(\underline{b}_i) = 0$, and (4.42) becomes

$$P(\underline{b}_i) = -\left[\frac{\sqrt{(m_{UU}(\underline{b}_i)+m_{VV}(\underline{b}_i))^2 - 4|m_{UV}(\underline{b}_i)|^2} + |m_{UU}(\underline{b}_i)-m_{VV}(\underline{b}_i)|}{2\sqrt{(m_{UU}(\underline{b}_i)+m_{VV}(\underline{b}_i))^2 - 4|m_{UV}(\underline{b}_i)|^2}}\right], \quad (4.44)$$

which is identical to (4.6) for the case $b_i = 1$. Alternatively, if there is no faded component in the received signal so that the channel is simply the additive white Gaussian noise channel, then $2\sigma^2 = 0$ in (2.4) and the moments in (4.43) become

$$m_{UU} = m_{VV} = 8N_0T$$

and

$$m_{UV} = 0.$$

If $b_i = 1$ and the transmitted signals are orthogonal, then $A(\underline{b}_i) = 0$, and $B(\underline{b}_i) = 2\alpha^2E/N_0$ and (4.42) becomes

$$P(\underline{b}_i) = \frac{1}{2}\exp\left[-\frac{\alpha^2E}{2N_0}\right]$$

(since $Q(0,x) = \exp(-x/2)$ [6]) which is the average error probability of FSK for the additive white Gaussian noise channel.

# CHAPTER 5

## ADAPTIVE EQUALIZATION TECHNIQUES FOR DIGITAL COMMUNICATIONS OVER FREQUENCY-SELECTIVE FADING CHANNELS

In Chapters 3 and 4, the performance of differentially coherent (DPSK) and noncoherent (FSK) communications via WSSUS frequency-selective fading channels was considered. It was shown that the average error probability for these systems is degraded by two effects that are each closely related to the multipath spread of the fading channel. The first effect is that of loss of available signal energy due to time-dispersion of the desired signal beyond the sampling window of the matched filter receiver. While this effect causes minor performance degradation for small time-bandwidth product signals and for adjacent-pulse-limited ISI, it can become a major consideration for large time-bandwidth product signals, and for channels which are more severely frequency-selective (dispersive in time).

The second adverse effect is due to the intersymbol interference introduced by the superposition of delayed versions of the transmitted signal at the channel output. The results in previous sections demonstrated that it is this effect which most severely limits the performance of digital communications over frequency-selective channels. In fact, we see from Figures 3.7 and 4.7 that for rms multipath spread $\mu$ as small as 0.05, intersymbol interference can result in irreducible error probabilities that are unacceptably large for many applications. Notice that the parameter $\mu = M/T$ is a linear function of both the rms delay M defined in (2.3) and the data-bit rate 1/T. Within the past decade, there has been increased interest in applications for high-frequency (HF) and troposcatter communications

[7,14,23,40] for which the rms multipath spread $\mu \simeq 0.5$. For all examples of delay spectra and modulation formats considered in previous chapters, the irreducible error probabilities resulting from this degree of frequency-selective are substantially larger than $10^{-1}$. Thus, in order to achieve reliable communications over dispersive fading channels, it is necessary to employ more complicated receiver structures which are less sensitive to the effects of intersymbol interference.

For channels, such as telephone lines and line-of-sight (LOS) microwave links, both linear and nonlinear equalizers (typically in the configuration of a tapped-delay-line (TDL)) have been effectively used to reduce the effects of intersymbol interference [20]. More recently, there has been interest in applications of similar equalization techniques to improve the performance of digital communications over classes of randomly time-variant linear channels [8,23]. The majority of channels for which equalization techniques have been considered are accurately modeled as WSSUS frequency-selective Rayleigh fading channels. While it is clear that the random character of the fading channel presents a number of additional difficulties (e.g., zero-mean unequalized signal amplitude) which must be overcome through the use of diversity or some form of redundant transmission, both simulation studies [8,24,41-43] and experimental evidence [14] indicate that for a given data rate, reliable communications can be achieved for fading channels with rms delays which would produce unacceptable limiting error probabilities if the system were not equalized. Alternatively, for a fading channel with a given value of rms multipath spread, equalization allows an increase of an order of magnitude in data rates for a specified bit-error probability [7].

Studies of equalization techniques for non-fading dispersive channels (e.g., high-speed digital telephone links) have been concentrated on linear equalizers, in general, and on linear TDL equalizers, in particular [21]. However, one of the characteristics of WSSUS frequency-selective channels is that the time-variant transfer function frequently exhibits nulls at various portions of the spectrum which result in "deep" fades of the spectrum of the received signal at these frequencies [9,13]. The primary goal of the equalizer is the elimination (or reduction) of the effects of intersymbol interference. More generally, the goal of equalization is to realize an equalizer filter such that the combination of the channel and equalizer yields an equivalent "channel" with flat frequency response [44]. Since practical linear TDL equalizers can only realize equalizer filters with Z-transform transfer functions consisting entirely of zeroes [21], linear equalizers are not well suited for applications to WSSUS frequency-selective fading channels [8].

There are several nonlinear equalizer structures that can be used to compensate for channels with nulls in the frequency response [21]. The nonlinear equalizer structure that has received the most attention, because of its relatively uncomplicated implementation and demonstrated effectiveness, is the class of TDL decision-feedback equalizers (DFE) [8,23]. The form of DFE receiver considered for applications in fading channels consists of a linear TDL equalizer operating on the received signal at some intermediate frequency (or passband [45]), a filter matched to the transmitted data pulse shape, and an additional TDL operating on the results of the (nonlinear) decisions of previous data symbols. The performance of the TDL equalizer strongly depends on the effectiveness of the linear TDL portion of the equalizer [24,44]. In

what follows, the characteristics of DFE equalizers are considered by first discussing the characteristics of linear TDL equalizers.

## 5.1 Linear Equalizer Characteristics

A model for a linear tapped-delay-line equalizer with $K_1 + K_2 + 1$ taps is shown in Fig. 5.1. Using narrowband signal representation, the input to the equalizer is given by

$$r(t) = \int_{-\infty}^{\infty} h(t,\xi)\ s(t-\xi)\ d\xi + n(t)\ . \tag{5.1}$$

The time-varying channel response function $h(t,\xi)$ is assumed to be that of a WSSUS Rayleigh fading channel as discussed in Chapter 2 and $n(t)$ is the equivalent low-pass Gaussian noise with (one-sided) spectral intensity $N_0$.

The tap-weight vectors $\underline{c}$ and $\underline{d}$ in Fig. 5.1 represent the real and imaginary parts of the equivalent complex-valued tap-weight vector $\underline{w} = \underline{c} - j\underline{d}$. We have, for simplicity, dropped the dependence on the time reference t. The remainder of the receiver is composed of in-phase and quadrature correlation receivers such as those shown in Fig. 3.1, which operate on the in-phase and quadrature outputs I(t) and Q(t) of the TDL equalizer. The sampled output of the composite receiver is given by

$$U = 2 \int_0^T v(t)\ e^{j\theta}\ r_0(t)\ dt\ , \tag{5.2}$$

where $r_0(t) = I(t) - jQ(t)$ is the output of the TDL equalizer and the slowly time-varying phase $\theta$ represents the combined phases of the transmitter, the channel, and the receiver. It is convenient to represent the output U in terms of the vector sum of the equalizer output as

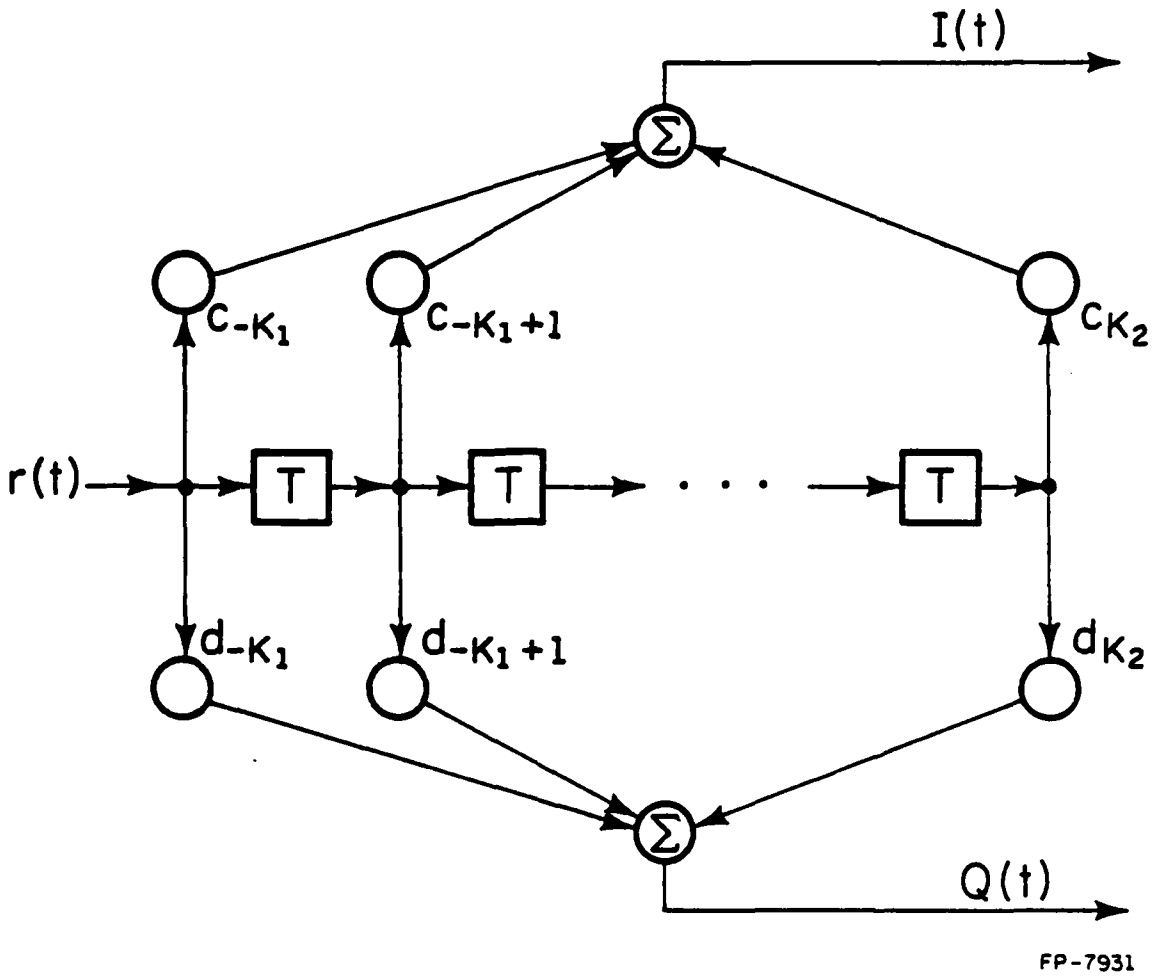


Figure 5.1. Linear TDL equalizer

$$U = \sqrt{\frac{8E}{T}}\ \underline{w}'\ \underline{R}\ \underline{b} + 2\underline{w}'\ \underline{n}\ , \qquad (5.3)$$

where $\underline{w}'$ represents the conjugate transpose of the column vector $\underline{w}$, T is the duration of the data pulse waveform v(t), and E is the transmitted energy per bit. The tap-weight vector $\underline{w}'$ in (5.3) is given by $\underline{w}' = [w^*_{-K_1}, \ldots, w^*_0, \ldots, w^*_{K_2}]$, where $(K_1+K_2+1)T$ is the width of the time window of the received signal r(t) represented by the equalizer output $r_0(t)$. The vector $\underline{b}$ represents the sequence of data bits which have influence on the receiver output U. Notice that the length of $\underline{b}$ depends on the number of equalizer taps as well as the time duration of the channel impulse response function $h(t,\xi)$.

Simulation studies [24] of the performance of linear TDL equalizers are often based on the assumption that the channel response to an impulse at t = 0 is non-zero only for relative delays $\xi$ in the range [-T,T]. Notice that this is similar to the adjacent-pulse-limited ISI assumption used in Chapters 3 and 4. In what follows we assume, for purposes of discussion, that the response function $h(t,\xi)$ is identically zero for $|t-\xi| > T$. Also, notice that there is some ambiguity as to the time reference of the equalizer receiver output relative to the transmitted signal. In fact, the determination of time reference (timing phase) is a major concern for the implementation of both linear and decision-feedback equalizers [23,46]. We adopt the common [24,44] assumption that the time reference is chosen so that the output of the zero-th tap, $w_0$, corresponds to the maximum channel output due to the desired data bit, $b_0$. Under the above assumptions, the data sequence $\underline{b}$ affecting the receiver output U is given by

$$\underline{b}' = [b_{K_2+1}, b_{K_2}, \ldots, b_{-K_1-1}]\ ,$$

where $K=K_1+K_2+1$ is the total number of equalizer taps.

The matrix $\underline{R}$ in (5.3) contains elements which represent the combined impulse response of the transmitted waveform v(t), the fading channel response function $h(t,\xi)$, and the matched filter correlation receiver. Under the adjacent-pulse-limited ISI assumption $\underline{R}$ is given by

$$\underline{R} = \begin{bmatrix} R(-N,1), & R(-N,0), & R(-N,-1), & 0 & , 0, \ldots, 0 \\ 0 & , R(-N+1,1), & R(-N+1,0), & R(-N+1,1), & 0, \ldots, 0 \\ & & \vdots & & \\ 0 & , \quad 0 \quad , \ldots, & R(N,1), & R(N,0), & R(N,-1) \end{bmatrix}, \quad (5.4)$$

where

$$R(n,k) = \int_{-T}^{T} \bar{R}(|\xi|)\, h(nT,\, kT+\xi)\, d\xi \,. \quad (5.5)$$

The function $\bar{R}(\cdot)$ in (5.5) is the aperiodic autocorrelation function of the time-limited pulse waveform v(t) defined by (3.14a). It is common to represent the combined response of the transmitter, fading channel, and receiver in this way. In fact, the rows of $\underline{R}$ are closely related to the discrete-time channel response functions discussed in [9] and the equivalent tapped-delay-line model for doubly selective fading channels considered in [10]. Note that the first argument of R(n,k) denotes the value of this integral for the channel response at time t = nT. The variation of the value of (5.5) as a function of n is related to the time-selectivity of the fading channel. For the present discussion we assume that the value of R(n,k) is independent of n for $n \in [-K_1-1,\ K_2+1]$.

One of the key characteristics of both HF and troposcatter channels is that the response function $h(t,\xi)$ is time varying. When the changes of the characteristics of the response function are sufficiently rapid that the above

assumption does not apply, the channel is modeled as a time-selective fading channel [9]. Typically, the degree of time-selectivity is measured in terms of the width of the Doppler power-density spectrum which is the temporal Fourier transform of the function $\rho(t-x,\cdot)$ defined in (2.4). Definitions of this type which are commonly used in the published literature are the distance between the 1/e points or the half-power bandwidth of the Doppler spectrum (e.g., see [3,9]). Alternatively, the time-selectivity of the WSSUS fading channel may be grossly characterized by the smallest value of $\tau$ for which $\rho(\tau,0) \approx 0$. This value, which is inversely proportional to the width of the Doppler spectrum, is referred to as the channel "decorrelation time" [7,24].

Since both HF and troposcatter fading channels are time-selective to some degree, a time-varying equalizer must be employed. For applications to WSSUS fading channels, the equalizer must adapt to the time-varying characteristics of the channel. One of the earliest applications of adaptive equalizers was to high-speed data communications over switched telephone-line networks [22]. In this situation, the receiver is designed to adapt to one of a number of links before the data is transmitted. Equalization of fading channels requires continuous adaptation in step with the changing characteristics of the fading channel. Moreover, it is crucial that the equalizer adapt in a time period which is much shorter than the channel decorrelation time. For many applications, this implies that the decorrelation time must be much larger than the data pulse duration T. Fortunately, this constraint, which is referred to as a <u>learning constraint</u> [40], does not preclude the use of equalization techniques for most fading channel applications. Typical values of the decorrelation time are on the order of $10^3 \cdot T$ for HF systems and $10^7 \cdot T$ for troposcatter links [7].

In order to reduce the effects of intersymbol interference, the tap-weights $\underline{w}$ are adjusted (adaptively) to minimize some cost function which, hopefully, is related to the resulting system performance. When the receiver bases the binary decision for each successive data bit on a single sampled output, the cost-function that is most often employed is the mean-square-error (MSE) [8,23,44].

The consideration of the performance of adaptive equalization techniques for slowly time-varying fading channels must, it seems, be based on the following basic assumption. At each time $t$ and for each sample function $h(t,\xi)$ of the channel impulse response, the TDL is adjusted in a manner such that the equalizer is able to "track" the slow changes in the channel. In this case it is not clear that knowledge of the channel statistics (zero-mean Gaussian for a Rayleigh fading channel) can be utilized to obtain a meaningful interim measure of system performance. On the other hand, if we assume that the equalizer is unable to track the channel, then the TDL would only serve to add additional intersymbol interference as well as correlated Gaussian noise. In this case it is reasonable to assume that it would be better not to attempt channel equalization.

Consider the receiver output $U$ for a fixed channel impulse response function $h(\cdot,\xi)$, which is a function only of the relative delay $\xi$. The mean-square-error (MSE), as defined for the consideration of fading channels [8,24,45] and for the consideration of deterministic channels [45,47], is given by

$$\text{MSE} = E_{\underline{R}}\{|U - k\sqrt{8ET}\, b_0|^2\} , \tag{5.6}$$

where $E$ is the transmitted energy per bit and $E_{\underline{R}}\{\cdot\}$ denotes the conditional

expectation given $\underline{R}$. The expectation in (5.6) is taken with respect to the data sequence $b_i$ for $i \neq 0$ and the additive noise samples $\underline{n}$. The scale factor k in (5.6) is a positive real constant which does not affect the form of the minimum MSE filter. Using the vector representation in (5.3) for U, we have

$$MSE = E_{\underline{R}}\{| \sqrt{\frac{8E}{T}}\ \underline{w}'\ \underline{R}\ \underline{b} + 2\underline{w}'\ \underline{n} - k\sqrt{8ET}\ b_0|^2\} \ . \tag{5.7}$$

If we assume that the data sequence is a sequence of independent, identically distributed random variables taking on the values -1, +1 with equal probability, (5.7) becomes

$$MSE = \frac{8E}{T}\ \underline{w}'\ \underline{R}\ \underline{I}\ \underline{R}'\ \underline{w} + 8N_0T\cdot\underline{w}'\underline{w} + k^2\cdot 8ET - 16kE\cdot Re\{\underline{w}'\underline{R}_0\} \ , \tag{5.8}$$

where

$$\underline{R}_0' = [R^*(\cdot,-K_1),\ \ldots,R^*(\cdot,0),\ \ldots,\ R^*(\cdot,K_2)] \ .$$

It can be shown [23,44,45] that the solution for the MSE optimum tap-weight vector $\underline{w}$ is given by

$$\underline{w}'\ \underline{A}\ \underline{w} = k\cdot\ Re\{\underline{w}'\ \underline{R}_0\} \tag{5.9}$$

or

$$\underline{w} = k\cdot\underline{A}^{-1}\ \underline{R}_0 \ ,$$

where the Hermitian matrix $\underline{A}$ is written as

$$\underline{A} = T^{-1}\ \underline{R}\ \underline{R}' + \frac{N_0T}{E}\cdot\underline{I} \ . \tag{5.10}$$

Using (5.9) and (5.8), the minimum MSE (MMSE) is given by

$$MMSE = k^2 8ET - k8E\cdot\ \underline{R}_0'\ \underline{A}^{-1}\ \underline{R}_0 \ . \tag{5.11}$$

Alternatively, the MMSE can be written as

$$\text{MMSE} = k^2 8ET - k8E \cdot \text{Re}\{\underline{w}' \underline{R}_0\} \ . \tag{5.12}$$

Notice that, for a particular channel response matrix $\underline{R}$, the second moment of the filter output U (for $b_0 = 1$) in (5.3) is related to the mean-square-error by

$$E_{\underline{R}}(|U|^2) = \text{MSE} - k^2 8ET + 16kE \cdot \text{Re}\{\underline{w}' \underline{R}_0\} \ . \tag{5.13}$$

Using the expression for the MMSE in (5.12) we have

$$E_{\underline{R}}(|U|^2) = \text{MMSE} - k^2 8ET + 16kE \cdot \text{Re}\{\underline{w}' \underline{R}_0\} \tag{5.14}$$

$$E_{\underline{R}}(|U|^2) = k8E \cdot \text{Re}\{\underline{w}' \underline{R}_0\} > 0 \ . \tag{5.15}$$

We have seen that the MSE or, in particular, the MMSE is related to the second moment of the receiver output U (cf. (5.14)). It is tempting to consider the possibility of characterizing an "average" MMSE by taking an additional expectation with respect to the channel statistics. Using the expression for MSE in (5.8) and averaging with respect to the channel ensemble (WSSUS zero-mean Gaussian) we have

$$\text{MSE} = \frac{8E}{T} \underline{w}' \underline{C} \underline{w} + 8N_0 T \underline{w}' \underline{w} + k^2 8ET \ ,$$

where the matrix $\underline{C}$ denotes the expected value of the quadratic form $\underline{R}\underline{R}'$. If there is no additional restriction on $\underline{w}$, then this implies that $\underline{w} = 0$ produces the minimum MSE. Alternatively, if we insist that $\underline{w}'\underline{w} = 1$, then it is easy to see, using an example where the fading channel is nonselective, that the above minimization produces the wrong result.

It is interesting to note that the last term in (5.8), which is also the right-hand side of (5.15), is just a constant times the real part of the output U due to the desired signal (corresponding to $b_0$=1). Then we see that (5.15) implies that the optimum tap vector $\underline{w}$ produces a "one-shot" receiver response whose real part has non-zero mean-value. Hence, we see that a linear TDL equalizer designed to minimize the MSE, not only reduces the average contribution of interfering adjacent data signals, but also provides phase-coherence between the transmitter and receiver. Moreover, using (5.8) and (5.15), it can be seen that for small values of $E/N_0$, the linear TDL equalizer receiver is closely related to the maximal ratio diversity combiner for a one-shot receiver [48] where the "diversity" links are produced by the time-dispersive properties of the channel. In a frequency-selective fading environment, the received signal can be characterized as the superposition of delayed versions of the transmitted signal. Thus, the efficient combining of these signal components at the receiver results in a potential for diversity gain. The diversity that is due to the time-dispersive nature of the frequency-selective fading channel is commonly referred to as "implicit" diversity [25] as opposed to explicit forms of diversity which can be realized by redundant transmissions over channels separated by space, time, frequency, or antenna polarization [6]. (Recall that maximal ratio combining is a linear, coherent diversity combining technique which achieves the maximum possible output signal-to-noise ratio for a single data pulse at each sampling instant.) If the matrix $\underline{A}$ in (5.10) is dominated by the term due to the additive noise, and if the contributions from interfering data signals are ignored, the statistic U in (5.3) becomes

$$U \approx \sqrt{\frac{8E}{T}}\ \underline{w}'\cdot\underline{R}_0\ b_0 + 2\underline{w}'\ \underline{n}$$

$$= \frac{kE}{N_0}\left[\sqrt{\frac{8E}{T}}\ \underline{R}_0'\ \underline{R}_0\ b_0 + \frac{2E}{N_0}\ \underline{R}_0'\ \underline{n}\right]. \qquad (5.16)$$

With U defined in this way, the signal-to-noise ratio is given by

$$SNR = \frac{E}{N_0 T^2}\ \underline{R}_0'\ \underline{R}_0 ,$$

which is precisely the definition of the instantaneous signal-to-noise ratio for maximal ratio combining considered in [6] and [48] where the order of the implicit diversity is related to the number of significant elements of $\underline{R}_0$. In light of the relationship between a MMSE linear TDL equalizer and coherent maximal ratio combining, it is not reasonable to assume that it is advantageous to consider signalling techniques other than coherent PSK. In fact, it is well known that coherent binary PSK produces smaller error probabilities than other common form of binary signalling (i.e., DPSK, and coherent and noncoherent FSK) for maximal ratio combining in a Rayleigh fading environment [6].

We have seen that for a given channel impulse response, the MMSE-TDL equalizer allows the use of coherent PSK detection. Using the solution for the MSE-optimal $\underline{w}$ in (5.9) for $k = 1$, the random variable U in (5.3) can be written as

$$U = \sqrt{\frac{8E}{T}}\ \underline{R}_0'\ \underline{A}^{-1}\ \underline{R}\ \underline{b} + 2\underline{R}_0'\ \underline{A}^{-1}\ \underline{n} . \qquad (5.17)$$

where $\underline{R}_0'$, $\underline{R}$, and $\underline{A}$ are all determined by the channel response function and the statistics of the additive noise. Conceptually, the conditional bit-error probability for a particular $h(\cdot,\xi)$ and a particular data sequence $\underline{b}$ can be obtained by finding the signal-to-noise ratio and computing $P_e(\underline{b})=Q(SNR^{1/2})$, where $Q(x)=1-F(x)$: the standard Gaussian cumulative distribution function. The average probability of error is then determined by averaging $P_e(\underline{b})$ over

the possible data sequence combinations. Unfortunately, the evaluation of both the conditional and average error probabilities is quite cumbersome even for non-fading channels and the results concerning the performance of MMSE equalizers are almost always in the form of simulation studies [21,44]. An exact evaluation of the average error probability for fading channels appears hopeless, since, in this case, it is necessary to perform additional averaging with respect to the channel response function h.

## 5.2 Decision-Feedback Equalizer Characteristics

The receiver structure of a DFE is similar to that of a linear TDL equalizer receiver with the addition of a feedback loop which forms a linear combination of the values of previously detected data symbols [8,23,42,49,50]. (The nonlinear nature of the equalizer is due to the effect of the hard decisions used to form the output of the feedback section.) The device used to form the feedback output D can be (and usually is [8]) represented as a linear TDL with tap spacing necessarily equal to the data symbol duration T. If we assume the current decision concerns the zero-th data bit $b_0$, the output of the feedback section of the DFE is given by

$$D = \sum_{i=1}^{N} d_i \bar{b}_{-i} , \tag{5.18}$$

where N is the number of feedback taps and $\bar{b}_i$ is the value of the decision on the i-th data bit. Using vector representation for the parameter D, the expression for the decision statistic U for a DFE can be written as

$$U = \sqrt{\frac{8E}{T}}\, \underline{w}'\, \underline{R}_f\, \underline{b} + \underline{d}'\bar{\underline{b}}_d + 2\underline{w}'\, \underline{n} , \tag{5.19}$$

where $\underline{d}' = [d_N^*,\ldots,d_1^*]$ and $\bar{\underline{b}}_d' = [\bar{b}_{-1},\ldots,\bar{b}_{-N}]$. Notice that there are now $K_1$ +

1 taps for the linear TDL portion of the equalizer so that $K_2=0$. The matrix $\underline{R}_f$ in (5.19) is obtained from (5.4) by deleting the last $K_2$ +1 columns and the last $K_2$ rows of the original channel response matrix.

The MSE criterion for the DFE is defined similarly as for the linear TDL equalizer and is based on the assumption [8,24,44] that the previously detected symbols in the feedback filter are correct, i.e., $\bar{b}_i = b_i$ for $i<0$. Using this assumption and the definition in (5.6), the MSE for the DFE is given by

$$MSE = E_{\underline{R}_f}\{| \sqrt{\frac{8E}{T}}\ \underline{w}'\ \underline{R}_f\ \underline{b}_f + \underline{d}'\underline{b}_d + 2\underline{w}'\ \underline{n} - k\sqrt{8ET}\cdot b_0|^2\}\ . \qquad (5.20)$$

Minimization of (5.20) with respect to $\underline{w}$ shows that the linear TDL that minimizes the MSE is given by the relation [44]

$$\underline{w}'\ \underline{A}_f\ \underline{w} = k\cdot\ Re\{\underline{w}'\ \underline{R}_{f0}\}$$

or

$$\underline{w} = k\cdot\underline{A}_f^{-1}\ \underline{R}_{f0}\ , \qquad (5.21)$$

where the matrix $\underline{A}_f$ is

$$\underline{A}_f = T^{-1}\ \underline{R}_f\ \underline{R}_f' + \frac{N_0T}{E}\cdot\underline{I}\ . \qquad (5.22)$$

The coefficients of the DFE are then chosen so that the resulting output D exactly cancels the intersymbol interference due to previously detected symbols or "precursors" [23]. In this case, the coefficients $d_i$ can be written in terms of the coefficients of the linear TDL section by

$$\underline{d} = \underline{w}'\ \underline{R}_1\ , \qquad (5.23)$$

where the matrix $\underline{R}_1$ is obtained from (5.4) by deleting the first $K_2$ columns and the first $K_2$+1 rows of $\underline{R}$.

For any practical implementation of DFE receivers (especially for Rayleigh fading channels) it is not reasonable to assume that all previous data decisions are correct. Moreover, in the case when a decision error is made, the output from the feedback portion of the equalizer adversely affects subsequent decisions causing error propagation. For nonfading channels, the increase in the average error probability due to this effect is considered in [20] using a Markov chain model. The analysis is carried out under the assumption that the tap weights for the linear TDL forward filter are chosen according to a zero-forcing (ZF) criterion [22,44]. The ZF cost function is closely related to the definition of the MSE in (5.7) by neglecting the term corresponding to additive channel noise. The zero-forcing criterion is simply the requirement that the intersymbol interference contribution at the output of the forward filter is forced to zero, at the cost of an enhancement of the additive noise. It should be pointed out that the zero-forcing criterion is not generally applicable to fading channels since ZF can be achieved only for channels with limited intersymbol interference [44]. Assuming ideal DFE characteristics and a particular nonfading channel response function, it is shown in [20] that error propagation is not a major source of degradation for typical values of signal-to-noise ratio and channel characteristics. A similar conclusion is obtained in [40] where a simulation study of the error propagation effect is carried out for a single-echo and an exponentially decaying multiple echo channel model.

From the discussion of linear TDL equalizer characteristics in Section 5.1, we see that the forward filter portion of the DFE has the potential of providing a degree of implicit diversity gain as well as some reduction of the effects of intersymbol interference, at the expense of an increase in the

effective noise power. In contrast, the feedback portion of the DFE is designed to eliminate the distortion due to previously transmitted data signals at the expense of a loss of diversity gain and some degradation due to error propagation. Hence, the DFE receiver can be viewed as a compromise between these two configurations.

Finally, we point out that for both linear TDL and DFE receivers, the ability to track the channel characteristics strongly depends of the available signal-to-noise ratio [44]. Clearly, if the received signal is dominated by the additive noise, there is little hope of maintaining equalization. In a Rayleigh fading environment, the instantaneous SNR can fall below the level necessary to maintain equalization so often that the equalizer performance is severly degraded. In order to overcome this difficulty, practical DFE modems are designed to process signals received from L explicit independent diversity links [23]. This is accomplished by employing a separate forward TDL filter for each of the L explicit links, appropriately combining the forward filter outputs by means of automatic gain control devices, and using a common data pulse filter and feedback loop TDL to process the combined output of the forward filters.

## 5.3 DFE Performance Considerations

The published analytical work on the evaluation of the average bit-error probability for DFE receivers in frequency-selective fading is almost entirely due to Monsen [24,40]. The analysis in [24] is carried out for a system without explicit diversity and is based on the fundamental assumption that the feedback portion of the equalizer precisely cancels the intersymbol interference due to pulses transmitted prior to $b_0$ (the desired bit). Under

this assumption, it is easy to see that the resulting analysis is independent of the parameters of the feedback portion of the equalizer. Hence, the development in [24] can be viewed as an analytical technique that can be applied to linear TDL equalizers.

Notice that the receiver output U in (5.3) can be written as

$$U = \sqrt{\frac{8E}{T}}\,\underline{w}'\,\underline{R}_{f0}b_0 + \sqrt{\frac{8E}{T}}\,\underline{w}'\,\tilde{\underline{R}}_f\tilde{\underline{b}}_f + 2\underline{w}'\underline{n}\ , \tag{5.24}$$

where $\tilde{\underline{R}}_f$ and $\tilde{\underline{b}}_f$ are obtained by deleting the column of $\underline{R}_f$ and the entry of $\underline{b}_f$ corresponding to the desired bit $b_0$. The first term of (5.24) then denotes the desired signal component, the second term is the output due to interfering signals, and the last term is due to the additive channel noise. In [24], Monsen approximates the interfering data bits $b_i$ for $i > 0$ as independent zero-mean complex Gaussian random variables with variance $\gamma^2$. (Recall that the intersymbol interference due to previous data pulses is assumed to be eliminated by the feedback portion of the equalizer.) With the intersymbol interference from future data pulses modeled as additive Gaussian noise, the minimization of the MSE with respect to the coefficients of the forward filter yields

$$\underline{w}'\ \underline{B}\ \underline{w} = k\cdot\mathrm{Re}\{\underline{w}'\ \underline{R}_{f0}\}\ ,$$

where the matrix $\underline{B}$ is given by

$$B = T^{-1}\gamma^2\ \tilde{\underline{R}}_f\ \tilde{\underline{R}}_f' + \frac{N_0T}{E}\cdot\underline{I}\ . \tag{5.25}$$

Substituting the solution for the MMSE forward filter tap weights into (5.24), the statistic U becomes

$$U = \sqrt{\frac{8E}{T}}\,\underline{R}_{f0}'B^{-1}\underline{R}_{f0}b_0 + \sqrt{\frac{8E}{T}}\,\underline{R}_{f0}'B^{-1}\tilde{\underline{R}}_f\tilde{\underline{b}} + 2\underline{R}_{f0}'B^{-1}\underline{n}\ . \tag{5.26}$$

Under the Gaussian noise characterization for the interfering data pulses, we see that the last two terms in (5.26) represent the contributions due to additive noise. Monsen defines an "equivalent signal-to-noise ratio" as

$$\text{SNR} = \frac{\frac{8E}{T}\left(\underline{R}'_{f0}\ \underline{B}^{-1}\ \underline{R}_{f0}\right)^2}{8N_0T\ \underline{R}'_{f0}\ \underline{B}^{-1}\ \underline{R}_{f0}}$$

$$= \frac{E}{N_0T^2}\ \underline{R}'_{f0}\ \underline{B}^{-1}\ \underline{R}_{f0}\ , \qquad (5.27)$$

which is the ratio of the output due to the desired data pulse to the average of the output due to both interfering data pulses and additive noise. Hence, we see that the intersymbol interference has been replaced with interference due to additional additive Gaussian noise.

The second approximation employed in [24] is to replace the matrix $\underline{B}$ by its mean value, $E\{\underline{B}\}$. However, even with these simplifying assumptions, it is still necessary to find the eigenvalues of the correlation matrix $E\{\underline{R}_{f0}\underline{R}'_{f0}\}$ of zero-mean correlated complex Gaussian random variables with means and covariances that depend on the channel response function $h(\cdot,\xi)$. When the eigenvalue distribution is obtained for a particular channel realization, it is then necessary to find the coefficients of a partial fraction expansion of a polynomial in the eigenvalues. The variance $\gamma^2$ of the interfering data bits is chosen in [24] to be 0.5 to allow the best agreement between calculated and simulated results.

Since, in reality, the average bit-error probability is dominated by the probability of a wrong decision for the worst case intersymbol interference, it would be useful to supplement the analysis in [24] by characterizing the

receiver output U for the worst-case data sequence. Using (5.24) we have

$$U = \sqrt{\frac{8E}{T}}\,\underline{w}'\,\underline{R}_{f0}\,b_0 + \sqrt{\frac{8E}{T}}\,\underline{w}'\,\tilde{\underline{R}}_f\,\tilde{\underline{b}} + 2\underline{w}'\underline{n}\ , \tag{5.28}$$

so that $\underline{w}'(\underline{R}_{f0} + \tilde{\underline{R}}_f\,\tilde{\underline{b}})$ represents the sampled output of the receiver for a particular data sequence. If we assume $h(\cdot,\xi) = 0$ for $|\xi| > T$ and that the forward TDL filter consists of only 2 taps, $(\underline{R}_0 + \tilde{\underline{R}}\,\tilde{\underline{b}})$ is given by

$$\begin{bmatrix} R(\cdot,-1) \\ R(\cdot,0) \end{bmatrix} = \begin{bmatrix} b_2R(\cdot,1) + b_1(R(\cdot,0) \\ b_1R(\cdot,1) \end{bmatrix}\ . \tag{5.29}$$

Unfortunately, even for this simple example it is not clear that the worst case interference and the resulting effect on the error probability can be adequately characterized.

### 5.3.1 Nonselective Fading Channel Approximation of DFE Performance

Since the forward TDL equalizer in each explicit diversity branch is assumed to achieve coherence with the channel, an interesting approximation of DFE system performance (which proves to be a reasonable estimate of the performance of practical DFE receivers) is the error probability of coherent PSK for maximal ratio combining of independent nonselective Rayleigh fading channels. If L denotes the order of the explicit diversity, the probability of error of maximal ratio PSK is given by [6],

$$P_c(L) = \int_0^\infty Q(\sqrt{2s})\cdot f_L(s)ds\ , \tag{5.30}$$

where s is the instantaneous combined signal-to-noise ratio and $f_L(s)$ is the probability density function of s for diversity L. Assuming identical diversity branch statistics (i.e., average branch signal-to-noise ratios), the

probability density function $f_L(s)$ is [6],

$$f_L(s) = \frac{1}{(L-1)!} \cdot \frac{s^{L-1}}{S^L} \cdot \exp(-s/S) , \qquad (5.31)$$

where the common per branch average signal-to-noise ratio $S=2\sigma^2E/N_0$. The results of the computation of $P_c(L)$ as a function of S are shown in Fig. 5.2 for diversity L = 1, 2, and 4. As a comparison for the results in Chapters 3 and 4 for the case of diversity reception, the error probability for square law diversity combining of DPSK in nonselective Rayleigh fading is also shown as a dashed line for the same orders of diversity. When the decision statistic for DPSK signalling is of the form of Z in (3.5), "square law" combining should be viewed as quadratic form combining (see [6]) of the received signals given by the sum of L independent variables $Z_n$ for n=1,L [17]. Since DPSK signalling can be represented as a particular form of orthogonal signalling on the interval [0,2T], this quadratic-form combining, which is the optimal combining technique for DPSK in Rayleigh fading if no channel estimate is available, is equivalent to square law combining of the orthogonal signals. It can be shown, using the results in [6] or [48], that the average error probability for square law DPSK in Rayleigh fading is given by

$$P_d(L) = P_e^L \cdot \sum_{n=0}^{L-1} (1-P_e)^n \, C(L-1+n,n) , \qquad (5.32)$$

where $P_e=(2+2S)^{-1}$ is the average error probability for DPSK in nonselective Rayleigh fading (cf. (3.18)), and C(m,n) is the binomial coefficient. The corresponding result for orthogonal FSK can be obtained from Fig. 5.2 by finding the value of the error probability corresponding to a 3 dB reduction of signal-to-noise ratio S. The effect of the limiting error probability on the square law diversity performance of DPSK and FSK can be approximately

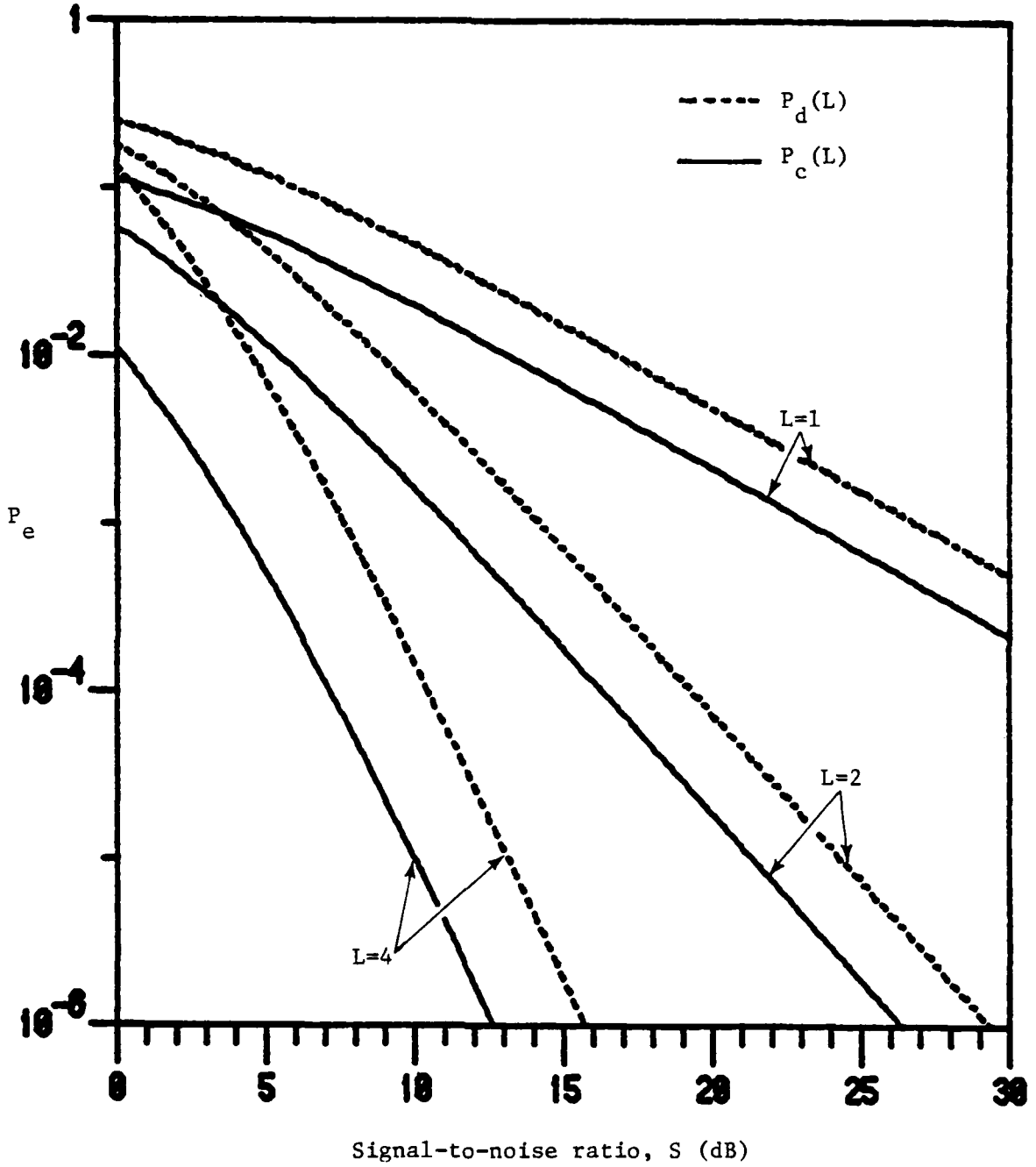


**Figure 5.2. Probability of error for maximal ratio PSK and square law DPSK for diversity L vs. per branch signal-to-noise ratio, S**

determined by finding the irreducible error probability for a particular value of rms multipath spread $\mu$ from Fig. 3.3 or Fig. 4.3, which is the exact result for L=1. The approximation of the limiting error probability for L=2,4 is then obtained by finding the corresponding value of S for the square law, L=1 curve and determining $P_d(L)$ with L=2 and L=4 for this value of S.

## 5.4 Simulation and Experimental Results on DFE Performance

### 5.4.1 Simulation Results

One of the earliest published records of computer simulation results for the performance of DFE for fading channels appears in [23]. For this simulation study, the Rayleigh fading channel is modeled with a rectangular delay power-density spectrum (cf. (2.16)) with the parameter $T_0$ ranging between 0 and 0.5/T where T is the data pulse duration. Notice that for all values of $T_0$ considered in this simulation, the frequency-selective channel satisfies the adjacent-pulse-limited ISI assumption for the received signal prior to equalization. From the definition of the rms multipath spread $\mu$ in Chapter 2, we see that these values of $T_0/T$ correspond to rms multipath spreads ranging from zero (i.e., nonselective fading), to a maximum value of 0.3 for $T_0 = 0.5/T$. The simulation is carried out for a DFE consisting of a single three-tap forward filter with data pulse interval tap spacing, and a three-tap feedback filter (i.e., $K_1+1 = N = 3$). The results of this study suggest that the implicit diversity gain resulting from the correct resolution of the multipath signal components can be realized in a simulated fading environment. This implicit diversity gain produced error probabilities less than the probability of error for coherent detection in nonselective fading (i.e., $P_c$) by an order of magnitude at S = 10 dB (representing a gain of 12

dB), and more than two orders of magnitude at S = 15 dB (for a gain of more than 20 dB) for an rms multipath spread of 0.3. The results in [23] also indicate that significant reduction in error probability (an order of magnitude for S = 15 dB) is achieved for values of $\mu$ as small as 0.18. For smaller rms multipath spreads (i.e., $\mu < 0.05$), the reported error probability is closely approximated by $P_c$ and is upper bounded by $P_c$ for all values of $\mu$ considered. It is interesting to note that the results in Chapter 3 indicate that for this channel model the irreducible error probability of rectangular pulse DPSK for $\mu = 0.3$ is approximately $6 \times 10^{-2}$ and that the average probability of error for DPSK is about $10^{-2}$ at S = 15 dB, even for nonselective Rayleigh fading. In contrast, no limiting probability of error was exhibited in the DFE simulation for error probabilities as low as $10^{-6}$.

In [24] simulation results are reported for an explicit diversity application of a high speed ($\approx$ 10 Mbits/second) troposcatter system described in [51]. The DFE modem was designed to employ rectangular pulse quadriphase shift keying (QPSK) and accommodate up to four independent diversity channels, each with a forward TDL filter of three taps spaced at one-half the data symbol interval T. The outputs of the forward filters are coherently combined and used as the input to in-phase and quadrature filters, each of which are followed by a three-tap feedback TDL with symbol-interval tap spacing. The simulation consisted of measuring the average bit-error probability performance for a prototype modem using a troposcatter channel simulator. The channel simulator is realized as a TDL filter with tap-weights driven by the outputs of Gaussian noise generators so as to realize a random channel with a fixed rms multipath spread for each simulation. Using this configuration, simulation results are obtained for values of rms multipath spreads as large

as 0.6 for diversity L=2 and 0.95 for diversity L=4. While the delay power-density spectrum model for the channel simulator is not explicitly discussed, it is reasonable to assume that a channel with a rectangular delay spectrum is employed since this model is used in [23], and the TDL channel simulator is most easily implemented for this model.

The results indicate that for dual diversity (L=2), and signal-to-noise ratios of less than 20 dB, the lowest error probabilities are obtained for rms multipath spreads between 0.25 and 0.4. For these values, it is shown that the DFE modem produces error rates which are lower than $P_c(2)$ by a factor of ten at S = 15 dB (for a gain of 5 dB), and an improvement of nearly two orders of magnitude at S = 20 dB (representing a gain of 10 dB) for S = 20 dB. In contrast to the results cited above, this simulation study establishes the existence of an irreducible error probability of approximately $10^{-6}$ for $\mu$ = 0.6 and $10^{-8}$ for $\mu$ = 0.45. In comparison, the results in Fig. 3.3 and Fig. 5.2 for L = 2, indicate that for $\mu$ = 0.45, the irreducible error probabilities for both rectangular pulse DPSK and sine pulse DPSK are about $3\times10^{-2}$ representing an equivalent per branch average signal-to-noise ratio of approximately 8 dB.

For fourth-order diversity, simulation results are obtained for values of $\mu$ as large as 0.95. As in the dual diversity simulation, the smallest average error probability is obtained for an rms multipath spread of about 0.45. In this case the resulting error probability is shown to be less than $P_c(4)$ by more than an order of magnitude for S = 10 dB (a gain of 3 dB) and about two orders of magnitude for S = 15 dB (a gain of 5 dB). For one simulation of fourth-order diversity, an irreducible error probability of about $10^{-7}$ was obtained for an rms multipath spread of 0.45. In comparison, the

approximation of the irreducible error probability for DPSK with L=4 is about $2x10^{-3}$, so that the use of DFE and coherent detection provides a reduction of more than four orders of magnitude for the limiting error probability in similar fading environments.

### 5.4.2 Results of Experimental Studies

In [14], live link test results are reported for the DFE modem described in [51] and used in the channel simulator studies cited above. In this test, the DFE modem was operated in both dual (L=2) and quadruple (L=4) diversity configurations and for two test "channels" with distinct fading characteristics. The two "channels" each consisted of a radio-frequency (RF) transmitter, fading channel, and an RF receiver producing an intermediate-frequency output (forward-filter input) for each diversity branch. The two channels considered in the test were the 900 MHz and 4.5 GHz troposcatter radio systems at the Rome Air Development Center test facility. The multipath profiles for these channels were measured with a channel probe using an m-sequence coded sounding signal. It was found that the delay density followed a basic triangular shape (cf. (2.14)) and that the shape of the delay density did not vary greatly from test to test (with the exception of the 900 MHz channel where a secondary triangular "hump" was occasionally observed). Data are presented in [14] for the 900 MHz channel with a measured rms multipath spread of $\mu$=0.45, and for the 4.5 GHz channel with $\mu$ measured as approximately 0.35. The probability of error for the DFE modem was measured by the bit-error rate averaged over twenty-minute periods as a function of the median received signal-to-noise ratio. In what follows, the performance of the DFE modem is discussed in terms of the mean value of the measured error

probabilities as a function of the per channel signal-to-noise ratio. It should be pointed out that the results in [14] exhibit sample points that vary from this mean value by as much as a factor of ten for a particular measured signal-to-noise ratio.

For all cases reported in [14], the test results show major discrepancies between measured DFE modem performance and the results of simulation studies discussed above. In particular, for the 900 MHz channel and dual diversity, test results are reported for measured signal-to-noise ratios ranging from 5 to 17 dB. These results indicate that the DFE modem error probability is on the average slightly larger than $P_c(2)$ for signal-to-noise ratios less than about 15 dB (differing by at most a factor of three at S = 5 dB, indicating a SNR degradation of about 5 dB). For S = 17 dB, the average error probability for the DFE modem was approximately equal to $P_c(2)$. Similar results were obtained with dual diversity for the 4.5 GHz channel with measured rms multipath spread 0.35. For this channel, test results are reported for signal-to-noise ratios ranging from 15 to 22 dB. The measured DFE error probabilities are slightly larger than $P_c(2)$ for S < 20 dB, and differ from $P_c(2)$ by less than a factor of two for the entire range of signal-to-noise ratios reported.

The test results for fourth-order diversity show that $P_c(4)$ is an excellent approximation of DFE performance for both channels considered. In particular, for the 900 MHz channel ($\mu$=0.45), the results show that the average measured DFE error probability is between $P_c(4)$ and $2xP_c(4)$ for all reported values of signal-to-noise ratio (0-15 dB) which corresponds to a degradation of less than 3 dB. Similarly, test results for the 4.5 GHz channel ($\mu$=0.35) show that the measured average error probabilities lie

between $1.2xP_c(4)$ and $3xP_c(4)$ for all signal-to-noise ratios which range between 5 and 17 dB for this channel.

The basic conclusion that can be drawn from the above experimental results is that the average error probability for maximal ratio PSK is a reasonable estimate of the performance of decision-feedback receivers for practical fading channel communication systems. This is in stark contrast to the implications of the simulation results which show that in certain cases, the DFE can realize error probabilities two orders of magnitude lower than $P_c(L)$, even in the case of no explicit diversity (L=1). It is reasonable to assume that some of the discrepancy between predicted and measured performance is due to the less than ideal characteristics of the RF transmitter and receiver employed for the experimental studies. However, by examining some of the very basic limitations of equalizer performance, it can be seen that the results of the simulation studies can be characterized as "optimistic."

Recall, from the discussion in Section 5.2, that the feedback portion of the DFE receiver is designed solely to eliminate the intersymbol interference due to previously transmitted data signals. Hence, the implicit diversity gain can only be realized by the coherent combining properties of the forward TDL filter. Thus, the potential for diversity gain with respect to the decision on the desired data bit, $b_0$ is characterized by the vector $\underline{R}_{f0}$ (cf. (5.24)). For the example of a rectangular delay delay power-density spectrum (2.16) with parameter $T_0=T/2$, which corresponds to the channel considered in [23], $\underline{R}_{f0}$ consists of only two entries, $R(\cdot,-1)$ and $R(\cdot,0)$, which are Gaussian random variables, linearly related to the response function $h(\cdot,\xi)$ through (5.5). Using (2.16) and the definition of the rectangular pulse correlation function in (3.14a), it is easy to see that the second moments of the

components of $\underline{R}_{f0}$ are related by

$$14 \cdot E\{R^2(\cdot,-1)\} = E\{R^2(\cdot,0)\} \ .$$

In general, the random variables R(·,-1) and R(·,0) are correlated Gaussian random variables by nature of the overlapping portions of the rectangular pulse autocorrelation function. However, in order to characterize a lower bound for DFE receiver performance, we proceed under the assumption that R(·,-1) and R(·,0) are uncorrelated and hence independent. (It is well known [6] that correlations among diversity links can only degrade the performance of maximal ratio diversity systems.) In this case, the error probability for maximal ratio PSK is given by (5.30) by neglecting the parameter L, where the probability density function of the instantaneous signal-to-noise ratio s is given by

$$f(s) = \frac{14}{13S} \cdot [\exp(-s/S) - \exp(-14s/S)] \ ,$$

and where S is the average signal-to-noise ratio corresponding to R(·,0). Calculation of the integral in (5.30) for this density function of s shows that for S between 10 and 30 dB, the maximal ratio error probability lies approximately mid-way between the curves corresponding to $P_c(1)$ and $P_c(2)$ shown in Fig. 5.2, and obtains a value of $5.4 \times 10^{-6}$ for S = 30 dB. Hence, we see that even under ideal conditions, the effective order of implicit diversity is between one and two. Moreover, it is not likely that the actual DFE performance would reflect much of this potential diversity gain since i) in reality, the implicit diversity branches are correlated, ii) the one-shot MMSE forward filter approaches the maximal ratio combining filter only <u>asymptotically</u> for small signal-to-noise ratios, and iii) the MMSE forward filter tap weights are largely determined by the character of the intersymbol

interference, especially for high signal-to-noise ratios. Thus, second-order diversity may be considered to be a gross upper bound for the effective order of implicit diversity for this example. In contrast, it is claimed in [23], that results of the simulation study for this channel model show that the DFE receiver realizes an implicit diversity order of approximately four. The discussion above and the results of experimental studies in [14] show that this is not the case.

We conclude that while some potential for implicit diversity gain does exist, it is not a significant factor for MMSE decision-feedback equalization. Rather, the main attributes of decision-feedback equalizers are the ability to establish a coherent communication environment, and the substantial reduction of the effects of intersymbol interference for practical systems within the limits of the capabilities of the equalizer. Thus, for a given order of explicit diversity L, the performance of DFE receivers in frequency-selective Rayleigh fading channels is both easily and accurately approximated by the average error probability for maximal ratio PSK defined in (5.31).

## 5.5 Additional Considerations

There are, of course, a number of design problems associated with the implementation of adaptive equalizers which largely determine the effectiveness of the equalizer. The aspect of equalizer implementation which most profoundly affects system performance is the realization of the algorithm used to adaptively adjust the coefficients of the TDL filters. In practice, the equalizer, and, hence, the tap-adjustment hardware, is designed to operate in two modes. At the start of operation, a known data sequence or training sequence is transmitted to allow the receiver to adjust to the initial state of the channel. The required length of the training sequence depends on the

total number of equalizer taps, the characteristics of the channel, and the speed of convergence of the adjustment algorithm [23,44,52]. At the end of the start-up mode, the receiver uses the results of previous data symbol decisions to continuously update the tap coefficients [40,44]. Thus, the primary performance criteria for tap-adjustment algorithms are the speed of convergence, the sensitivity to occasional decision errors, and the complexity or cost of implementation.

The most commonly implemented adjustment algorithm for both linear TDL and decision-feedback MSE equalizers is a form of stochastic gradient or steepest descent algorithm [23,49,50]. In this implementation, the tap-vector $\underline{w}$ is recursively adjusted according to the relation

$$\underline{w}_{k+1} = \underline{w}_k + \Delta \varepsilon_k \underline{U}_k^* ,$$

where $\underline{U}_k$ is the vector of received samples U given by (5.3), $\varepsilon_k$ is the difference between the k-th output and the decision on the k-th output, and $\Delta$ is a scale factor which must be chosen small enough to ensure equalizer convergence [44]. While the steepest descent algorithm has the advantage of ease of implementation, it is characterized by a slow rate of convergence [47]. It has been shown [53] that steepest descent algorithms require training sequences of length 10xN, where N is the total number of equalizer taps. A primary constraint for the equalization of fading channels is the need to track the sometimes rapidly varying channel. For applications to Rayleigh fading channels, it is necessary to insert training sequences at periodic intervals to ensure stable equalizer operation. For example, in [8] the results of a simulation study of a DFE consisting of ten forward and ten feedback taps with no explicit diversity are presented. The study was

implemented using a channel simulator to realize a channel with average decorrelation time on the order of $10^4$ data pulse durations. In order to maintain channel equalization, it was necessary to insert a 100-bit training sequence at 2000-bit intervals in the data sequence.

The slow rate of convergence of the steepest descent algorithm is a limiting factor in determining the applicability of adaptive equalizers implementing this algorithm. Within the last decade, a number of studies have been directed toward finding rapidly converging algorithms that can be implemented with minimum additional complexity [47,53-56]. Of these, the algorithms that have received the most attention are those derived from the work of Godard [53] who first applied the Kalman estimation algorithm to the problem of equalizer adjustment. These investigations show that it is possible to obtain near MSE-optimal equalizer adjustment using training sequences of length N, where N is the total number of equalizer taps [54]. Moreover, it is suggested that equalizer adjustment algorithms of this type are capable of tracking the occasionally rapid changes experienced in a fading environment. The two main disadvantages of these algorithms are additional sensitivity to additive noise [44] and increased complexity [44]. The additional computational burden for even the most efficient of these algorithms is roughly 2N times the complexity of steepest descent algorithms for an N-tap equalizer.

# CHAPTER 6

## SUMMARY AND CONCLUSIONS

In this thesis, we have investigated the effects of frequency-selective fading on the average probability of error for DPSK and FSK communications. By considering the effects of frequency-selective fading in both the frequency domain and the delay domain, we have examined the interaction between the characteristics of the fading channel, the transmitted signal, and the quadratic nature of the detection process employed for DPSK and noncoherent FSK communications. We have identified the system parameters that are of fundamental importance in determining the average error probability. It has been shown that the performances of DPSK and FSK can be approximated in terms of one or two parameters that can be obtained from rms-type channel measurements. Lastly, we have examined the basic limitations of equalizer performance and have developed a method of obtaining estimates of adaptive equalizer performance for practical systems.

The analysis of DPSK and FSK for several examples of multipath models (delay power-density spectra) leads to several conclusions. For DPSK systems, the average error probability as well as the irreducible error probability strongly depend on the shape of the data-pulse waveform. These examples also indicate that the lowest error probabilities are obtained when small time-bandwidth product pulses are employed. In particular, the sine-pulse, which is the smallest time-bandwidth product pulse waveform considered [39], also produces the lowest error probability of any pulse shape considered. Large time-bandwidth product pulse shapes (e.g., phase-coded pulses generated by m-sequences) exhibit increased sensitivity to the effects of intersymbol

interference as well as larger error probabilities for practical values of signal-to-noise ratio.

Similar conclusions apply to the relationship between the data-pulse shape and the probability of error for FSK systems. In addition, the modulation index as well as the relative phases between successive transmitted signals play an important role in determining the system error probability. The lowest error rates for FSK are obtained for continuous-phase signals with small modulation indices.

Comparing the results for DPSK and FSK, we find that the error probabilities for these systems depend on a number of common factors, and in certain cases, the effects of frequency-selectivity on both DPSK and FSK systems can be characterized by the same parameter. A technique for obtaining bounds on system performance in terms of the key system and channel parameters applies to the evaluation of both DPSK and FSK systems for the several examples of channel models and signaling formats. Finally, the error probabilities for systems employing complicated pulse shapes and for channels which are difficult to fully characterize can be predicted from the key system parameters and the performance data contained in this thesis.

For channels with rms multipath spreads less than about 0.1, it is possible to substantially reduce the irreducible error probabilities for both DPSK and FSK systems by choosing system parameters which minimize the sensitivity to intersymbol interference. However, for many practical systems the effects of ISI can severely limit the performance of these forms of digital communications. In Chapter 5, the characteristics of adaptive equalizers commonly employed for fading-channel communications are described and the results of several simulation and experimental studies are compared.

It is revealed, that while claims of "implicit diversity gain" abound in the literature, the significant attributes of adaptive equalization techniques are the ability to establish a coherent communication link and the substantial reduction of the effects of intersymbol interference. Comparing the results of simulation studies and experimental investigations of equalizer performance with the analytical results for the error probabilities of DPSK and FSK systems reveals that reliable communications can be achieved through channel equalization even in fading environments that produce unacceptably high error probabilities for unequalized systems.

It should be pointed out that one of the factors limiting the implicit diversity gain for signals with small time-bandwidth products is the inability to resolve the multipath components in the received signal. For rectangular data pulse waveforms with duration T, it is clear that signals arriving at the receiver with relative delays of less than T seconds cannot be resolved into independently faded components. In fact, for WSSUS fading channels, the statistical correlation between signals received with relative delay $\xi$ is completely determined by the product of the delay power-density spectrum and the autocorrelation function of the data pulse waveform evaluated at $\xi$.

Within the last five years, there has been considerable interest in the application of equalization techniques to both coherent and noncoherent spread-spectrum communication systems employing phase-coded waveforms. The analysis [57] and test results [58,59] indicate that the use of this type of signal with large time-bandwidth product allows resolution and coherent (maximal ratio) combining for both HF and troposcatter channels. The development of useful bounds and approximations of the performance of adaptive equalizers for both spread-spectrum and conventional communications in

frequency-selective fading channels is an area where much further work is needed.

The current interest in applications of adaptive equalization techniques to digital communications over frequency-selective fading channels is in large part due to the well-documented effectiveness of these techniques in nonfading systems. While it is true that reliable communications can be achieved through the use of adaptive equalizers, it is not clear that channel equalization is the most efficient way to reduce the effects of intersymbol interference. Unfortunately, the published literature is void of the consideration of alternative techniques that could be used in practical systems to obtain acceptable performance.

One example of a possible alternative which deserves consideration is the use of M-ary orthogonal signalling in conjunction with error correcting codes. In particular, suppose that the source data rate R = $10^6$ bits/sec and the channel rms delay M = $3\text{x}10^{-5}$ sec are fixed design parameters. Hence, for binary signaling the rms multipath spread $\mu_2 = M/T = 0.3$. If 8-ary orthogonal FSK is used to transmit the binary data, the effective rms multipath spread is reduced to $\mu_8 = 0.1$. Unfortunately, the evaluation of the probability of error for M-ary orthogonal FSK in frequency-selective Rayleigh fading is at present an unsolved problem. While it is true that the introduction of an error-correcting code has the effect of increasing the channel data rate (and, hence, increasing the effective rms multipath spread), it may be possible to realize error rates significantly lower than those achieved through adaptive channel equalization. The investigation of alternative methods of achieving reliable communications over frequency-selective fading channels is an area which appears to be both promising and challenging.

## REFERENCES


[1] IEEE Transactions on Communications: Special Issue on Spread-Spectrum Communications, vol. COM-30, no. 5, May 1982.

[2] E. A. Geraniotis and M. B. Pursley, "Error probabilities for slow-frequency-hopped spread-spectrum multiple-access communications over fading channels," IEEE Transactions on Communications, vol. COM-30, no. 5, pp. 986-1009, May 1982.

[3] F. D. Garber and M. B. Pursley, "Effects of time-selective fading on slow-frequency-hopped DPSK spread-spectrum communications," Conference Record, IEEE National Telecommunications Conference, (New Orleans, Louisiana: Nov. 3-5, 1981), vol. 4, pp. G8.1.1-5.

[4] E. A. Geraniotis, "Error probabilities for coherent hybrid slow-frequency-hopped direct-sequence spread-spectrum multiple-access communications," Conference Record, IEEE National Telecommunications Conference, (New Orleans, Louisiana: Nov. 29 - Dec. 3, 1981), vol. 4, pp. G8.6.1-5.

[5] F. D. Garber and M. B. Pursley, "Effects of frequency-selective fading on slow-frequency-hopped DPSK spread-spectrum multiple-access communications," Proceedings of the 1982 IEEE Military Communications Conference, (Boston, Massachusetts: Oct. 18-20, 1982), vol. 2, pp. 35.2.1-6.

[6] M. Schwartz, W. R. Bennett, and S. Stein, Communication Systems and Techniques, McGraw-Hill, New York, 1966, part III.

[7] P. Monsen, "Fading channel communications," IEEE Communications Magazine, vol. 18, no. 1, pp. 16-25, Jan. 1980.

[8] R. L. Bogusch, F. W. Guigliano and D. L. Knepp, "Frequency-selective scintillation effects and decision feedback equalization in high data-rate satellite links," Proceedings of the IEEE, vol. 71, no. 6, pp. 754-767, June 1983.

[9] P. A. Bello, "Characterization of randomly time variant linear channels," IEEE Transactions on Communication Systems, vol. CS-11, pp. 360-393, Dec. 1963.

[10] T. Kailath, "Channel characterization: time-variant dispersive channels," Chapter 6, in Lectures on Communications System Theory, E. Baghdady, Ed., McGraw-Hill, New York, 1961.

[11] P. A. Bello and B. D. Nelin, "The influence of fading spectrum on the binary error probabilities of incoherent and differentially-coherent matched filter receivers," IRE Transactions on Communication Systems, vol. CS-10, pp. 160-168, June 1962.

[12] D. E. Borth and M. B. Pursley, "Analysis of direct-sequence spread-spectrum multiple-access communication over Rician fading channels, IEEE Transactions on Communications, vol. COM-27, no. 10, pp. 1566-1577, Oct. 1979.

[13] P. A. Bello, "Some techniques for the instantaneous real-time measurement of multipath and Doppler spread," IEEE Transactions on Communication Technology, vol. COM-13, pp. 285-292, Sept. 1965.

[14] L. Ehrman and P. Monsen, "Troposcatter test results for a high-speed decision-feedback equalizer modem," IEEE Transactions on Communications, vol. COM-25, no. 12, pp. 1499-1504, Dec., 1977.

[15] E. D. Sunde, "Digital troposcatter transmission and modulation theory," Bell System Technical Journal, vol. 43, part 1, pp. 143-214, Jan. 1964.

[16] C. C. Bailey and J. C. Lindenlaub, "Further results concerning the effect of frequency-selective fading on differentially coherent matched filter receivers," IEEE Transactions on Communication Technology, vol. COM-16, pp. 749-751, Oct. 1968.

[17] P. A. Bello and B. D. Nelin, "The effect of frequency selective fading on the binary error probabilities of incoherent and differentially coherent matched filter receivers," IEEE Transactions on Communication Systems, vol. CS-11, pp. 170-186, June 1963.

[18] L. B. Milstein and D. L. Schilling, "The effect of frequency-selective fading on a noncoherent FH-FSK system operating with partial-band tone interference," IEEE Transactions on Communications, vol. COM-30, no. 5, pp. 904-912, May 1982.

[19] P. A. Bello, "Binary error probabilities over selectively fading channels containing specular components," IEEE Transactions on Communication Technology, vol. COM-14, no. 4, pp. 400-406, Aug. 1966.

[20] D. L. Duttweiler, J. E. Mazo, and D. G. Messerschmidt, "An upper bound on the error probability in decision-feedback equalization," IEEE Transactions on Information Theory, vol. IT-20, no. 4, pp. 490-497, July, 1974.

[21] J. G. Proakis, "Advances in equalization for intersymbol interference ," in Advances in Communication Systems, vol. 4, pp. 123-198, Academic Press, New York, 1975.

[22] S. Qureshi, "Adaptive equalization," IEEE Communications Magazine, vol. 20, no. 2, pp. 9-16, Mar. 1982.

[23] P. Monsen, "Feedback equalization for fading dispersive channels," IEEE Transactions on Information Theory, vol. IT-17, no. 1, pp. 56-64, Jan. 1971.

[24] P. Monsen, "Theoretical and measured performance of a DFE modem on a fading multipath channel," IEEE Transactions on Communications, vol. COM-25, no. 10, pp. 1144-1153, Oct. 1977.

[25] P. Monsen, "Digital transmission performance on fading dispersive diversity channels," IEEE Transactions on Communications, vol. COM-21, no. 1, pp. 33-39, Jan. 1973.

[26] M. B. Pursley, "Spread-spectrum multiple-access communications," in Multi-User Communication Systems, G. Longo, Ed., Springer-Verlag, New York, pp. 139-199, 1981.

[27] M. B. Pursley, F. D. Garber and J. S. Lehnert, "Analysis of generalized quadriphase spread-spectrum communications," (Invited Paper) Conference Record, IEEE International Conference on Communications, (Seattle, Washington: June 8-12, 1980), vol. 1, pp. 15.3.1-6.

[28] M. B. Pursley, "Performance analysis for phase-coded spread-spectrum multiple-access communication -- Part I: System analysis," IEEE Transactions on Communications, vol. COM-25, no. 7, pp. 795-799, Aug. 1977.

[29] M. B. Pursley and D. V. Sarwate, "Performance analysis for phase-coded spread-spectrum multiple-access communication -- Part II: Code sequence analysis," IEEE Transactions on Communications, vol. COM-25, no. 7, pp. 800-803, Aug. 1977.

[30] D. V. Sarwate and M. B. Pursley, "Crosscorrelation properties of pseudorandom and related sequences," (Invited Paper) Proceedings of the IEEE, vol. 68, no. 5, pp. 593-619, May 1980.

[31] E. A. Geraniotis and M. B. Pursley, "Coherent direct-sequence spread-spectrum communications in a specular multipath fading environment," Proceedings of the 1982 Conference on Information Sciences and Systems, (Princeton University, Princeton, New Jersey: Mar. 17-19, 1982), pp. 401-406.

[32] F. J. MacWilliams and N. J. A. Sloane, "Pseudo-random sequences and arrays," Proceedings of the IEEE, vol. 64, no. 12, pp. 1715-1729, Dec. 1976.

[33] L. E. Dubins, "On extreme points of convex sets," Journal of Math Analysis and Applications, vol. 5, pp. 237-244, 1962.

[34] H. S. Witsenhausen, "Some aspects of convexity useful in information theory," IEEE Transactions on Information Theory, vol. IT-26, no. 3, pp. 265-271, May 1980.

[35] R. Ash, Real Analysis and Probability, Academic Press, New York, 1972.

[36] G. D. Hingorani, "Error rates for a class of binary receivers," IEEE Transactions on Communications Technology, vol. COM-15, no. 2, pp. 209-215, Apr. 1967.

[37] G. L. Turin, "The characteristic function of Hermitian quadratic forms in complex normal variables," Biometrika, vol. 47, pts. 1, 2, pp. 149-201, June, 1960.

[38] R. Price, "Some non-central F-distributions expressed in closed form," Biometrika, vol. 51, pts. 1, 2, pp. 107-122, June 1964.

[39] M. B. Pursley, "Digital communications," Chapter 24 of Reference Data for Radio Engineers, Seventh edition, E. C. Jordan, Ed., Howard W. Sams Publishing Co., Indianapolis Indiana, 1983.

[40] P. Monsen, "Adaptive equalization of the slow fading channel," IEEE Transactions on Communications, vol. COM-22, no. 8, pp. 1064-1075, Aug. 1974.

[41] P. Monsen, "MMSE equalization of interference on fading diversity channels," Conference Record, IEEE International Conference on Communications, (Denver, Colorado: June 14-18, 1981), vol. 1, pp. 12.2.1-5.

[42] P. Monsen, "Decision-feedback equalization performance on mixed diffraction/scatter paths," Conference Record, IEEE International Conference on Communications, (Philadelphia: June 13-17, 1982), vol. 2, pp. 3H.2.1-4.

[43] P. A. Bello and K. Pahlavan, "Performance of adaptive equalization for staggered QPSK and QPR over frequency-selective LOS microwave channels," Conference Record, IEEE International Conference on Communications, (Philadelphia: June 13-17, 1982), vol. 2, pp. 3H.1.1-6.

[44] J. G. Proakis, Digital Communications, McGraw-Hill, New York, 1983.

[45] R. D. Gitlin, E. Y. Ho and J. E. Mazo, "Passband equalization of differentially phase-modulated data signals," Bell System Technical Journal, vol. 52, no. 2, pp. 219-238, Feb. 1972.

[46] S. U. H. Qureshi and G. D. Forney Jr., "Performance and properties of a T/2 equalizer," Conference Record, IEEE National Telecommunications Conference, Dec. 1977, pp. 11:1.1-9.

[47] J. Salz, "Optimum mean-square decision feedback equalization," Bell System Technical Journal, vol. 52, no. 8, pp. 1341-1373, Oct. 1973.

[48] D. G. Brennan, "Linear diversity combining techniques," Proceedings of the IRE, vol. 47, pp. 1075-1102, June 1959.

[49] D. A. George, R. R. Bowen, and J. R. Storey, "An adaptive decision-feedback equalizer," IEEE Transactions on Communication Technology, vol. COM-19, no. 6, pp. 281-293, June 1971.

[50] C. A. Belfiore and J. H. Park, "Decision feedback equalization," Proceedings of the IEEE, vol. 67, no. 8, pp. 1143-1156, Aug. 1979.

[51] C. J. Grzenda, D. R. Kern, and P. Monsen, "Megabit digital troposcatter subsystem," Conference Record, IEEE National Telecommunications Conference, (New Orleans, Louisiana: Dec. 1975), pp. 28.15-19.

[52] J. G. Proakis, "Adaptive filters," in Communications Systems and Random Process Theory, J. K. Skwirzinski, Ed., Sitjhoff and Noordhoff, Alphen aan der Rijn, The Netherlands, pp. 661-678, 1978.

[53] D. Godard, "Channel equalization using a Kalman filter for fast data transmission," IBM Journal of Research and Development, pp. 267-273, May 1974.

[54] M. S. Mueller, "On the rapid initial convergence of least-squares equalizer adjustment algorithms," Bell System Technical Journal, vol. 69, no. 10, pp. 2345-2358, Dec. 1981.

[55] D. D. Falconer and L. Ljung, "Application of fast Kalman estimation to adaptive equalization," IEEE Transactions on Communications, vol. COM-26, no. 10, pp. 1439-1446, Oct. 1978.

[56] F. M. Hsu, "Square-root Kalman filtering for high-speed data received over fading dispersive HF channels," IEEE Transactions on Information Theory, vol. IT-28, no. 5, pp. 753-763, Sept. 1982.

[57] J. S. Lehnert and M. B. Pursley, "Multipath diversity reception of coherent direct-sequence spread-spectrum communications," Proceedings of the 1983 Conference on Information Sciences and Systems, (The Johns Hopkins University, Baltimore, Maryland: Mar. 23-25, 1983), pp. 770-775.

[58] E. T. Tsui and R. Y. Ibaraki, "An adaptive spread-spectrum receiver for multipath/scatter channels," Proceedings of the 1982 IEEE Military Communications Conference, (Boston, Massachusetts: Oct. 18-20, 1982), vol. 2, pp. 35.3.1-4.

[59] J. Low and S. M. Waldstein, "A direct-sequence spread-spectrum modem for wideband HF channels," Proceedings of the 1982 IEEE Military Communications Conference, (Boston, Massachusetts: Oct. 18-20, 1982), vol. 2, pp. 29.6.1-6.

# VITA

Frederick Dwight Garber was born in Brookville, Ohio on October 1, 1951. He received the B.S. degree with honors from Tri-State College in 1975, and the M.S. degree from the University of Illinois in 1978. From June 1976 to September 1983 he was a research assistant in the Coordinated Science Laboratory at the University of Illinois. He has co-authored the following papers:

"Quadriphase spread-spectrum multiple-access communications," IEEE International Conference on Communications, Conference Record, pp. 7.3.1-7.3.5, June, 1978. (with M. B. Pursley)

"Analysis of generalized quadriphase spread-spectrum communications," IEEE International Conference on Communications, Conference Record, pp. 15.3.1-15.3.6, June, 1980. (with M. B. Pursley and J. S. Lehnert)

"Optimal phases of maximal length sequences for asynchronous spread-spectrum multiplexing," Electronics Letters, vol. 16, no. 19, pp. 756-757, September 1980. (with M. B. Pursley)

"Performance of offset quadriphase spread-spectrum multiple-access communications," IEEE Transactions on Communications, vol. COM-29, no. 3, pp. 305-314, March 1981. (with M. B. Pursley)

"Effects of time-selective fading on slow-frequency-hopped DPSK spread-spectrum communications," IEEE National Telecommunications Conference Record, pp. G8.1.1-G8.1.5, November 1981. (with M. B. Pursley)

"Effects of frequency-selective fading on slow-frequency-hopped DPSK spread-spectrum communications," 1982 IEEE Military Communications Conference Record, pp. 35.2.1-35.2.6, October, 1982. (with M. B. Pursley)

"Performance of differentially-coherent digital communications over frequency-selective fading channels," submitted to: IEEE Transactions on Communications. (with M. B. Pursley)

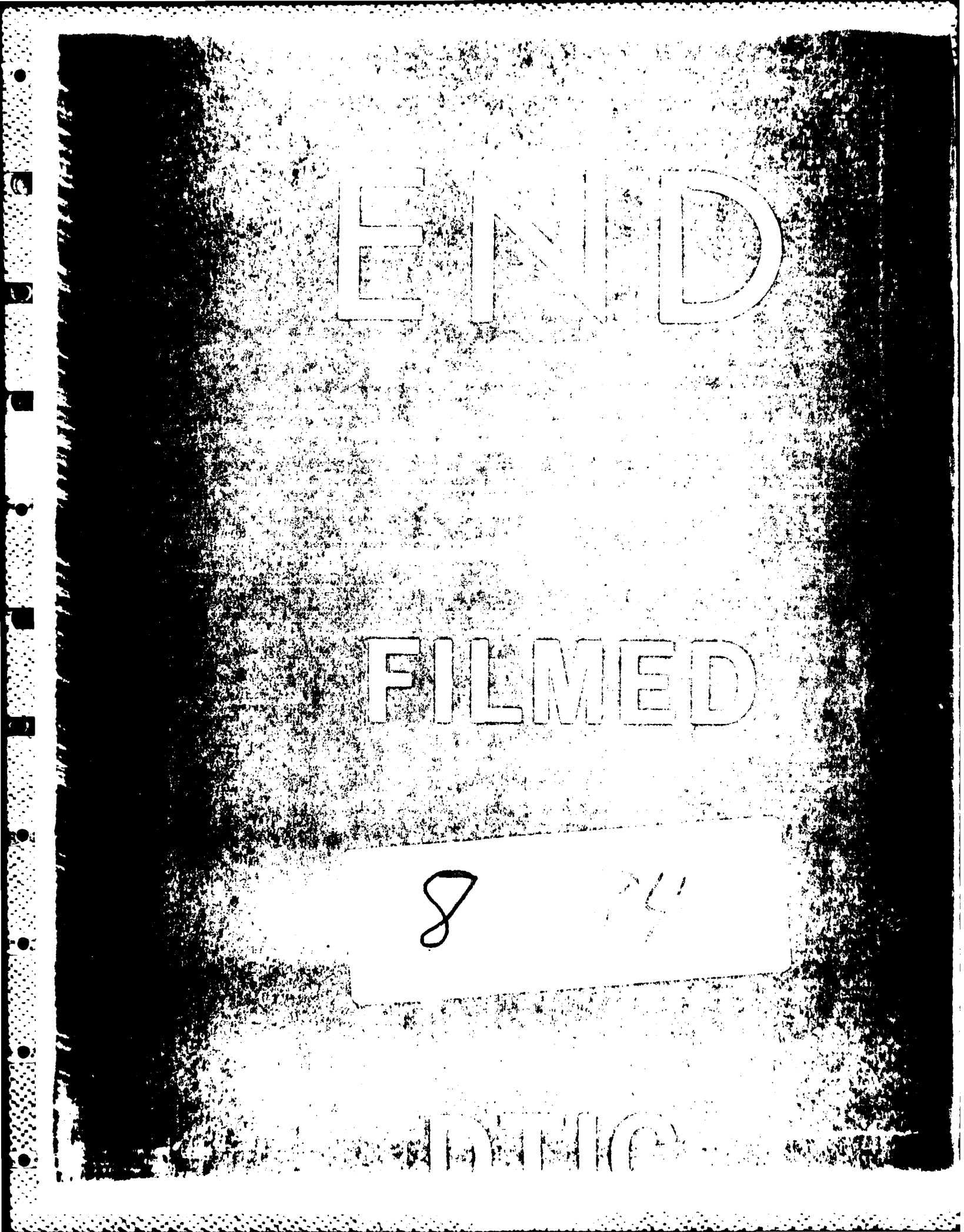
END
FILMED
8